

5-2011

MODIFICATION AND IMPLEMENTATION OF THE RPC HETEROGENEOUS THORAX PHANTOM FOR VERIFICATION OF PROTON THERAPY TREATMENT PROCEDURES

Anthony Blatnica

Follow this and additional works at: https://digitalcommons.library.tmc.edu/utgsbs_dissertations

 Part of the [Other Physics Commons](#)

Recommended Citation

Blatnica, Anthony, "MODIFICATION AND IMPLEMENTATION OF THE RPC HETEROGENEOUS THORAX PHANTOM FOR VERIFICATION OF PROTON THERAPY TREATMENT PROCEDURES" (2011). *The University of Texas MD Anderson Cancer Center UTHealth Graduate School of Biomedical Sciences Dissertations and Theses (Open Access)*. 110.

https://digitalcommons.library.tmc.edu/utgsbs_dissertations/110

This Thesis (MS) is brought to you for free and open access by the The University of Texas MD Anderson Cancer Center UTHealth Graduate School of Biomedical Sciences at DigitalCommons@TMC. It has been accepted for inclusion in The University of Texas MD Anderson Cancer Center UTHealth Graduate School of Biomedical Sciences Dissertations and Theses (Open Access) by an authorized administrator of DigitalCommons@TMC. For more information, please contact digitalcommons@library.tmc.edu.

MODIFICATION AND IMPLEMENTATION OF THE RPC HETEROGENEOUS THORAX PHANTOM FOR VERIFICATION OF PROTON THERAPY TREATMENT PROCEDURES

By
Anthony (Tony) Blatnica, B.S.

Approved:

Geoffrey S. Ibbott, PhD.
Supervisory Professor

David S. Followill, PhD.

Ronald X. Zhu, PhD.

Peter A. Balter, PhD.

R. Allen White, PhD.

APPROVED:

Dean, The University of Texas
Health Science Center at Houston
Graduate School of Biomedical Sciences

**MODIFICATION AND IMPLEMENTATION OF THE RPC
HETEROGENEOUS THORAX PHANTOM FOR
VERIFICATION OF PROTON THERAPY
TREATMENT PROCEDURES**

A

THESIS

Presented to the Faculty of
The University of Texas
Health Science Center at Houston
and
The University of Texas
M.D. Anderson Cancer Center
Graduate School of Biomedical Sciences
in Partial Fulfillment

of the Requirements

for the Degree of

MASTER OF SCIENCE

By

Anthony (Tony) Blatnica, B.S.

May 2011

ACKNOWLEDGMENTS

The author wishes to express sincere appreciation to his committee, Drs. Ibbott, Followill, Zhu, Balter and White for their guidance through the course of my research. I would also like to thank the staff at the RPC for their assistance in helping me understand the inner workings of the RPC. I would like to thank John Costales, at UH for his expertise in machining the insert that made this project possible. I would also like to thank Drs. Gillin and Sahoo, as well as the staff at the PTC-H for all of their assistance. I would also like to thank Ryan Grant, Mike Silosky and my other fellow medical physics graduate students for all their help and support during this project. Most importantly I would like to thank my wife Becky and my son Jake for their support and for tolerating me and my schedule during this entire process.

ABSTRACT
MODIFICATION AND IMPLEMENTATION OF THE RPC HETEROGENEOUS
THORAX PHANTOM FOR VERIFICATION OF PROTON THERAPY TREATMENT
PROCEDURES

By: Anthony (Tony) Blatnica

Chairperson of the Supervisory Committee: Geoffrey S. Ibbott, PhD.

The Radiological Physics Center (RPC) provides heterogeneous phantoms that are used to evaluate radiation treatment procedures as part of a comprehensive quality assurance program for institutions participating in clinical trials. It was hypothesized that the existing RPC heterogeneous thorax phantom can be modified to assess lung tumor proton beam therapy procedures involving patient simulation, treatment planning, and treatment delivery, and could confirm agreement between the measured dose and calculated dose within 5%/3mm with a reproducibility of 5%. The Hounsfield Units (HU) for lung equivalent materials (balsa wood and cork) was measured using a CT scanner. The relative linear stopping power (RLSP) of these materials was measured. The linear energy transfer (LET) of Gafchromic EBT2 film was analyzed utilizing parallel and perpendicular orientations in a water tank and compared to ion chamber readings. Both parallel and perpendicular orientations displayed a quenching effect underperforming the ion chamber, with the parallel orientation showing an average 31 % difference and the perpendicular showing an average of 15% difference. Two treatment plans were created that delivered the prescribed dose to the target volume, while achieving low entrance doses. Both treatment plans were designed using smeared compensators and expanded apertures, as would be utilized for a patient in the clinic. Plan 1a contained two beams that were set to orthogonal angles and a zero degree couch kick. Plan 1b utilized two beams set to 10

and 80 degrees with a 15 degree couch kick. EBT2 film and TLD were inserted and the phantom was irradiated 3 times for each plan. Both plans passed the criteria for the TLD measurements where the TLD values were within 7% of the dose calculated by Eclipse. Utilizing the 5%/3mm criteria, the 3 trial average of overall pass rate was 71% for Plan 1a. The 3 trial average for the overall pass rate was 76% for Plan 1b. The trials were then analyzed using RPC conventional lung treatment guidelines set forth by the RTOG: 5%/5mm, and an overall pass rate of 85%. Utilizing these criteria, only Plan 1b passed for all 3 trials, with an average overall pass rate of 89%.

CONTENTS

Signature Page	i
Title Page.....	ii
Acknowledgments	iii
Abstract	iv
List of Figures	x
List of Tables.....	xv
CHAPTER 1: Introduction and Background.....	1
1.1 Introduction	1
1.2 Statement of Problem	1
1.3 Proton Therapy	2
1.3.1 History	2
1.3.2 Properties of Protons.....	3
1.3.3 Properties of The Proton Beam.....	3
1.3.4 Modification of the Proton Beam	4
1.3.5 Range	9
1.3.6 Relative Biological effectiveness.....	10
1.4 New Insert	11
1.4.1 Existing Thorax Phantom	11
1.4.2 Lung Equivalent material	13
1.4.3 Film and Air Gaps in Current Insert	14

1.5	Hypothesis and Specific Aims	15
CHAPTER 2: Materials and Methods		16
2.1	Phantom Design and Construction	16
2.1.1	Lung Insert Material	17
2.2	Material Relative Linear Stopping Power	18
2.2.1	Depth Dose Scanning	19
2.2.2	Stopping Power analysis.....	20
2.3	Construction	21
2.4	Treatment Planning	23
2.4.1	Eclipse	24
2.4.2	Stopping power Comparison	24
2.4.3	Treatment Plan 1A.....	25
2.4.4	Treatment Plan 1b.....	27
2.5	Dosimeters.....	29
2.5.1	TLD	29
2.5.2	GAFChromic® Film.....	32
2.5.3	Treatment Delivery for Lung insert.....	36
2.5.4	TLD and Film Registration.....	37
2.6	Treatment Evaluations.....	38
2.6.1	TLD Comparisons	38

2.6.2	Film vs. Treatment plan comparisons.....	38
CHAPTER 3:	Results and Discussion.....	42
3.1	Phantom Design and Construction	42
3.1.1	Material Relative Linear Stopping Powers.....	42
3.1.2	Compression	46
3.1.3	Comparison of Plans.....	47
3.2	LET Dependence of GAFChromic Film	50
3.2.1	Parallel Film Orientation	50
3.2.2	Perpendicular Film Orientation	53
3.3	Phantom Irradiation Evaluation.....	54
3.3.1	TLD	54
3.3.2	CT to Eclipse registration	58
3.3.3	TLD Registration.....	59
3.3.4	Film scanning and registration.....	59
3.3.5	Gamma Analysis.....	61
3.3.6	DTA Profile Comparisons	73
CHAPTER 4:	Conclusions	86
4.1	Summary.....	86
4.2	Conclusions	88
4.3	Future Work.....	89
CHAPTER 5:	Appendix	90

5.1	Gamma Analysis – 5%/3mm	90
5.1.1	Plan 1a	90
5.1.2	Plan 1a – PVC contoured.....	93
5.1.3	Plan 1b	96
5.1.4	Plan 1b- PVC Contoured	99
5.2	DTA Profile Comparisons	102
5.2.1	Plan 1A	102
5.2.2	Plan 1b	109
	References	117
	Vita	121

LIST OF FIGURES

<i>Number</i>	<i>Page</i>
Figure 1-1 Schematic of nozzle components of the passively scattered beams lines.....	5
Figure 1-2 Comparison of Percent Depth Dose curves	6
Figure 1-3 Steps on an aluminum range modulation wheel (RMW) used at the PTC-H.....	7
Figure 1-4 Bronze collimator plate.....	8
Figure 1-5 Acrylic range compensator	8
Figure 1-6 RPC Thorax Phantom – phantom shell.....	12
Figure 1-7 Disassembled, original cork lung imaging/dosimetry insert.....	13
Figure 2-1 Random sample of lung patient's CT images	17
Figure 2-2 CT Image of balsa block suspended in air.....	18
Figure 2-3 Balsa sample being scanned for RLSP analysis at PTC-H.....	20
Figure 2-4 Cross section of tapered outer balsa ring	21
Figure 2-5 Schematic of an individual wedges assembled in a wireframe.....	22
Figure 2-6 Balsa imaging/dosimetry insert	23
Figure 2-7 Axial view of treatment plan 1A at isocenter.	26
Figure 2-8 Axial view of Plan 1b	28
Figure 2-9 Configuration of GAFChromic® EBT2 film	32
Figure 2-10 Dose response curve of lot# A06221004 GAFChromic EBT2 film.....	33
Figure 2-11 GAFChromic film in perpendicular orientation	35
Figure 2-12 GAFChromic film in parallel orientation	36
Figure 2-13 Screen capture of RPCFILM analysis for Plan 1b trial 2	39
Figure 3-1 Comparison of balsa and reference ion chamber depth dose curves	43

Figure 3-2 Lung Material RLSP-HU chart comparing phantom values to calibrated Eclipse curves..	45
Figure 3-3 High resolution CT scan of imaging/dosimetry insert.....	47
Figure 3-4 Gamma analysis of Std. Plan and PVC contoured plan in the axial plane.	48
Figure 3-5 Gamma analysis of Std. Plan and PVC contoured plan in the coronal plane	49
Figure 3-6 Gamma analysis of Std. Plan and PVC contoured plan in the sagittal plane	49
Figure 3-7 Comparison of depth dose curves.....	51
Figure 3-8 Comparison of depth dose curves.....	52
Figure 3-9 Comparison of depth dose curves.....	54
Figure 3-10 Plan 1b trial 2 film prick localizers.....	60
Figure 3-11 Plan 1a Trial 2 Axial Gamma Analysis	63
Figure 3-12 Plan 1a Trial 2 Coronal Gamma Analysis	63
Figure 3-13 Plan 1a Trial 2 Sagittal Gamma Analysis.....	64
Figure 3-14 Plan 1b Trial 2 Axial Gamma Analysis	64
Figure 3-15 Plan 1b Trial 2 Coronal Gamma Analysis.....	65
Figure 3-16 Plan 1b Trial 2 Sagittal Gamma Analysis.....	65
Figure 3-17 Plan 1a Trial 2 Axial Gamma Analysis with PVC Shell contoured	67
Figure 3-18 Plan 1a Trial 2 Coronal Gamma Analysis with PVC Shell contoured	67
Figure 3-19 Plan 1a Trial 2 Sagittal Gamma Analysis with PVC Shell contoured	68
Figure 3-20 Plan 1b Trial 2 Axial Gamma Analysis with PVC Shell contoured.....	68
Figure 3-21 Plan 1b Trial 2 Coronal Gamma Analysis with PVC Shell contoured	69
Figure 3-22 Plan 1b Trial 2 Sagittal Gamma Analysis with PVC Shell contoured.....	69
Figure 3-23 Plan 1a Trial 2 Axial Gamma Analysis 5%/5mm.....	71
Figure 3-24 Plan 1a Trial 2 Coronal Gamma Analysis 5%/5mm.....	71
Figure 3-25 Plan 1a Trial 2 Sagittal Gamma Analysis 5%/5mm	72
Figure 3-26 Plan 1b Trial 2 Axial Gamma Analysis 5%/5mm	72
Figure 3-27 Plan 1b Trial 2 Coronal Gamma Analysis 5%/5mm	73

Figure 3-28 Plan 1b Trial 2 Sagittal Gamma Analysis 5%/5mm.....	73
Figure 3-29 Plan 1a Trial 2 Anterior Posterior Profile Axial Plane	75
Figure 3-30 Plan 1a Trial 2 Right Left Profile Axial Plane.....	76
Figure 3-31 Plan 1a Trial 2 Superior Inferior Profile Coronal Plane	77
Figure 3-32 Plan 1a Trial 2 Right Left Profile Coronal Plane.....	77
Figure 3-33 Plan 1a Trial 2 Anterior Posterior Profile Sagittal Plane.....	78
Figure 3-34 Plan 1a Trial 2 Superior Inferior Profile Sagittal Plane.....	79
Figure 3-35 Plan 1b Trial 2 Anterior Posterior Profile Axial Plane.....	80
Figure 3-36 Plan 1b Trial 2 Right Left Profile Axial Plane	81
Figure 3-37 Plan 1b Trial 2 Superior Inferior Profile Coronal Plane.....	82
Figure 3-38 Plan 1b Trial 2 Right Left Profile Coronal Plane	82
Figure 3-39 Plan 1b Trial 2 Anterior Posterior Profile Sagittal Plane.....	83
Figure 3-40 Plan 1b Trial 2 Superior Inferior Profile Sagittal Plane.....	84
Figure 3-41 Plan 1b Trial 1 Right Left Profile Axial Plane	85
Figure 5-1 Plan 1a Trial 1 Axial Gamma Analysis	90
Figure 5-2 Plan 1a Trial 1 Coronal Gamma Analysis	90
Figure 5-3 Plan 1a Trial 1 Sagittal Gamma Analysis.....	91
Figure 5-4 Plan 1a Trial 3 Axial Gamma Analysis	91
Figure 5-5 Plan 1a Trial 3 Coronal Gamma Analysis	92
Figure 5-6 Plan 1a Trial 3 Sagittal Gamma Analysis.....	92
Figure 5-7 Plan 1a Trial 1 Axial Gamma Analysis	93
Figure 5-8 Plan 1a Trial 1 Coronal Gamma Analysis	93
Figure 5-9 Plan 1a Trial 1 Sagittal Gamma Analysis.....	94
Figure 5-10 Plan 1a Trial 3 Axial Gamma Analysis	94
Figure 5-11 Plan 1a Trial 3 Coronal Gamma Analysis	95
Figure 5-12 Plan 1a Trial 3 Sagittal Gamma Analysis.....	95

Figure 5-13 Plan 1b Trial 1 Axial Gamma Analysis	96
Figure 5-14 Plan 1b Trial 1 Axial Gamma Analysis	96
Figure 5-15 Plan 1b Trial 1 Sagittal Gamma Analysis.....	97
Figure 5-16 Plan 1b Trial 3 Axial Gamma Analysis	97
Figure 5-17 Plan 1b Trial 3 Coronal Gamma Analysis.....	98
Figure 5-18 Plan 1b Trial 3 Sagittal Gamma Analysis.....	98
Figure 5-19 Plan 1b Trial 1 Axial Gamma Analysis	99
Figure 5-20 Plan 1b Trial 1 Axial Gamma Analysis	99
Figure 5-21 Plan 1b Trial 1 Sagittal Gamma Analysis.....	100
Figure 5-22 Plan 1b Trial 3 Axial Gamma Analysis	100
Figure 5-23 Plan 1b Trial 3 Coronal Gamma Analysis	101
Figure 5-24 Plan 1b Trial 3 Sagittal Gamma Analysis.....	101
Figure 5-25 Plan 1a Trial 1 Anterior Posterior Profile Axial Plane	103
Figure 5-26 Plan 1a Trial 1 Right Left Profile Axial Plane.....	103
Figure 5-27 Plan 1A Trial 1 Right Left Profile Coronal Plane.....	104
Figure 5-28 Plan 1A Trial 1 Superior Inferior Coronal Plane	104
Figure 5-29 Plan 1A Trial 1 Anterior Posterior Sagittal Plane.....	105
Figure 5-30 Plan 1A Trial 1 Superior Inferior Sagittal Plane.....	105
Figure 5-31 Plan 1A Trial 1 Right Left Profile Axial Plane	106
Figure 5-32 Plan 1A Trial 3 Anterior Posterior Axial Plane	106
Figure 5-33 Plan 1A Trial 3 Right Left Coronal Plane	107
Figure 5-34 Plan 1A Trial 3 Superior Inferior Coronal Plane	107
Figure 5-35 Plan 1A Trial 3 Anterior Posterior Sagittal Plane.....	108
Figure 5-36 Plan 1A Trial 3 Superior Inferior Sagittal Plane.....	108
Figure 5-37 Plan 1b Trial 1 Right Left Axial Plane	110
Figure 5-38 Plan 1b Trial 1 Anterior Posterior Axial Plane.....	110

Figure 5-39 Plan 1b Trial 1 Right Left Coronal Plane	111
Figure 5-40 Plan 1b Trial 1 Superior Inferior Coronal Plane.....	111
Figure 5-41 Plan 1b Anterior Posterior Sagittal Plane	112
Figure 5-42 Plan 1b Trial 1 Superior Inferior Sagittal Plane	112
Figure 5-43 Plan 1b Trial 3 Right Left Axial Plane	113
Figure 5-44 Plan 1b Trial 3 Anterior Posterior Axial Plane.....	113
Figure 5-45 Plan 1b Trial 3 Right Left Coronal Plane	114
Figure 5-46 Plan 1b Trial 3 Superior Inferior Coronal Plane.....	114
Figure 5-47 Plan 1b Trial 3 Anterior Posterior Sagittal Plane	115
Figure 5-48 Plan 1b Trial 3 Superior Inferior Sagittal Plane	115
Figure 5-49: Monitor Unit Calculation Sheet.....	116

LIST OF TABLES

<i>Number</i>	<i>Page</i>
Table 1 Plan 1a Treatment Parameters. Prescribed dose is 200 cGyRBE.....	27
Table 2 Plan 1b Treatment Parameters. Prescribed dose is 200 cGyRBE.....	29
Table 3 DTA Profile co-ordinates for Axial, Coronal, and Sagittal films.....	41
Table 4 Relative stopping linear stopping powers of phantom materials.....	44
Table 5 Relative linear stopping power of three lung equivalent lung materials	46
Table 6 Comparison of Parallel film methods to Ion chamber readings	53
Table 7 Comparison of Perpendicular film method to Ion chamber readings.....	53
Table 8 TLD formula constants for B07	55
Table 9 Plan 1a TLD dosimetry data.....	55
Table 10 Plan 1b TLD dosimetry data	56
Table 11 Plan 1a TLD average, Std. Deviation and CV for 3 trials	57
Table 12 Plan 1b TLD average, Std. deviation, and CV for 3 trials.....	57
Table 13 CT registration landmarks	58
Table 14 Table of TLD physical registration locations for RPCFILM, in mm.....	59
Table 15 Film registration prick locations.....	60
Table 16 Gamma analysis results for Plans 1a and 1b utilizing a 5%/3mm criteria	62
Table 17 Gamma analysis results for Plans 1a and 1b utilizing a 5%/3mm criteria	66
Table 18 Gamma analysis results for Plans 1a and 1b utilizing a 5%/5mm criteria	70
Table 19 Dose levels for linear regressions utilized to calculate DTA	74
Table 20 Plan 1a DTA data averaged over 3 trials.....	79
Table 21 Plan 1b DTA averaged over 3 trials	84

Table 22 DTA values per film per profiles for Plan 1a, in mm.....	102
Table 23 DTA values per film per profiles for Plan 1b, in mm.....	109

CHAPTER 1: INTRODUCTION AND BACKGROUND

1.1 Introduction

Lung cancer is a growing problem in the United States and the world in general. The American Cancer Society estimates that there will be 157,300 deaths (86,220 among men and 71,080 among women) in the United States from lung cancer in 2010, accounting for about 28% of all cancer related deaths. In addition, lung cancer occurs mainly in older people, with 2 out of 3 lung cancer diagnoses coming from people older than 65. (American Cancer Society 2010). Preservation of lung function is an important criterion in deciding treatment options for these patients. Proton therapy allows for superior dose distributions to be delivered to the targets, and it has been suggested that this will allow for more conformal treatment without increasing the dose to the surrounding tissue, while escalating the dose to the tumor site (A. R. Smith 2006). Because of these reasons, proton therapy is beginning to be a treatment option that many with lung cancer are becoming interested in receiving.

1.2 Statement of Problem

As of March 15, 2010, the Advanced Technology Consortium has given guidelines for the use of proton therapy in National Cancer Institute (NCI) sponsored cooperative clinical trials. Before patient trials can begin, any participating institute must be appropriately credentialed to perform proton radiation therapy. This credentialing procedure also requires a successful site visit from the Radiological Physics Center (RPC) which will include the usage of an anthropomorphic phantom. The mission of the RPC is to assure the NCI and cooperative groups that the institutions participating in the trial are delivering consistent and comparable doses of radiation accurately (D. Followill 2010) . To enable this assurance, the RPC utilizes mail-able heterogeneous phantoms which contain both radiochromic film and thermoluminescent dosimeters (TLD). As of this writing, there are no heterogeneous phantoms that have been commissioned to evaluate proton lung therapy. There is an existing RPC thorax phantom that is used to evaluate standard photon radiation therapy

and intensity modulated radiation therapy (IMRT). The purpose of this study is to discover if there is a method to modify the existing phantom in such a way that the phantom can be utilized to evaluate proton lung treatment procedures.

1.3 Proton Therapy

1.3.1 HISTORY

All atoms are composed of a nucleus surrounded by electrons. The particles that make up the nucleus are called nucleons, and can be either neutrons or protons. Proton particles were first proposed by Rutherford in 1919. Utilizing a natural radioactive source to provide energetic α particles, he bombarded nitrogen nuclei and showed that hydrogen nuclei were created, giving the name protons to these hydrogen nuclei. (Sundaresan 2001).

In 1946, Robert R. Wilson discussed the possibilities of using “fast protons.” These protons could be accelerated to energies above 125MeV and perhaps as high as 400MeV to treat patients, and as such could penetrate deep enough into a patient to reach any part of the body. A unique property of these protons is that as they pass through tissue, they follow a straight trajectory, allowing the proton beam to be used to treat a strictly localized region within the body. The total distance travelled by the protons along this trajectory is known as the range of the protons, and is determined by the amount of energy imparted to the protons by the accelerator. For protons accelerated to 140MeV, the energy imparted over the last centimeter is almost six times that at the surface. (Wilson 1946) This lower surface dose contributes to a tissue sparing effect on the entrance of the beam. The large deposit of energy at the the distal end of the proton’s range is known as the Bragg peak, and is immediately followed by a rapid decrease in dose, thus allowing a target to be treated with little to no exit dose.

In 1990, Loma Linda University Medical Center (LLUMC) became the first hospital based proton facility in the United States. (Slater, et al. 1992) Until this point, patients were previously treated in the US using high energy protons only as part of research protocols at facilities where the

machines were primarily used for research. The University of Texas M.D. Anderson Cancer Center (MDACC) Proton Therapy Center Houston (PTC-H) was commissioned in 2003 and opened for patient treatments in May 2006. The PTC-H has four treatment rooms; three utilizing rotating gantries, and one with two horizontal beam lines with capabilities for both large- and small-field treatments. The rotating gantries utilize passive scattering in two rooms, and the third contains a scanning pencil beam, that can eventually be utilized for intensity modulated proton treatments. (Smith, et al. 2003) This study was performed at the M. D. Anderson facility.

1.3.2 PROPERTIES OF PROTONS

The proton is an elementary particle having a positive charge that is equal yet opposite to that of an electron. The mass of the proton is 1.6×10^{-27} kg, which is approximately 1840 times larger than that of the mass of an electron. (Khan 2010)

1.3.3 PROPERTIES OF THE PROTON BEAM

Proton beams can be modified to manipulate the depth and shape of the beam. The energy loss properties of protons in matter can allow the range of the protons to be predicted based on the initial energy of the protons and the density of the materials through which they travel. As the protons pass through matter, they ionize the atoms that they encounter, gradually losing energy along the way predominately from inelastic collisions with electrons. The average rate of energy loss of a particle per unit path length in a specified medium is called the stopping power. The linear stopping power ($-dE/dx$) is the loss of energy ($-dE$) over some specified range (dx) and is measured in units of MeV/cm . The linear energy transfer (LET) of the particle is determined by removing the dependence on the density of the medium from stopping power tables by calculating ranges in units of g/cm^2 . (Khan 2010)

Stopping powers at higher energies, such as those used in proton therapy, are calculated according to Bethe's formula (ICRU 1993), where the mass collision stopping power is shown below:

$$(1/\rho)S_{col} = -(1/\rho)(dE/dx)_{el} = \frac{4\pi r_e^2 mc^2}{\beta^2} \frac{1}{u} \frac{Z}{A} z^2 L(\beta) \quad \text{Equation 1}$$

In the Bethe formula, r_e is the classical electron radius, mc^2 is the electron rest mass energy, μ is the atomic mass unit, β is the particle velocity in units of the velocity of light, Z is the atomic number, A is the relative atomic mass of the target atom, and z is the charge number of the projectile. $L(\beta)$ is the stopping number and it depends upon 3 factors:

1. The mean excitation energy of the medium, which quantifies the electron binding energy. The mean excitation potential is theoretically related to the orbital frequencies of electrons, and is usually determined from experimental data.
2. The contribution to stopping power from protons interacting with K-shell electrons lessens as the velocity of the projectile decreases. This is known as shell correction, and at low velocities, the assumption that electrons are stationary is not valid.
3. The density-effect correction, which accounts for the reduction of the stopping power due to the incident particle polarizing the medium through which it travels. (ICRU 1993)

The LET for charged particles, such as protons, increases at the end of the path forming what is known as the Bragg Peak. The depth, of the peaks can be modified in one of two ways: the protons can be accelerated to a different energy, higher or lower, shifting the peak further or closer respectively or by introducing a specified thickness of material or specific devices into the beam slowing the protons down thus reducing the range of the beam and possibly changing its shape.

1.3.4 MODIFICATION OF THE PROTON BEAM

The treatment gantry used for this research at the PTC-H delivers a passively scattered beamline, utilizing a double scattering technique. The protons are first accelerated by high RF voltage in the synchrotron. Once the selected beam energy is reached, the protons are extracted and

delivered to the treatment gantry through the beamline, via a series of proton spills. Once the spill of protons arrives at the nozzle of the treatment gantry it can then be modified. A diagram showing the path of the beam as it is modified is shown in Figure 1-1. (Sahoo, et al. 2008)

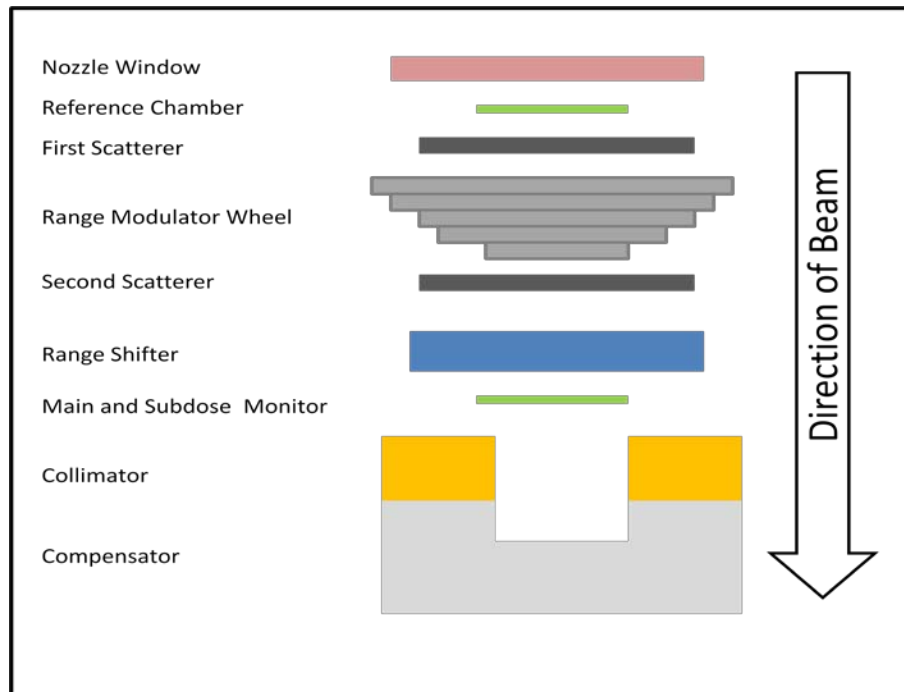


Figure 1.1 Schematic of nozzle components of the passively scattered beams lines at the PTC-H utilizing a double scattering technique

As the proton beam enters the nozzle, it can be shaped using filters and the range can be adjusted using a variety of modifiers. A double scattering technique allows the beam to be uniform in intensity over the beam's cross section. As the proton beam hits the first foil scatterer, the beam is laterally spread into a Gaussian shape across the beam's cross section. A second scatterer made of a high Z-material with a thickness that varies radially is placed further down the beam path, ensuring uniform proton energy, effectively flattening the intensity of the beam.

For proton therapy treatments, the peak of high dose deposition needs to be enlarged to conform to the target volume. This can be achieved using multiple independent peaks to cover the

proximal and distal sides of the target volume. When these peaks are combined they form a spread out Bragg peak (SOBP) in a technique called range modulation. The properties of the SOBP allow a level plateau of dose to be deposited at some depth in a patient with a much lower entrance exposure and almost no dose after the distal end of the peak. In contrast, a photon beam will exhibit a higher dose towards the end of its path, called the exit dose. This can be seen below in Figure 1-2.

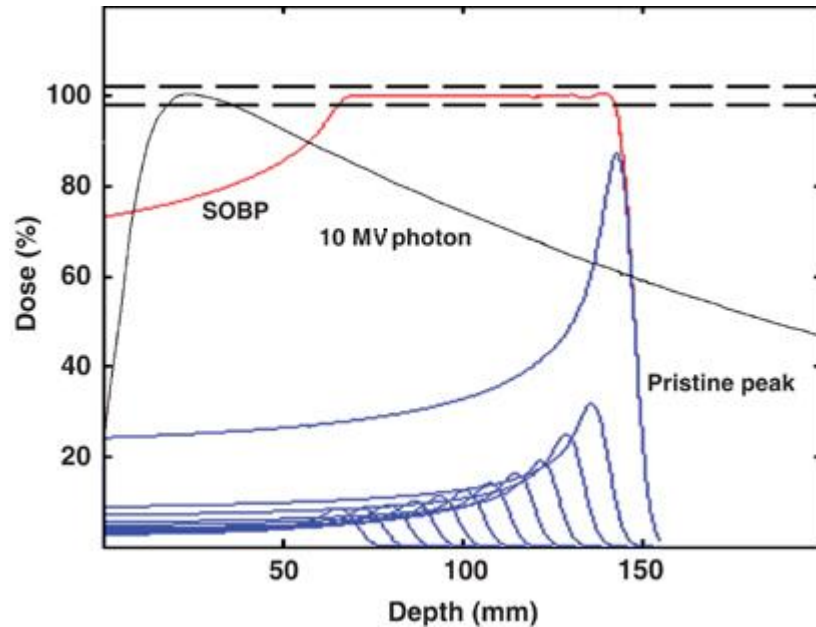


Figure 1.2 Comparison of Percent Depth Dose curves for 10 MV Photons (black line), a series of pristine Bragg peaks (blue lines), and a spread out Bragg peak (SOBP) (red lines).

The production of the SOBP is accomplished by using a called a range modulation wheel (RMW), first described by Robert Wilson. (Wilson 1946) The RMW has a series of steps machined into a specific material, dependent upon the desired energy of the proton beam, which can be rotated at high speeds. The effect of this rotation is that the RMW rapidly changes the range of the beam, effectively positioning the Bragg peaks at varying depths. These steps can be seen on a close up picture of part of a RMW shown in Figure 1-3.



Figure 1.3 Steps on an aluminum range modulation wheel (RMW) used at the PTC-H

The beam, can pass through a series of range shifters, if required, that reduce the range of the distal edge of the SOBP to achieve the desired depth. As the protons travel through the air and equipment that is located upstream of the patient, the protons suffer repeated elastic coulomb scattering.

The beam is collimated to cover the treatment area using custom designed bronze collimator plates, collectively referred to as the aperture. The thickness and number of plates is determined by the energy of the treatment beam. An example of one of these plates can be seen in Figure 1-4.

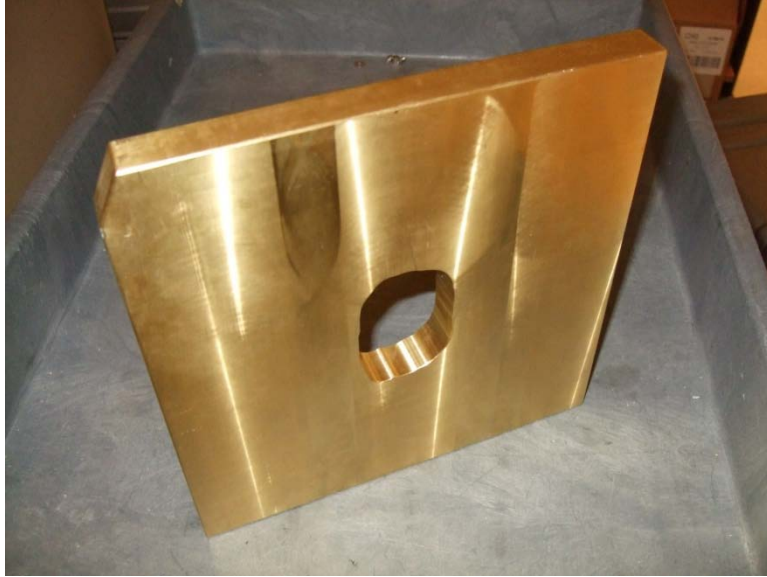


Figure 1.4 Bronze collimator plate

The beam is finally passed through a range compensator. The compensator acts to modify the range of the beam such that the distal end of the SOBP conforms to the distal surface of the target volume. (DeLaney and Kooy 2008) An example of a range compensator made from acrylic is shown below in Figure 1-5.



Figure 1.5 Acrylic range compensator

The cumulative effect of the scatterers, the RMW, the ranger shifters, the aperture and the compensators causes a deflection from the original particle direction and is known as multiple coulomb scattering (MCS). To minimize lateral dose fall-off of the beam caused by MCS in air after the beam has been effectively flattened, the snout should be manipulated as close to the patient as possible, thereby keeping the volume of air between the patient and the snout to a minimum. (DeLaney and Kooy 2008)

1.3.5 RANGE

The path length of protons determined by both their initial energy and their energy loss as they travel through the target material is known as the range of the proton. This range can be calculated using the continuous-slowing-down-approximation (CSDA) which allows a very close approximation to the average path length traveled by a charged particle as it slows down to rest. As the protons travel along this path, they will lose energy according to the stopping power of the material in which they are travelling. In this approximation, the rate of energy loss for all points along the track is assumed to be equal to the total stopping power. The CSDA range is obtained by integrating the reciprocal of the total stopping power with respect to energy, with units of distance travelled per unit energy loss. The individual protons path lengths differ slightly from each other as they do not lose the same amount of energy with each interaction. These energy-loss fluctuations of the energy imparted by individual protons due to multiple coulomb scatterings are called range straggling and neglected in the CSDA. (ICRU 1993)

Since the range of the proton is directly related to its energy, as the energy of the proton beam increases, then penetration depth also increases. A 125MeV proton has a range of 12cm in water and a 200MeV proton has a range of 27cm in water. (Wilson 1946) A proton beam composed of 160MeV protons has a mean range of 17cm in water. Due to the range straggling mentioned above, not all these protons stop at exactly 17cm. Because of the statistics of the multitude of

interactions involved, this can result in a approximately a 1% fluctuation of the range. (DeLaney and Kooy 2008)

1.3.6 RELATIVE BIOLOGICAL EFFECTIVENESS

As radiation from charged particles is absorbed in a biological material, ionization occurs and most of the lost energy is deposited to liberated electrons along the track of the charged particles. This distribution is characteristic of the particular type or energy of the radiation involved and is also dependent upon the energy of the particles. These different particles have different degrees of effectiveness when irradiating tissues in biological systems. The concept of relative biological effectiveness (RBE) was developed to compare these radiation sources and describes the amount of dose from a radiation source that is needed to produce the same biological effect as a known standard source of radiation. (Johns and Cunningham 1983)

$$RBE = \frac{\text{Dose from Standard Source to Produce Biological Effect}}{\text{Dose from Test Source to Produce Biological Effect}} \quad \text{Equation 2}$$

Recently for proton therapy, the accepted value of RBE has been under scrutiny, based on whether the calculations were performed on tissues or tissue substitutes related to the α/β ratio of the materials involved. For higher energy protons, the ionization track is wide, causing a low LET where the ionization is widely dispersed allowing for tissue repair. As the energy decreases, the track narrows, and the LET increases as the ionizations happen much closer together. However, the RBE is not consistent across a pristine Bragg Peak, where the ionization at the very end of the distal range is mixed because of range straggling, mentioned above. When multiple peaks are overlapped, forming an SOBP, there is a leveling of the RBE, with an increase in RBE occurring towards the distal end of the SOBP, most likely due to an increase of the LET. Due to this increase in the RBE and LET, the penetration of the beam is actually extended by a few

millimeters. (Paganetti, et al. 2002) For our study, the commonly accepted RBE value of 1.1 that was determined in the clinical setting using in-vivo laboratory studies with a standard error of 0.01 will be utilized.

1.4 New Insert

1.4.1 EXISTING THORAX PHANTOM

The RPC currently uses several different anthropomorphic quality assurance phantoms used for site credentialing purposes for sites that participate in NCI sponsored clinical trials. The RPC thorax phantom was initially created for verification of stereotactic body radiation therapy (SBRT) procedures for lung tumors. This phantom was built to simulate actual patient anatomy and when used in a photon beam, the reproducibility of the dose delivery to the target was 0.5% and radiation field localization was less than 2.5mm. (Followill, et al. 2007) The RPC Thorax phantom consists of a main phantom body (referred to from here on as the phantom shell) that is filled with water and has materials designed to replicate different organs and a removable imaging/dosimetry insert. The phantom shell is shown below in Figure 1-6, where the insert's location can be seen on the right.



Figure 1.6 RPC Thorax Phantom – phantom shell

The thorax phantom is intended not just to measure results of the radiation treatment, but the entire treatment procedure from participating institutions, from CT through planning to treatment. Accuracy in simulation and treatment planning are just as critical as accuracy in set-up and treatment of the phantom. Since the phantom is anthropomorphic and mimics the organs and shape of a human torso, it offers a realistic simulation and requires a patient equivalent dose calculation to be performed. The original imaging/dosimetry insert is comprised of cork, as is the remaining lung material in the phantom and is shown below in Figure 1-7 The dosimetry insert also doubles as an imaging insert and allows the phantom to be shipped “fully loaded” with film and TLD, eliminating possible errors that might be incurred by assembly by non experienced personnel. The film contained in the insert verifies the accuracy of the CT simulation and treatment planning systems. The TLD

provides verification of the physical dose distribution for the treatment delivery. (Followill, et al. 2007)

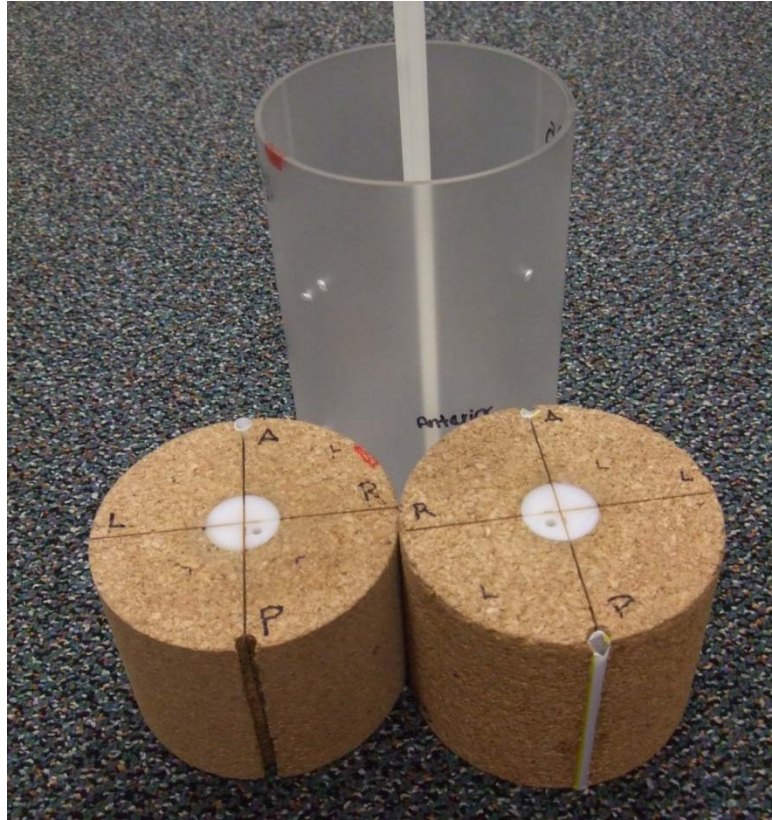


Figure 1.7 Disassembled, original cork lung imaging/dosimetry insert

It was decided at the start of this project that usage of the thorax phantom as is, was not possible due to two main construction issues: lung equivalency of the insert material and air gaps around the radiochromic film.

1.4.2 LUNG EQUIVALENT MATERIAL

Several lung equivalent materials were evaluated for usage in a proton beam. The relative linear stopping power (RLSP) is defined as the linear stopping power of the phantom material relative to water. The RLSP for the phantom material needs to be close to that of the corresponding standard human lung tissue for that material to be considered lung equivalent. Several materials

including Jelotong wood, and vendor specific lung materials such as The Phantom Laboratory (TPL) Lung material and Radiation Measurements Incorporated (RMI) Lung material have RLSP's from 0.303 at 135 MeV to 0.404 at 225 MeV. (Moyers, et al. 2010) The RPC thorax phantom was designed using cork as the lung equivalent material. Cork is not easily characterized in a proton beam, due to an inhomogeneity of the material caused by the many large air pockets contained within the structure. Balsa wood contains micro air pockets within the grain that could potentially cause fewer issues with distal edge degradation of the SOBP when compared to cork.

1.4.3 FILM AND AIR GAPS IN CURRENT INSERT

Another issue with cork is the difficulty with machining tight tolerances in the insert itself. The current insert has slots that house the radiochromic film, as well as multiple air channels created from the pin prick straws and the closure screws

In the current insert there are gaps alongside the film that allow the film to slide into the insert. Depending upon the orientation of the film and the beams selected for treatment these gaps along the film can introduce errors. Film was placed inside the imaging/dosimetry insert in 3 planes: Axial, Coronal, and Sagittal, and compressed to remove air gaps. In a study performed in 2005 using GAFChromic® MD-55 film, film gap and response versus orientation was explored. For films aligned parallel to the beam, an air gap equivalent to one thickness (0.26mm) of GAFChromic® film showed an 18% over response of the film. When that gap was increased to 3 times the thickness of the film (0.78mm), the over response was 22%. When the film was perpendicular to the beam or no air gap was present, the difference in response was 3% or less. (Nerbun 2005) This result was verified using EBT film by Zhao and Das, where they state that serious artifacts and errors are present in the depth dose distributions displayed on film, and that the dose errors increase as the gap increases. (Zhao and Das 2010)

1.5 Hypothesis and Specific Aims

The existing RPC heterogeneous thorax phantom can be modified to assess lung tumor proton beam therapy procedures involving patient simulation, treatment planning, and treatment delivery confirming agreement between the measured dose and calculated dose within 5%/3mm with a reproducibility of 5%.

Selection of phantom materials and design plans were created allowing the existing phantom to be utilized in a proton beam. The phantom was then simulated on a CT scanner at the PTC-H, planned and treated using clinical techniques to emulate a lung tumor treatment with proton therapy. The agreement criteria in the hypothesis were then tested through the completion of the specific aims listed below. Throughout the entire process, modifications were made and the specific aims were tested and verified. The specific aims to complete this research were:

- 1) Determine the equivalency of phantom lung material to the patient anatomy counterpart, and modify the existing thorax phantom/insert correspondingly.
- 2) Determine the LET dependence of radiochromic film for parallel and perpendicular orientation in water.
- 3) Image the modified insert and thorax phantom to create clinically relevant treatment plans, and irradiate the phantom with these treatment plans.
- 4) Measure the delivered dose distribution and the dose to specific points within the irradiated thorax phantom and compare the calculated and measured doses and dose distributions to determine the deviations and reproducibility.

CHAPTER 2: MATERIALS AND METHODS

2.1 Phantom Design and Construction

It was decided to base the lung phantom for protons on the existing RPC Thorax phantom. The only change would be to re-design a new dosimetry/imaging insert that would be appropriate for use in a proton beam. The material selected would need to be lung density equivalent. Based on long accepted research lung density can range from 0.348 g/cm³ to 0.193 g/cm³ depending on age and whether or not the lung tissue is normal or abnormal. (Van Dyk, Keane and Rider 1982) The average density of the target material was decided to be approximately 0.300 g/cm³, agreeing with the materials evaluated in the Moyers paper, where the average density was in the 0.300-0.400 g/cm³ range. (Moyers, et al. 2010)

Multiple patient images were examined, including both normal and abnormal lung tissue to determine a range of acceptable Hounsfield Units (HU) for the phantom material. The calculation of HU is shown below:

$$HU = \left(\frac{\mu_{\text{Material}} - \mu_{\text{Water}}}{\mu_{\text{Water}}} \right) \times 1000 \quad \text{Equation 3}$$

Based on multiple patient images such as the ones shown in Figure 2-1, it was determined that the range of acceptable HU's was between -300 and -900 depending upon the levels of inflation and density of the lungs where the ROI's were drawn.

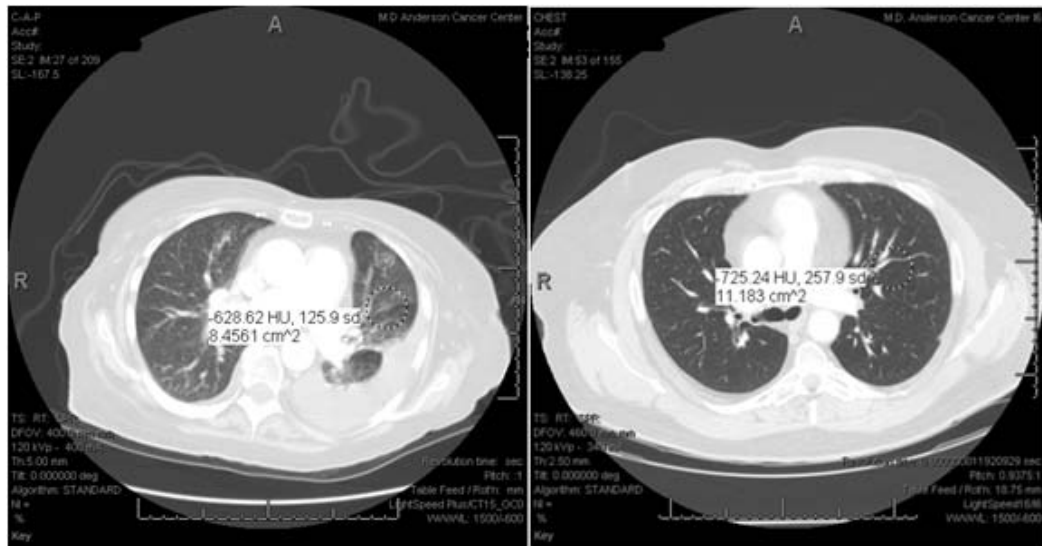


Figure 2.1 Random sample of lung patient's CT images

2.1.1 LUNG INSERT MATERIAL

To find an equivalent lung material, the material had to have a density similar to the density of average lung tissue, and also have a HU number comparable to the average of patient lung tissue. Several materials were researched, and based on cost and ability to be machined to tight tolerances, extra heavy balsa wood was selected. Extra heavy balsa is specific type of balsa with a density over 20 lbs./ft³. Multiple blocks of balsa stock were ordered, measured and weighed to calculate the average density of the sample. The density range of the sample was from 0.300 to 0.340 g/cm³, which was deemed acceptable. The samples were then suspended in air and CT's were performed on the blocks using a standard chest protocol on a GE Lightspeed X/Qi CT scanner (GE Healthcare , Waukesha, WI) and regions of interest (ROIs) were measured across the different blocks to determine the HU numbers of the samples. A sample image is shown below in Figure 2-2.

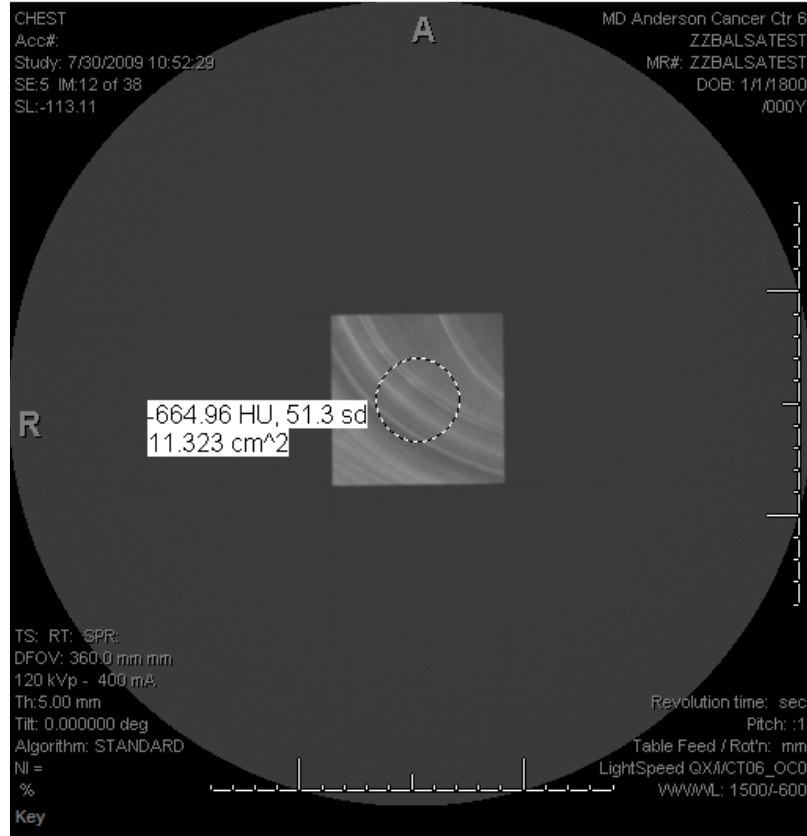


Figure 2.2 CT Image of balsa block suspended in air

The HU numbers of the sample ranged from -590 to -790 with a mean of -670, which places the material right in the middle of the range of patient numbers discussed in the previous section. The balsa was then stored in a climate controlled office with temperature set to 72 degrees Fahrenheit to maintain steady moisture content of the wood.

2.2 Material Relative Linear Stopping Power

As discussed in Section 1.3.5, protons will lose energy according to the stopping power of the material in which they are travelling. This loss of energy is also related to the initial energy and the relative linear stopping power (RLSP) of the materials in the beam's path. Depth dose curves are characterized using a water tank and parallel plate chamber for every energy, SOBP, and range combination available for each snout size. When a material of different RLSP than water is inserted into the tank displacing an equal volume of water, the distal edge of the Bragg peak is shifted either

shallower, for materials of RLSP, or deeper, for materials of lower RLSP. The materials for the phantom shell were initially designed for usage in photon beams for SBRT, and were characterized in proton beams when the RPC commissioned their Pelvis Phantom. (Grant 2010) Two additional materials needed to have their RLSP's measured for this study: cork and balsa.

2.2.1 DEPTH DOSE SCANNING

The RPC possesses a portable water tank phantom and scanner that is used for remote site visits. This scanner was used to measure the RLSP of both the cork and balsa samples. The primary scanning ion chamber used with this scanner was an Exradin P11 parallel plate chamber (Standard Imaging, Middleton, WI). The reference ion chamber, placed in from of the window was an Exradin A12 thimble chamber (Standard Imaging, Middleton, WI). The tank was filled with water to a level higher than the mylar entrance window of the tank. The proton treatment gantry was then set to 270 degrees with a source to axis distance of 270 cm to the inside of the mylar window.

A reference curve of the beam in water was acquired to be used as a baseline for calculating the RLSP. A sample of cork that was used to construct the insert was measured with calipers and then taped to the front of the window outside of the water tank, and a depth dose curve was acquired. The same beam conditions were used for scanning the materials as were used for the reference curve. This procedure was then repeated for the balsa sample, shown in Figure 2-3 .

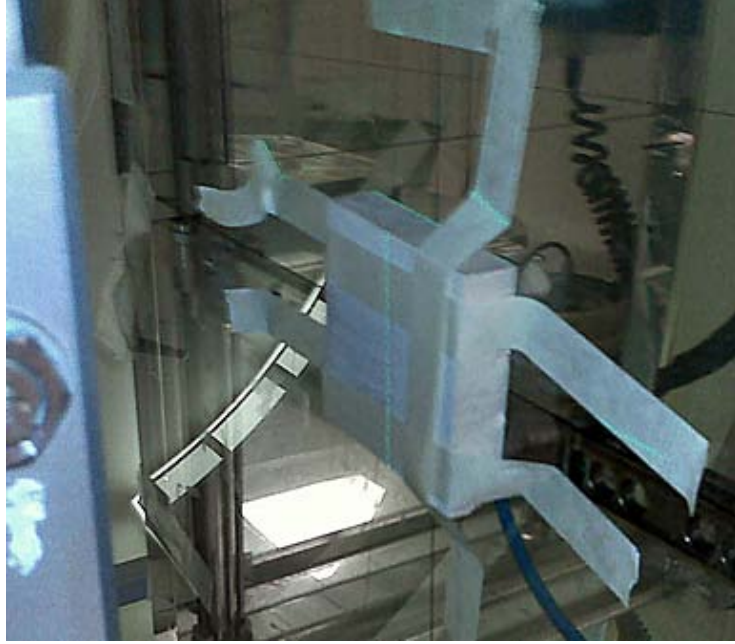


Figure 2.3 Balsa sample being scanned for RLSP analysis at PTC-H

2.2.2 STOPPING POWER ANALYSIS

Using the average of 5 maximum points located at the beginning of the SOBP, the individual curves for both the balsa and the cork were each normalized to to the reference depth dose curve. To determine the stopping power, the difference between the reference curve and each material curve at the distal 90% points was then calculated. The formula to calculate the RLSP from this data was taken from the Moyer's paper. (Moyers, et al. 2010) The material was attached to the front of the water tank, not displacing any water, as both the cork and balsa are hygroscopic and would absorb water if placed in the tank. The RLSP equation is shown below, where $R_{90,W}$ is the distance to the distal 90% point on the reference curve, $R_{90,m}$ is the distance to the 90% point on the material curve, and t_m is the thickness of the material.

$$RLSP = \frac{(R_{90,W} - R_{90,m})}{t_m} \quad \text{Equation 4}$$

2.3 Construction

The imaging/dosimetry insert was redesigned to utilize extra heavy balsa and to minimize air gaps. The new insert design was based on a series of tapered wedges that fit into a tapered ring, a cross section is shown below in Figure 2-4.

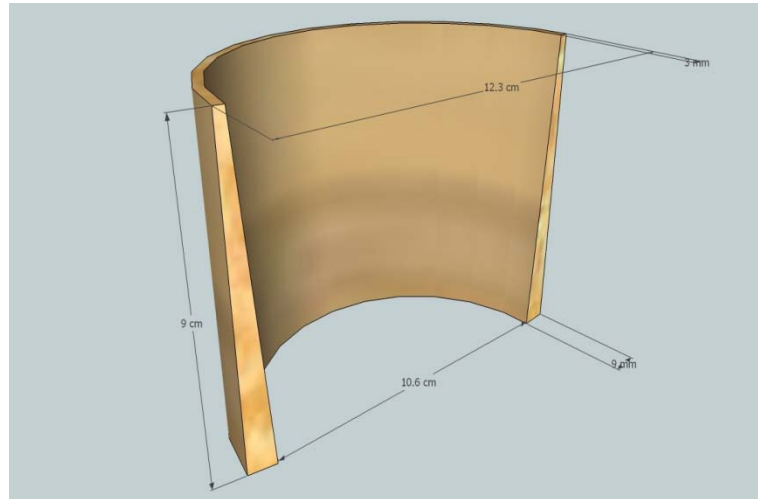


Figure 2.4 Cross section of tapered outer balsa ring

Two sets of these rings and wedges were utilized; one for each the superior and inferior sections of the insert, housing the sagittal and coronal films, and when compressed into the outer hi-impact polystyrene outer housing, straddle the central axial film slice. Located at the center of the insert, cut into 8 quarter wedges is the hi-impact polystyrene insert that mimics the tumor and is assigned the Gross Tumor Volume (GTV) when treatment planned. The tumor inserts and film planes can be seen in Figure 2-5.

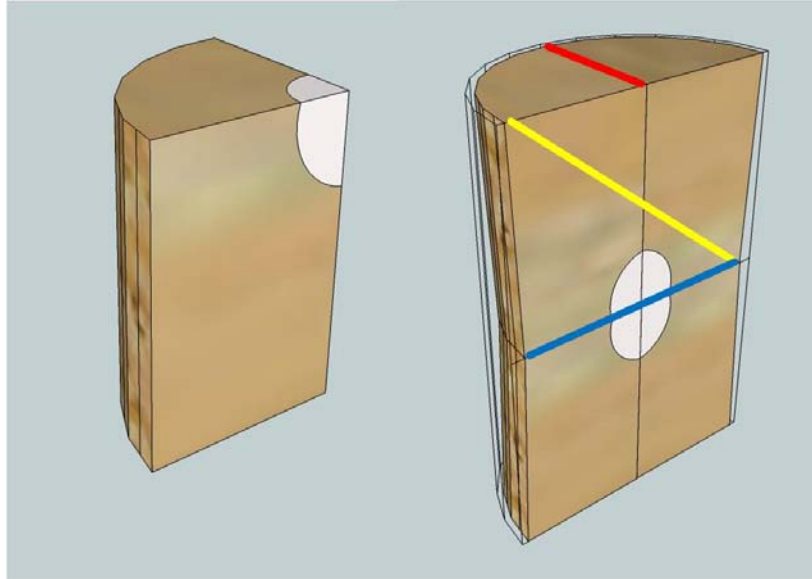


Figure 2.5 Schematic of an individual wedge (left), and half of the wedges shown stacked assembled in a wireframe that represents the outer tapered balsa ring (right). The tumor insert is shown in white. The colored lines depict the film plane: blue – axial, red – sagittal, yellow – coronal.

The outer housing of the insert has removable end caps that screw closed providing compression that laterally tightens all of the wedges together effectively removing the air gap around the films. Before machining, all of the individual balsa blocks were imaged with a CT scanner and the only blocks that were close in HU were utilized. After construction, the parts were then assembled and imaged again with a CT scanner using the smallest field of view (FOV) possible to increase resolution, to verify compression. All of the parts for the insert are shown below in Figure 2-6.



Figure 2.6 Balsa imaging/dosimetry insert. Assembled inferior wedge and ring shown on the right. The sleeve and superior endcap are shown in the back. The individual superior wedges and ring are shown in front.

2.4 Treatment Planning

The dosimetry/imaging insert was assembled with dummy film and TLD to simulate how the insert will be loaded under treatment. Since the purpose of the RPC lung phantom is to evaluate the entire treatment process, care was taken to treat the phantom as a patient would be imaged and treated. The outer phantom shell was filled with water, and rocked to remove air bubbles. The balsa insert was aligned in the proper orientation and inserted into the outer shell where tape was placed to keep it from moving.. The assembled phantom was imaged at the PTC-H on an in-house GE Lightspeed RT16 Computed Tomography scanner (GE Healthcare , Waukesha, WI) calibrated for proton treatment . The phantom was placed on the CT table, and after careful alignment of the phantom using multiple scout images, the outer shell was marked at the localization laser points with pen marks and plastic fiducial BBs were placed at those marks. The BBs were used to verify that the phantom was aligned to the set-up lasers as all of the BBs appeared in the same plane. The BBs

would later be contoured out when planning the treatment, so as not to add additional material to the path of the beam that might affect beam delivery. The protocol used was the free breathing lung prescription that is utilized on patients, yielding 2.5mm image slices. Multiple plans were developed and evaluated. Plan 1a and Plan 3 were selected, and will be referred to in the remaining portions of the paper as Plan 1a and Plan 1b, respectively, to eliminate confusion.

2.4.1 ECLIPSE

The treatment planning system (TPS) utilized by the PTC-H to create patient treatment plans is Eclipse (Varian Medical Systems, Palo Alto, CA). The TPS utilizes a calibration curve that converts the HU from a calibrated CT scanner to relative linear stopping powers that match those of human tissue. The CT scan of the lung phantom was uploaded to Eclipse to determine the exact HU for each material in the phantom. Profiles were drawn across each balsa wedge, 10 sample points were taken for each and averaged together, yielding the HU for balsa. The same was repeated for a section of cork in the anterior lung segment on the patient left side of the phantom.

2.4.2 STOPPING POWER COMPARISON

Once the HU values of the materials were determined, they were plotted against the measured RLSPs as mentioned in section 2.2.2 Stopping Power analysis. These values were then plotted on the TPS calibration curve, along with points for PVC, Hi-impact (HI) Polystyrene, and Acrylic- PMMA. Traditionally, multiple organ samples were measured to set the points for bone, soft tissue, fat, brain matter, etc. Because the ex-vivo lung tissue samples could not be inflated, the value for lung tissue had to be estimated, resulting in possible discrepancies of lung tissue density. The stopping power curve at densities less than water was determined by drawing a straight line from the HU of air (-1000 HU) to the HU of water (0 HU). The RLSP comparisons were then made to validate the new lung insert's usage in proton therapy, and possibly predict differences between treatment plans based on the calibrated curve, and by using points based on measured material specific RLSP.

2.4.3 *TREATMENT PLAN 1A*

The first of two treatment plans to be developed was based on using two orthogonal beams set at 0 and 90 degrees, entering the anterior and patient left side of the phantom. It had been noted that delivering dose to film in a phantom where the film is aligned in the parallel orientation can introduce errors, possibly due to the protons streaming down the film (which has a different RLSP than the surrounding material) or possibly due to air gaps surrounding the film. It was decided to develop a plan this way so that the results could be compared with a second plan where the beams would not be parallel to the films. To insure that the beams would be parallel to all of the films, the treatment couch was set to a zero degree couch kick, so that the axial films would also be parallel to the incident beams. The outer shell was contoured to remove the BBs as mentioned at the beginning of Section 2.4. All of the remaining structures in the phantom, including the heart, spine, and right lung, were then contoured. The two orthogonal beams as placed, were termed the initial beams, and initially formed a tight box around the tumor, or GTV. The range and SOBPs were modified to ensure smooth coverage on the distal end of the GTV. Since the tumor was not moving, no margins were added and the GTV was prescribed to receive 100% of the dose. Also, when treating patients we modify both the compensator and the collimator to ensure complete coverage of the GTV. This is accomplished by smearing the milling steps defining the distal edge of the tumor site by 10mm and expanding the treatment aperture by 10mm, thereby accounting for any unobserved motion or set up errors that might cause the tumor to be slightly off target. As the purpose of the phantom is to verify the treatment planning of a patient, the range compensator was therefore smeared by 6mm, also the aperture was expanded by 10mm. (DeLaney and Kooy 2008) This expansion results in a dose overshoot on the lateral edges of the treatment field and can be seen in Figure 2-7. The TPS then designed the correct apertures and compensators for both fields, and this information was transferred to the machine shop at the PTC-H for construction.

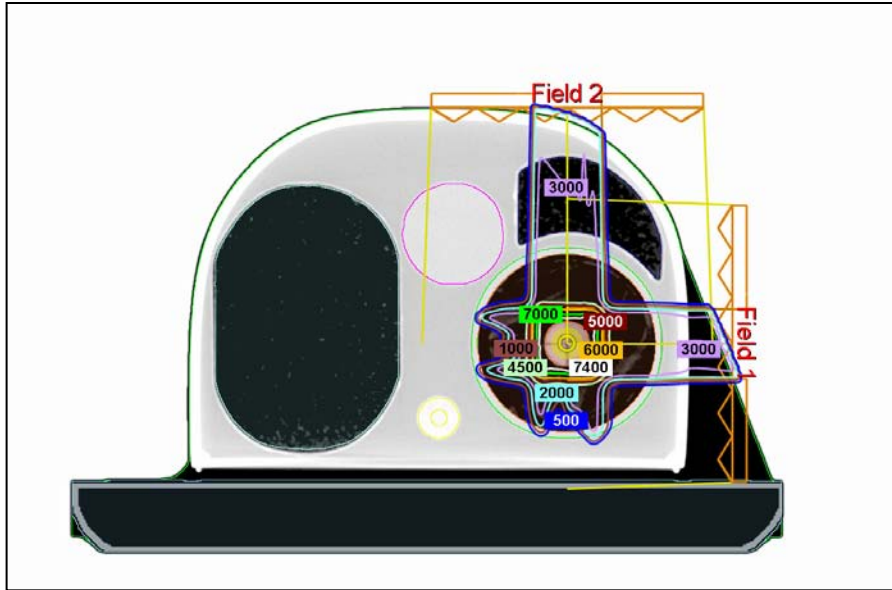


Figure 2.7 Axial view of treatment plan 1A at isocenter. Both apertures for fields 1 and 2 are shown. Notice the overshoot "horns" on the lateral edges of each field.

Upon approval of the plan, the dose was scaled back from 37 fractions at 200 cGy, giving a total dose of 7400cGy, to 200 cGy at the GTV. This would test the treatment system's ability to deliver a single fraction to the phantom. Three fractions would be utilized to yield a combined dose 600 cGy. The beam parameters for plan 1a are shown in Table 1.

	Field 1	Field 2
Nominal Energy	140 MeV	160 MeV
SAD	270 cm	270 cm
Snout Size	18 cm x 18 cm	18 cm x 18 cm
Gantry Angle	90	0
Couch Angle	0	0
Planned Distal Target Distance	8.1 cm	11.9 cm
Nominal SOBP Width	5.0 cm	5.0 cm
Snout Position	30.0 cm	30.0 cm
Range Modulator	RM 85	RM 84
Range (Distal 90%)	10.2 cm	13.4 cm
Range Shifter	RS 22	RS 16
Shifted distance	2.1 cm	1.5 cm
GTV dose	101.0 cGy	99.0 cGy

Table 1 Plan 1a Treatment Parameters. Prescribed dose is 200 cGy.

2.4.4 TREATMENT PLAN 1B

For the next treatment plan, the gantry angles and couch angles were adjusted to eliminate the proton streaming issues. It has been reported that tilt angles of as little as 2 degrees (Zhao and Das 2010) can reduce this effect; however the effect is still present on the distal end of the SOBP. Our study utilized a 10 degree tilt angle, with gantry angles of 10 and 80 degrees, comparable to a technique in a study that irradiated a film insert that was located near a critical structure (Vatnitsky, et al. 1997). The couch was then rotated -15 degrees to 345 degrees. The two initial beams, as placed, formed a tight diamond-shaped dose distribution around GTV. The range and SOBP were modified to ensure smooth coverage on the distal end of the GTV, and then the compensator and

apertures were modified and smeared the same way as in plan 1a. The beam parameters are shown below in Table 2 and the placed field is shown in Figure 2-8 .

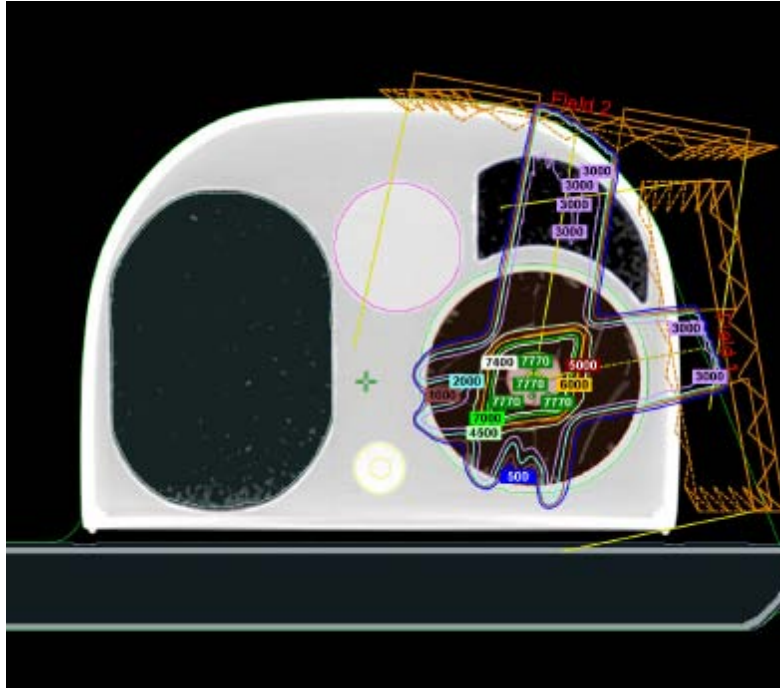


Figure 2.8 Axial view of Plan 1b Note the fields have been angles to 10 and 80 degrees. Also note that the overshoot "horns" on the lateral edges of each field.

	Field 1	Field 2
Nominal Energy	140 MeV	160 MeV
SAD	270 cm	270 cm
Snout Size	18 cm x 18 cm	18 cm x 18 cm
Gantry Angle	80	10
Couch Angle	345	345
Planned Distal Target Distance	8.1 cm	11.0 cm
Nominal SOBP Width	5.0 cm	5.0 cm
Snout Position	30.0 cm	30.0 cm
Range Modulator	RM 85	RM 84
Range (Distal 90%)	10.2	13.4
Range Shifter	RS 22	RS 25
Shifted distance	2.1 cm	2.4 cm
Tumor dose	102.4 cGy	97.6 cGy

Table 2 Plan 1b Treatment Parameters. Prescribed dose is 200 cGy.

2.5 Dosimeters

Two types of dosimeters were used in to evaluate the irradiation inside the phantom: thermoluminescent dosimeters TLD (Quantaflux, LLC, Dayton, Ohio) and GAFChromic® EBT2 radiochromic film (International Specialty Products, Wayne, NJ). The TLD allows for the absolute dose to be measured at two specific sites in the tumor site in the lung insert. The film dose, once calibrations are applied, can then be scaled to this point, thereby allowing for two dimensional (2D) profiles to be drawn in each film plane: axial, sagittal, and coronal.

2.5.1 TLD

Thermoluminescent dosimeters (TLDs) utilize trapping centers of varying energies to capture electrons that are released by incident radiation from the valence band to the conduction band. (Knoll 2000) The TLDs can then be read by exposing the dosimeter to heat, thereby releasing the trapped electrons back to the valence band in turn releasing visible light. This light can then be read by a photomultiplier tube (PMT), which amplifies and converts the input thermoluminescent (TL) signal to a measurable electronic reading. This signal can then be compared to the temperature at the time of the light emission and an output glow curve is produced. This glow curve contains multiple peaks that correspond to the different energy traps in the TLD. The lower energy traps are unreliable as they tend to not be stable at room temperature, releasing their electrons back to the valence band using spontaneous recombination. By waiting at least 10 days to read out the TLD, most of these traps have already lost their TL signal, and the remaining low energy traps are relieved of their electrons by preheating the crystal before the actual reading takes place. The integrated TL signal under the remaining glow curve directly corresponds to the number of photons released. This reading, along with several correction factors will give the total absorbed dose delivered to the TLD. This is shown below in Equation 5.

$$D = T \times K_L \times K_E \times K_F \times S \quad \text{Equation 5}$$

The absorbed dose, D, is calculated by adjusting T, which is the total TL signal divided by the mass of the powder, using several factors: K_L , the linearity correction; K_E , the energy correction; K_F , the fading correction; and S, the sensitivity of the system. The readout of the TLD was performed by the RPC. Since these K factors are consistent for each batch of TLD, they are only measured and calculated during the commissioning of the batch, in this case Batch 07.

The K factors are determined using a variety of methods. The linearity correction factor, K_L , accounts for the supra-linearity response of each individual TLD batch over the range of 1-40Gy. To acquire this factor, several TLD capsules are irradiated over the designated range, and a least squares

fit is applied to reading vs. dose curve. This calculation is shown below, using batch specific quadratic parameters a,b, and c in Equation 6.

$$K_L = ax^2 + bx + c \quad \text{Equation 6}$$

The energy correction factor, K_E , is derived by comparing the dose response of the TLD in a specific beam to the known response of TLD in a ^{60}Co beam for the same absorbed dose. The fading correction factor, K_F , is calculated using the equation shown below, in Equation 7, where the parameters a, b, c, d and N are all batch specific, and X is the time (in days) from irradiation.

$$K_F = N / (a \times e^{-bX} + c \times e^{-dX}) \quad \text{Equation 7}$$

The system sensitivity, S, can vary from reading session to reading session, and as such is calculated at every reading session. These variations can be caused by heater characteristics, reflectivity of the heated planchette, and subtle variation in the readout electronics. (Kirby, Hanson and Johnston 1992) The system sensitivity correction factor, S, is shown below in Equation 8, and utilizes the previously discussed correction factors. The system sensitivity correction factor is calculated using standard doses (“standards”) that are read out at the beginning and end of each session. And based on the time point of each reading taken between them, the individual reading system sensitivity can be interpolated.

$$S = D_{\text{standard}} / (T_{\text{standard}} \times K_{F \text{ standard}} \times K_{L \text{ standard}}) \quad \text{Equation 8}$$

The TLD used as for this experiment were capsules containing lithium fluoride (LiF) TLD-100 powder. The capsules utilized were double loaded, which means that there are two separate “loads” or aliquots of TLD powder contained in the capsule, each containing approximately 22 mg of powder. These double loads allow for multiple measurements to be taken to improve the readout statistics of the final dose measurements.

2.5.2 GAFCHROMIC® FILM

Radiochromic film was used to measure the relative dose distributions of the treatment plans. Film is an effective way to gather spatial information in two dimensions, and when calibrated and dose adjusted using an absolute dosimeter, such as TLD, the film can give an accurate description of the dose distribution. This is accomplished by evaluating the optical density of the film, which changes by polymerization within the active layer of the film as a function of the dosage received. The radiochromic film used in this study was GAFChromic EBT2 Dosimetry Film (lot A06221004, expiration 4343), in the 8" x 10" size.. A schematic of the film is shown below in Figure 2-9. (International Specialty Products 2009)

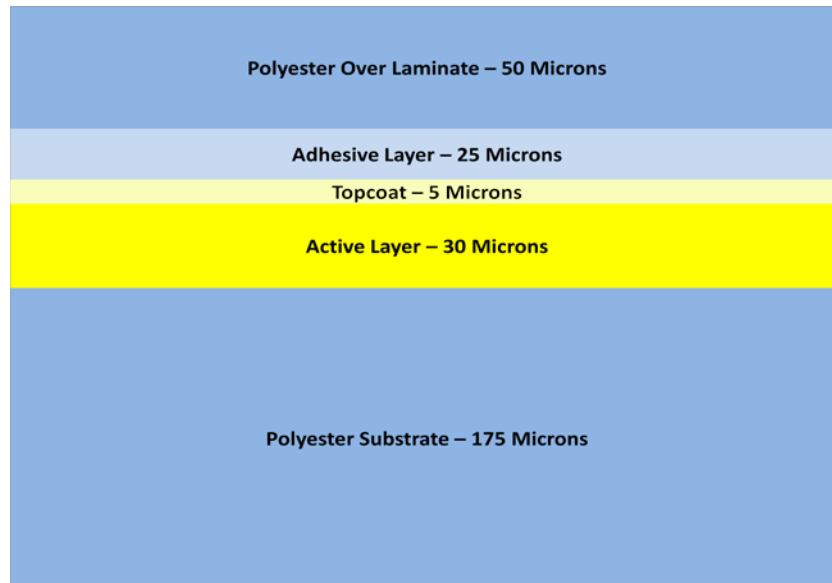


Figure 2.9 Configuration of GAFChromic® EBT2 film

2.5.2.1 FILM CALIBRATION

The film was calibrated according to RPC protocol. To reduce uncertainty in our measurements, three readings were taken for each irradiation level. To ensure that all film samples could be taken from the same piece of film, thereby removing another source of variation, 3 cm by 6cm sized pieces of film were utilized. These calibration films were then individually placed at 1.5 cm depth of solid water (d_{\max} for 6MV photons) utilizing a Varian Clinac 600C (Varian Medical

Systems, Palo Alto, CA), . An additional 9cm of solid water was placed beneath the calibration films on a leveling acrylic block to act as backscatter. The calibration films were progressively irradiated from 50 monitor units to 1350 monitor units in a 20 cm by 20 cm field.

The individual films were then scanned using the RPC's film scanner, a CCD100 Microdensitometer by the Photoelectron Corporation (North Billerica, MA). The scanned films were exported as X bit .FIT files and analyzed with ImageJ, an open source image analysis software developed by the Research Services Branch of the NIH in Bethesda, MA.

For each irradiation level, the individual films were analyzed for the mean optical density over an area approximately 90% of the size of the film to reduce fluctuations caused by possible separation of the film along the cut edges. This was repeated for each film and the average mean optical density was recorded for each irradiation level. Since the films were located at Dmax, no percent depth dose correction was applied, and the only correction was by multiplying the monitor units by the output factor of a 20 cm x 20cm field.

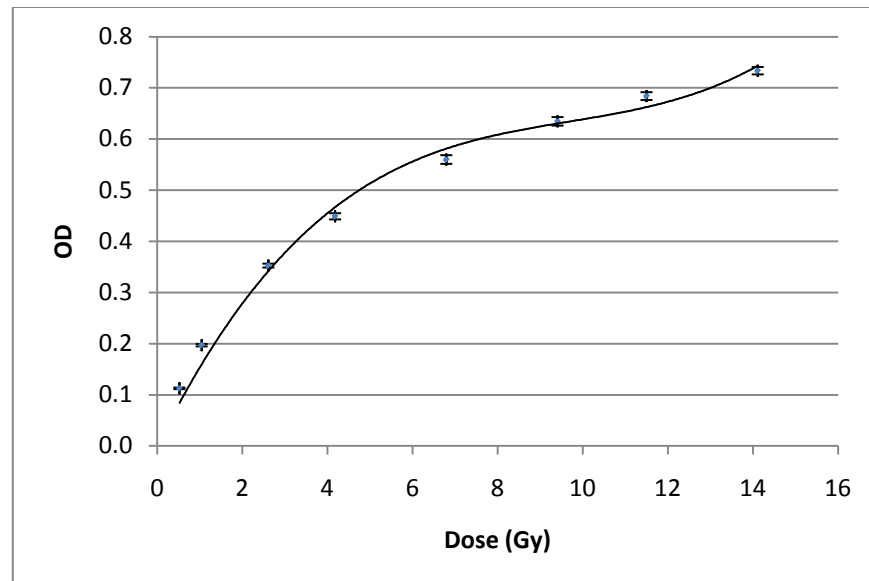


Figure 2.10 Dose response curve of lot# A06221004 GAFChromic EBT2 film; the chart plots the optical density against the dose.

To convert the OD of the film to dose, a correction supplied by the inverse of the above curve was generated. Per RPC protocols a 3rd order polynomial was generated with an R²= 0.997, and is shown below:

$$Dose(OD) = 38.855(OD^3) - 10.813(OD^2) + 6.1518(OD) \quad \textbf{Equation 9}$$

This calculation was then input into the CERR and utilized to measure the relative dose distribution. These measured distributions were then corrected by the TLD dose and compared to the dose maps generated by the Eclipse treatment planning system.

2.5.2.2 LET DEPENDENCE OF GAFCHROMIC EBT2 FILM

When looking at an SOBP, the distal-most portion of the dose plateau region contains mostly high LET particles, while the more proximal portion of the region contains higher energy, lower LET particles. This increase in LET, usually seen in the distal one third of the SOBP, is also directly related to an increase in RBE, which is what makes particle beam therapy so effective at cell killing. (DeLaney and Kooy 2008)

2.5.2.2.1 Film Response

In researching how film responds when used for proton dosimetry, almost every article shows an under-response in the area under the Bragg peak. Low energy (less than 6.7MeV) proton beam studies were performed on standard EBT film and show that there is an LET quenching effect that can be seen in film dosimetry. Two purposed reasons for this are suggested: LET quenching is purely due to the single hit detector nature of radiochromic films, or that the quenching of free radicals in the film is responsible for this underperformance. (Kirby, et al. 2010)

2.5.2.2.2 Evaluating film orientation

There are two ways to orient the film when evaluating the LET dependence of the film: parallel or perpendicular. In a recent study, it was shown that when the film is placed in a parallel orientation to the beam a 9-18% dose reduction can be seen in the film at the Bragg peak region. When the film is placed perpendicular to the beam, the issue of air gaps introducing artifacts and

response changes becomes apparent. To eliminate these air gaps, the film can be tilted up to 10 degrees. (Zhao and Das 2010)

To eliminate the effect of air gaps, samples of film were irradiated while submersed in a water tank. These OD values, once plotted were compared to the ion chamber central axis PDD data for the exact specific gantry and beam parameters. A bracket was designed and constructed that could allow for rotation of 90 degrees, and could be mounted to the stepper motors of the RPC travelling water tank, discussed in section 2.2.1. This bracket is shown with a piece of film prior to irradiation in Figure 2-11.

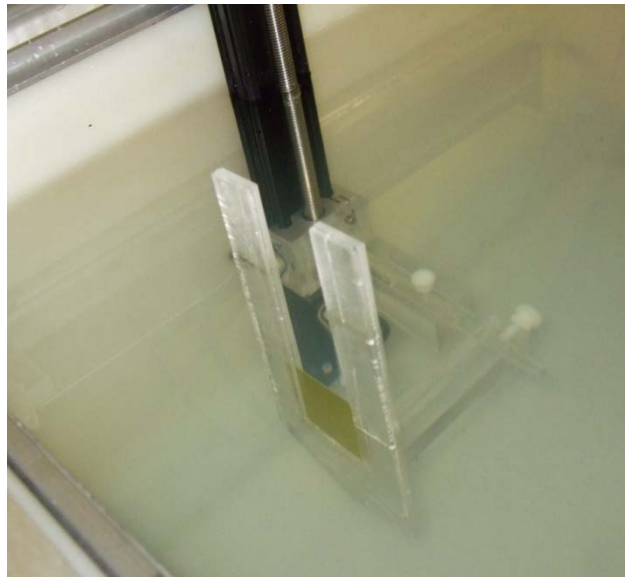


Figure 2.11 GAFChromic film in perpendicular orientation in the RPC portable water tank prior to irradiation.

The film bracket was mounted to the stepper motor of the RPC portable water phantom, and its level of plumb was verified using an electronic level, that was zeroed using the patient treatment couch as level (in relation to the gantry, at 90 or 270 degrees gantry angle). For both orientations the tank was positioned with isocenter located at the center of the chosen SOBPs to initiate a point of reference. The bracket was first set to the parallel alignment, with a 2 degree separation between film and beam

planes. A long piece of film was inserted and abutted with the inside of the 2mm mylar scanning window. Using the patient alignment lights the film was centered in the beam. This orientation is shown below with a piece of film, post irradiation in Figure 2-12. For the perpendicular orientation, the film was then zeroed using an alignment bracket, that when combined with the thickness of the mylar window gives a known depth. Six depths were then selected, and film was irradiated at each location. The stepper motor was used to move the film to each desired depth. Vertical alignment within the center of the beam was handled using the patient alignment lights from the snout. A physical measurement with a ruler was taken to verify accuracy.

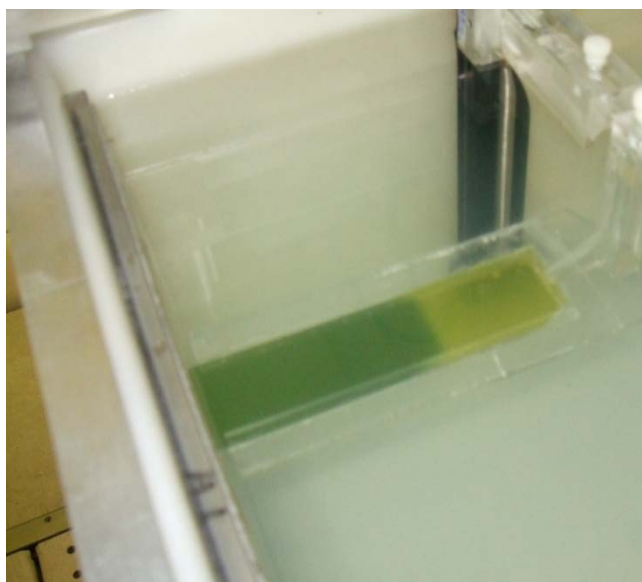


Figure 2.12 GAFChromic film in parallel orientation in the RPC portable water tank post irradiation.

After irradiating film at both orientations, the film was scanned using in house software and the OD values were measured and compared to acceptance testing depth dose curves for the specific gantry/snout combination provided by the PTC-H.

2.5.3 TREATMENT DELIVERY FOR LUNG INSERT

To evaluate treatment delivery of the various treatment plans, the lung insert was loaded with TLD and film, inserted into the thorax phantom and placed on the patient treatment table in PTC-H Gantry2. The phantom was positioned with lasers, and then alignment was verified using orthogonal digital reconstructed radiographs (DRR). Alignment was then evaluated utilizing the tumor as the visible marker of interest. Upon verification the apertures and compensators for the first field to be treated were installed into the snout and treatment delivery was prepared. The beam parameters and the MUs required by the record and verify system were input into the console and the phantom was irradiated. This was performed for two fields for each irradiation trial. Both treatment plans, Plan 1a and Plan 1b, were irradiated 3 separate times with new film and TLD inserted for each trial. The position of the thorax phantom on the treatment couch was noted, and verified after each placement of the insert, to ensure no changes to alignment were made.

2.5.4 TLD AND FILM REGISTRATION

The irradiated films from each phantom trial were scanned 3 days post irradiation following RPC protocols using the CCD100 film scanner. The 512 by 512 .FIT images generated contain both OD values and spatial values, thus allowing them to be overlaid onto a corresponding CT slice or a dose map generated by Eclipse. The phantom insert dimensions were measured from the CT scan of the phantom and 5 fiducial points were selected for image registration: The center of the wedges in both the superior and inferior ends of the insert, and 3 points on the center slice of the insert, the top cylinder wall, left cylinder wall and center of the phantom, which is designated coordinate (0,0,0). The TLD coordinates were also designated for each of the 3 scan planes.

After the film was loaded into the insert, the individual pieces were pricked at known coordinates. These locations were verified both with physical measurements and from the CT images and along with locations of TLD coordinates and saved for future usage as Proton Lung Phantom 1. This data was then input into the in-house analysis software, called RPCFILM, that enables registration between the measured dose distribution and the CT exam utilized to generate the

treatment plan. This software then integrates with CERR (Computational Environment for Radiotherapy Research), and enables the calculated treatment plans to be compared to measured dose distribution. (Deasy, Blanco and Clark 2003)

As mentioned in section 2.1.2, there are 3 planes of film that were analyzed: Sagittal (2 pieces of film), Coronal (two pieces of film), and Axial (single piece of film). The films from each of the irradiated trials were then uploaded by plane and registered using the above mentioned points, and the relative dose distribution calculated by the film and TLD compared to the dose maps from the TPS. Dose profiles were generated 5mm off center to reduce edge errors that might be introduced by the slotting of the film for both the sagittal and coronal planes. The profiles in the sagittal plane were drawn in the inferior-superior direction and the anterior posterior direction. The profiles in the coronal planes were drawn in the inferior-superior and the left-right planes. The axial film had the dose profiles drawn through the origin in both the anterior-posterior and left-right planes.

2.6 Treatment Evaluations

2.6.1 *TLD COMPARISONS*

The TLDs for the phantom trials were read by RPC employees 30 days post irradiation. The readings from the TLD session were imported into an Excel spreadsheet and all of the calculations previously discussed were used to calculate the measured dose of each trial. This measured value was then directly compared to the expected dose at that corresponding point in RPCFILM and a correction ratio was applied to the 512 by 512 matrix of OD values on the film, scaling the film to match the TLD reading.

2.6.2 *FILM VS. TREATMENT PLAN COMPARISONS*

The delivery of the treatment plan to the phantom was evaluated using two methods: gamma analysis and comparison of distance to agreement (DTA) profiles in 2D both utilizing the film data and the TPS dose maps. The scanned.FIT images, acquired in section 2.5.4, were loaded into RPCFILM. RPCFILM allows the user to select specific settings for the desired phantom. Analysis

was based on the selected film plane orientation. Once the desired plane was selected, the physical film alignment pricks were registered to known coordinates on the corresponding CT images, by selecting the registration points. RPCFILM includes a magnified view pane in the lower right corner that enables finer placement of the alignment marks. The magnification window and registration points, seen as black X's overlaid on the film, in a screen capture of RPCFILM shown in Figure 2-13 below

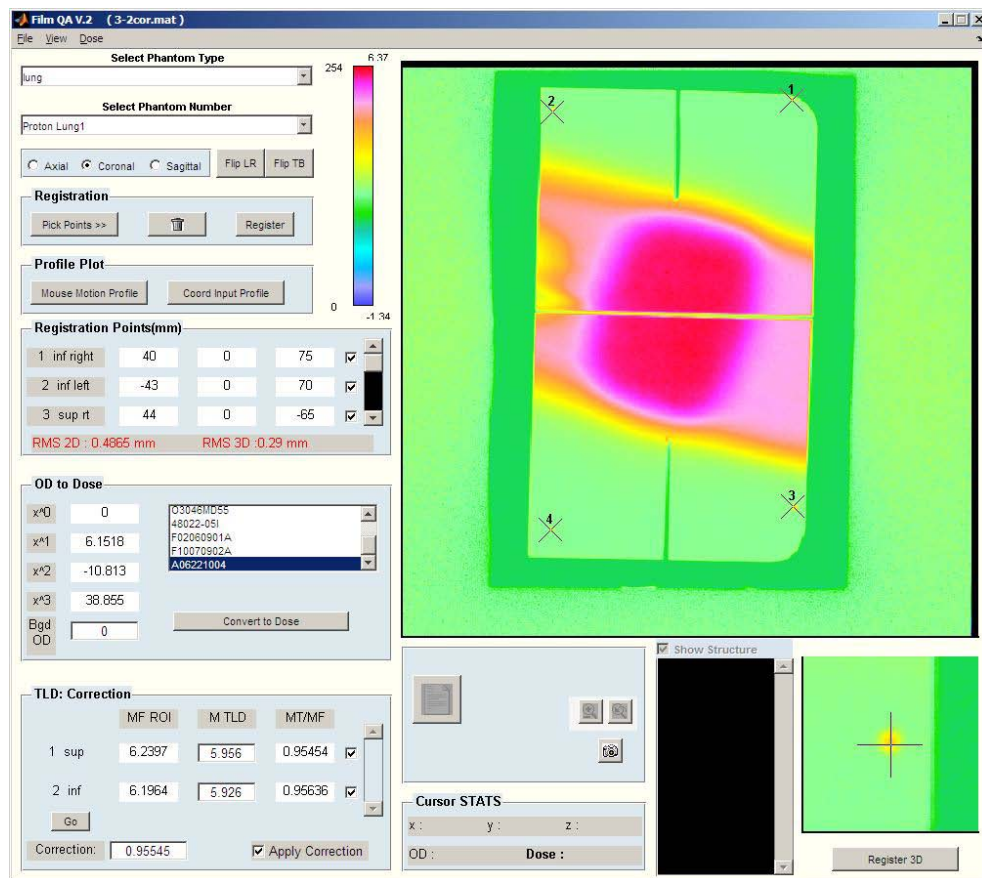


Figure 2.13 Screen capture of RPCFILM analysis for Plan 1b trial 2

After registering the measured distribution on the film to the TPS dose maps, the film calibration curve for the specific batch of film used during the irradiation was selected. The calibration curve, discussed in section 2.5.2.1, converts the OD of each pixel on the scanned film to a physical dose. The user then inputs the corresponding TLD data, discussed in above in section 2.6.1,

normalizing the film dose data to the TLD dose. At this point the user has completed the image registration, and both the gamma analysis and the DTA can be performed.

2.6.2.1 GAMMA ANALYSIS

Gamma analysis is a tool that can be utilized to determine the accuracy of radiation treatment and as such is useful in performing quality assurance of a treatment plan. Gamma analysis takes both DTA and percent difference in dosage when comparing planar dose distributions. Applying a 2D spatial coordinate system to a dose gradient takes advantage of the complementary nature of the dose gradient sensitivities of DTA and percent dose differences. In registering the film dose distribution to the Eclipse dose distribution, the gamma analysis allows the percentage dose difference and DTA for each pixel to be calculated as components of a vector. The vector is normalized to the desired criteria. If the magnitude of this vector at each pixel exceeds 1, then that pixel fails the defined criteria (Low, et al. 1998).

Gamma analysis was performed using CERR and RPCFILM, by selecting the desired criteria and running the gamma tool, returning the percentage of pixels passing. At M.D. Anderson, for daily IMRT QA we utilize a 5% / 3mm, where the dose distribution assessment will fail the gamma analysis if less than 80% of the pixels have magnitudes less than 1. (Childress, et al. 2005) The irradiated films will be compared against these gamma-index criteria, 5% dose difference and 3mm DTA, and is stated in the hypothesis. However, it is worth noting, that for RPC anthropomorphic lung phantoms treated for SBRT using photons, the gamma index criteria are 5%/5mm, where each film plane must have greater than an 80% pass rate, and the average of the planes must be greater than an 85% pass rate. The irradiated films also will be compared against the RPC gamma index criteria to enable a comparison to current anthropomorphic photon quality assurance.

2.6.2.2 DTA PROFILES

DTA profiles were acquired 5mm off center on the sagittal and coronal planes to avoid artifacts in the OD of the physical dose distribution caused by the slots cut into the film that enables them to interlock. The DTA for the axial film was taken directly across the center in both directions, as shown below in Table 3. These film profiles were then compared to profiles taken from the Eclipse dose distribution using the same coordinates.

		Start (mm)	Stop (mm)
AXIAL (x,y)	RL Profile	(-65,0)	(65,0)
	AP Profile	(0,-65)	(0,65)
CORONAL (x,z)	RL Profile	(-65,5)	(65,5)
	SI Profile	(5,-65)	(5,-65)
SAGITTAL (y,z)	AP Profile	(-65,5)	(65,5)
	SI Profile	(5,-65)	(5,-65)

Table 3 DTA Profile co-ordinates for Axial, Coronal, and Sagittal films

CHAPTER 3: RESULTS AND DISCUSSION

3.1 Phantom Design and Construction

3.1.1 MATERIAL RELATIVE LINEAR STOPPING POWERS

3.1.1.1 RELATIVE LINEAR STOPPING POWER ANALYSIS

Any material placed into the path of the beam will reduce the range of the protons. The materials used for the phantom have different stopping powers than water. For materials of equal thicknesses and different stopping powers, the range is affected differently. It is this difference in stopping powers that needs to be calculated.

The depth dose scans for both balsa and cork were obtained with each of the materials attached to the outside of the water phantom, and then compared to a depth dose scan of a beam in water, as discussed in section 2.2.1. Both the cork and balsa are used to represent tissue in the phantom, and needed to be characterized. The depth dose curve for the balsa is shown in Figure 3-1. A similar curve was created for the cork sample.

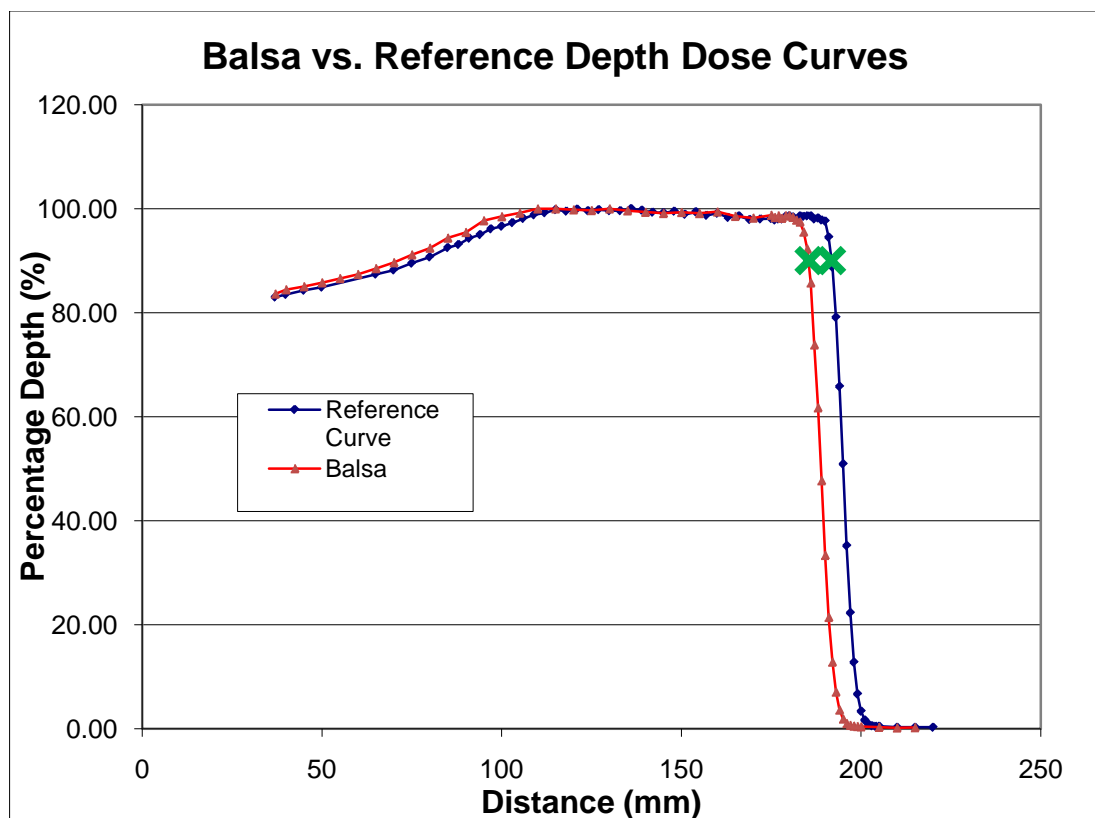


Figure 3.1 Comparison of balsa and reference ion chamber depth dose curves. Note that the 90% locations are designated with the green X on both curves

The depth dose curve for both the balsa and cork beams were overlaid onto the depth dose curve in water, called the reference curve. The distal 90% points for both the material curves and the reference curve were calculated using a cubic spline interpolation, and are marked on Figure 3-1 using green “X”s. Utilizing the methods and formulas in Section 2.2, for balsa it was determined that $R_{90,W} = 191.8\text{mm}$ and $R_{90,m} = 185.1\text{mm}$. The thickness of the balsa sample was determined by taking the average of five measurements using calipers at the center of the sample, resulting in $t_m = 20.1\text{mm}$, with a standard deviation of 0.04 mm, ensuring a uniform sample. Balsa was then calculated to have an $RLSP = 0.313$. The same procedures were repeated for the cork sample, yielding an $RLSP = 0.227$.

The RPC utilizes other phantoms made from the same materials as the thorax phantom. For the lung phantom, Poly-vinyl chloride (PVC) was utilized in the shell, acrylic was utilized as the sleeve into which the imaging/dosimetry insert is placed, high impact (HI) polystyrene was utilized as both the shell of the insert and as the tumor target, water fills the phantom body to simulate soft tissue, cork is utilized as lung tissue outside of the insert, and balsa is utilized as the lung tissue inside the insert. In a previously commissioned RPC anthropomorphic phantom, the RLSP for the materials, other than balsa and cork, in the phantom had already been calculated. (Grant 2010) These values, including the balsa and cork RLSP's are shown in Table 4, and the phantom material values are plotted against the calibrated values from Eclipse in Figure 3-2.

	HU Eclipse	SP Phantom
PVC	800	1.23
Acrylic	125	1.21
HI Polystyrene	-30	1.07
Water	17.6	1.00
Balsa	-672.3	0.313
Cork	-690	0.277

Table 4 Relative stopping linear stopping powers of phantom materials

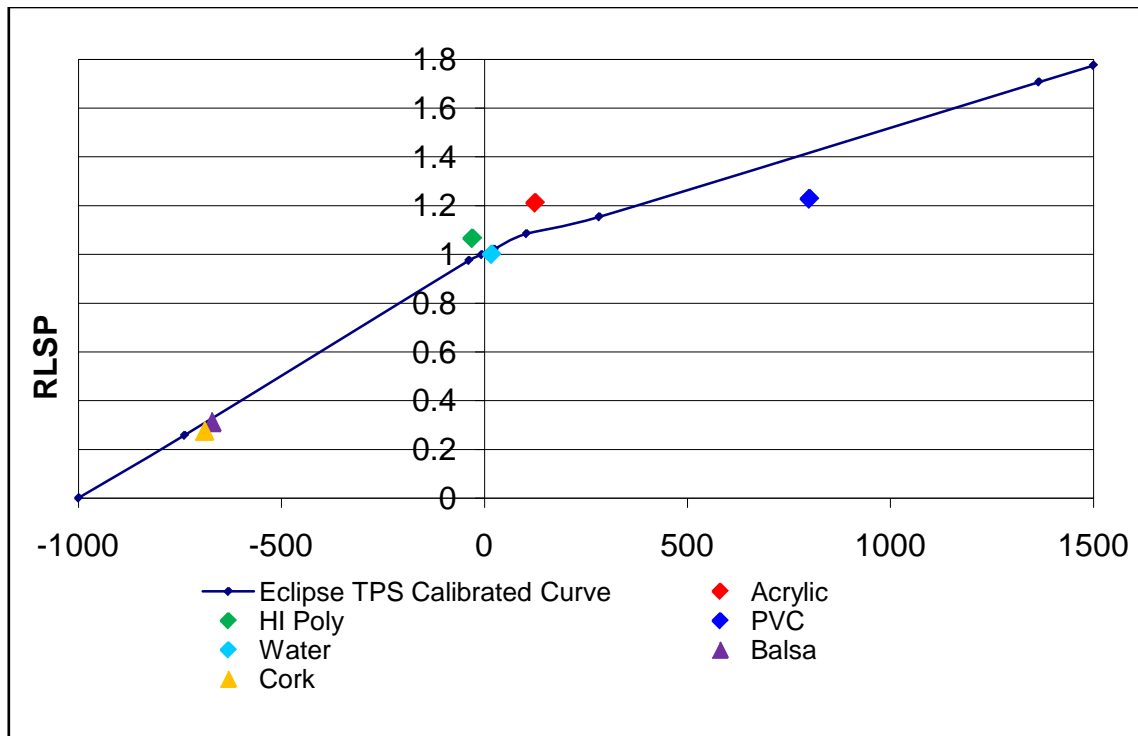


Figure 3.2 Lung Material RLSP-HU chart comparing phantom values to calibrated Eclipse curves

3.1.1.2 STOPPING POWER COMPARISON

The RLSP for almost all tissues in the human body have been reported previously in literature, due to ex vivo scanning techniques. However, lung tissue has not been scanned primarily because the tissue cannot show proper levels of inflation in an ex-vivo sample. Most treatment planning systems, including Eclipse, create a linear plot from air to the first known tissue sample, and place the RLSP for lung tissue at some predetermined HU number along this line. For Eclipse this is placed at -739.1 HU, giving a RLSP of 0.258. Previous studies compared different lung equivalent materials, both natural and man-made, to determine an effective phantom equivalent RLSP for lung tissue. In Table 5, three different materials had depth dose curves taken at three different energies to determine RLSP. (Moyers, et al. 2010)

Material	PD (g/cm ³)	HU ³	135Mev RLSP	175Mev RLSP	225Mev RLSP
TPL Lung	0.307	-679	0.303	0.305	0.305
RMI Lung	0.342	-655	0.35	0.337	0.345
Jelutong Wood	0.429	-580	0.4	0.402	0.404

Table 5 Relative linear stopping power of three lung equivalent lung materials

The three materials show very little difference in calculated RLSP based on energy, thus proving that each material is relatively energy independent, with the RMI Lung fluctuating the most. The extra heavy balsa utilized in the project has a measured density ranging from 0.30 to 0.34 g/cm³, and an average HU of -672.3. The stopping powers were compared to these literature values, and when compared to the TPL lung, the difference in HU and RLSP were 0.99% and -2.85% respectively. For RMI lung, the differences in HU and RLSP were -2.64% and 9.01%. For the only natural material on the list, Jelutong wood, the differences in HU and RLSP were -15.91% and 22.14%. Based on these comparisons and taking into account the cost and availability of the materials, it was determined that balsa would be an acceptable material to utilize in a lung phantom.

3.1.2 COMPRESSION

After construction of the imaging/dosimetry insert was completed, the removal of air gaps via a compression technique needed to be verified. The insert consists of a series of tapered wedges inserted into a corresponding tapered ring. When indexed into the HI poly shell, the end caps apply pressure squeezing the wedges into the rings, and providing lateral compression, that removes the air gaps near the film channels. The insert was placed on a GE Lightspeed X/Qi CT scanner (GE Healthcare , Waukesha, WI) and utilizing an HQ pitch with a DFOV = 18.3cm, yielded a resolution of 0.35 mm/pixel, shown in . The profiles across the film channels were then compared and if more than one pixel of gap was observed between the film and the insert, the insert was recompressed and shot again. It was determined that one wedge set needed to be re-machined, as it could not remove

the gap sufficiently. Upon re-machining, it passed visual inspection verifying that the compression technique was adequate to remove air gap.

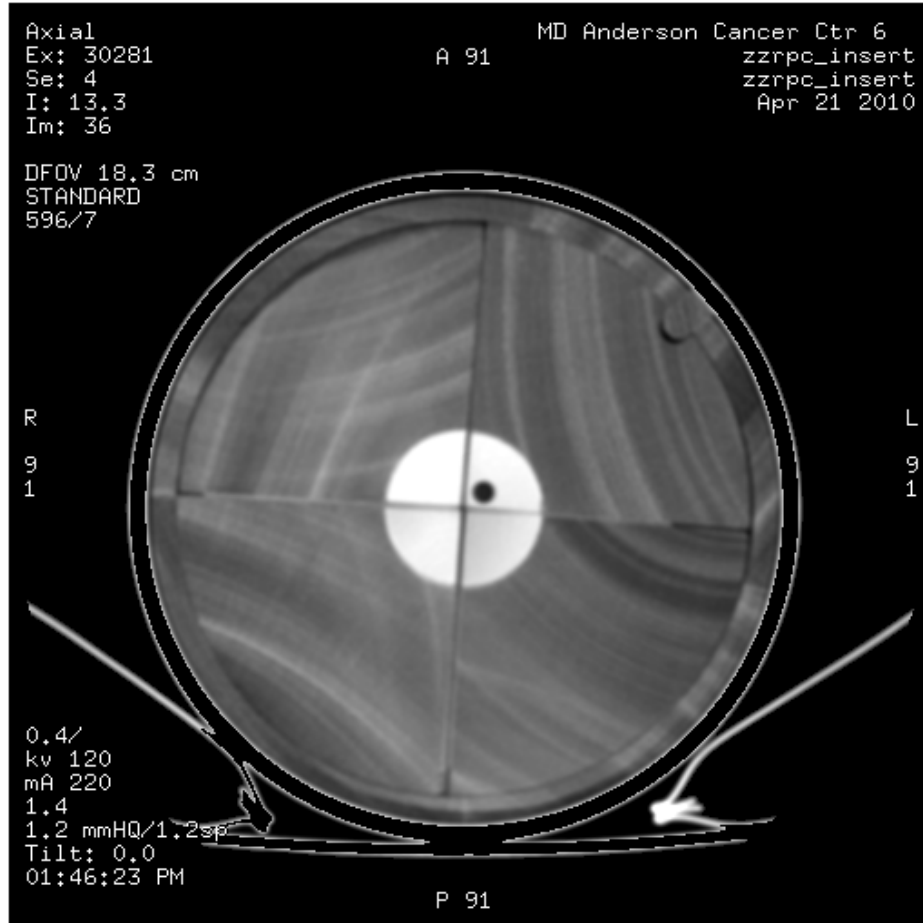


Figure 3.3 High resolution CT scan of imaging/dosimetry insert

3.1.3 COMPARISON OF PLANS

Due to the large difference of the PVC material RLSP when compared to the RLSP of a similar HU number on the calibrated Eclipse curve, a separate plan was created with the PVC shell contoured. A comparison of this new plan to the standard plan would help to evaluate differences, if any, which might appear in the treatment of the phantom. The body of the phantom was contoured and a HU of 427.3 was selected based on the measured RLSP of PVC. There is a tapering of the PVC shell in the treatment area which introduces a partial volume effect. A profile was drawn across

the shell and the HU for PVC was set for 80% of that profile, placing the shell closer to the calibrated Eclipse RLSP curve. To ensure that there would be no differences due to physical modifiers of the beam; neither the compensator nor the aperture was modified for the new plan. The beam conditions were then calculated in Eclipse, and the results did not differ from those reported in sections 2.4.3 and 2.4.4. From here forward, the unmodified original version of each plan will be known as Std. Plan, and the modified versions of each plan will be the PVC Contoured Plan. Using CERR, gamma analysis was performed on the Std. Plan vs. the PVC Contoured Plan, for the axial, sagittal and coronal planes, shown below.

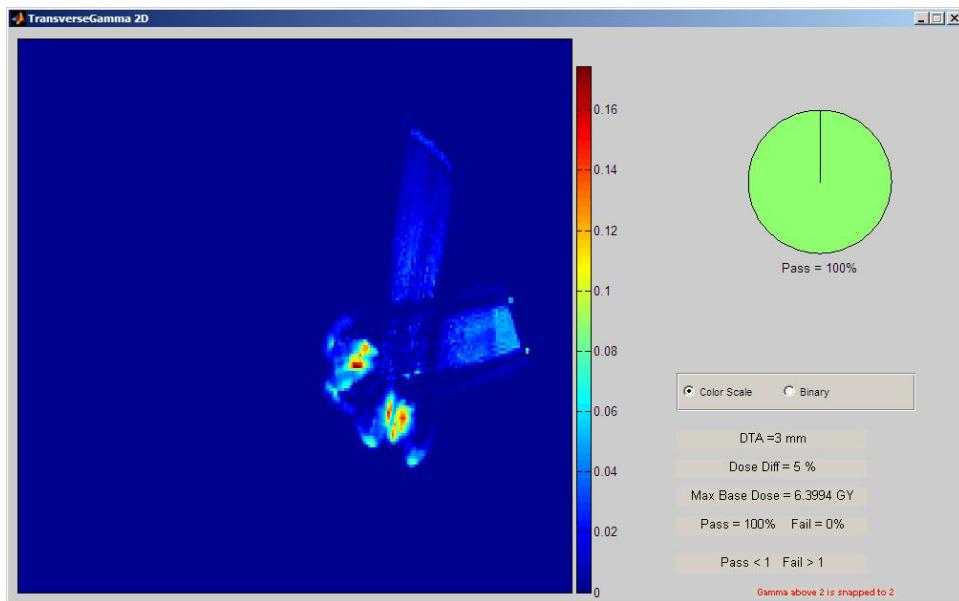


Figure 3.4 Gamma analysis of Std. Plan and PVC contoured plan in the axial plane. Gamma criteria were set to 5%/3mm

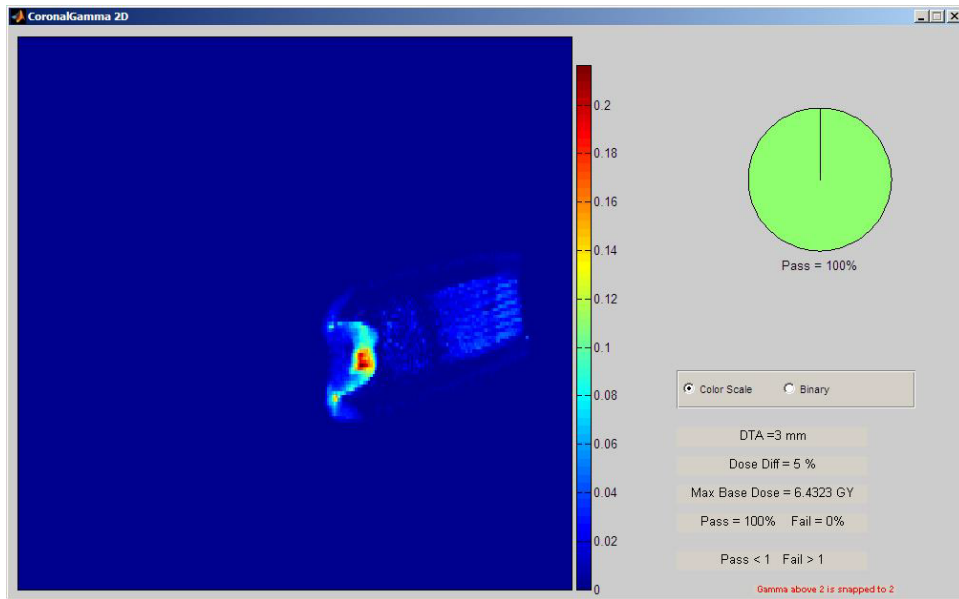


Figure 3.5 Gamma analysis of Std. Plan and PVC contoured plan in the coronal plane. Gamma criteria is set to 5%/3mm

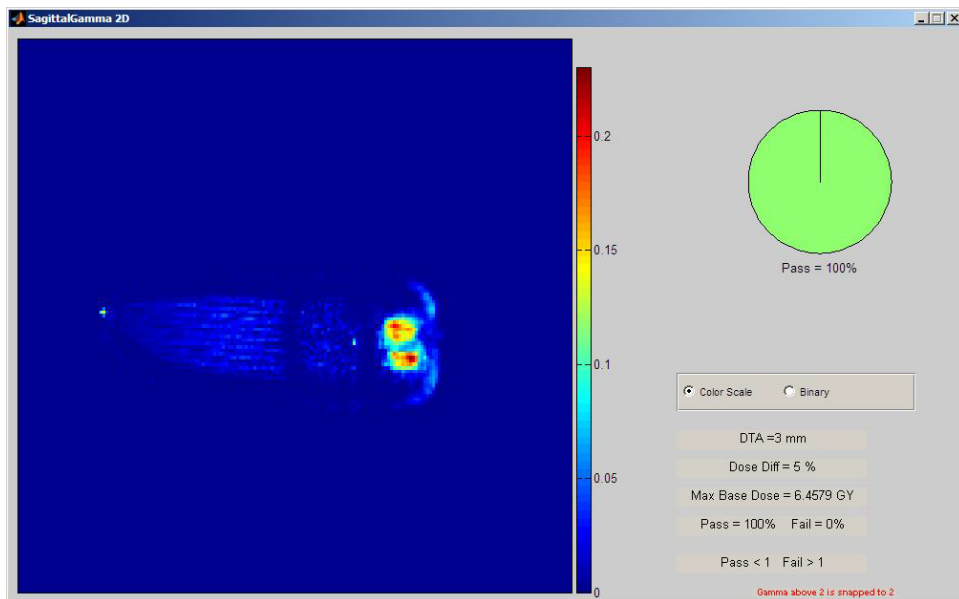


Figure 3.6 Gamma analysis of Std. Plan and PVC contoured plan in the sagittal plane. Gamma criteria is set to 5%/3mm

It is worth noting that at the criteria of 5%/3mm, a 100% pass rate was observed, with no pixels having a gamma value greater than 1; and therefore no pixels fail the comparison. This would lead us to believe that there would be little if any difference when comparing the treated film to the different contoured plans, as minimal error will be introduced that will be larger than the 5%/3mm criteria.

3.2 LET Dependence of GAFChromic Film

The possibility of LET dependence of the EBT2 film based on orientation, parallel or perpendicular might cause differences in comparison of 2D dose using film in the insert.

3.2.1 *PARALLEL FILM ORIENTATION*

Artifacts can arise when the film is placed directly parallel to the beam, so the film for the first part of this section was placed at a 2 degree declination to the beam to help reduce this effect. This was achieved by placing the gantry at 272degrees and the film horizontally at 270 degrees. After irradiation, the film was scanned in house utilizing RPCFILM. Five profiles of the OD were taken across the film and averaged.. The OD values were compared to acceptance testing depth dose curves provided by the PTC-H. The two curves were normalized at 6cm and are shown below in Figure 3-7 .

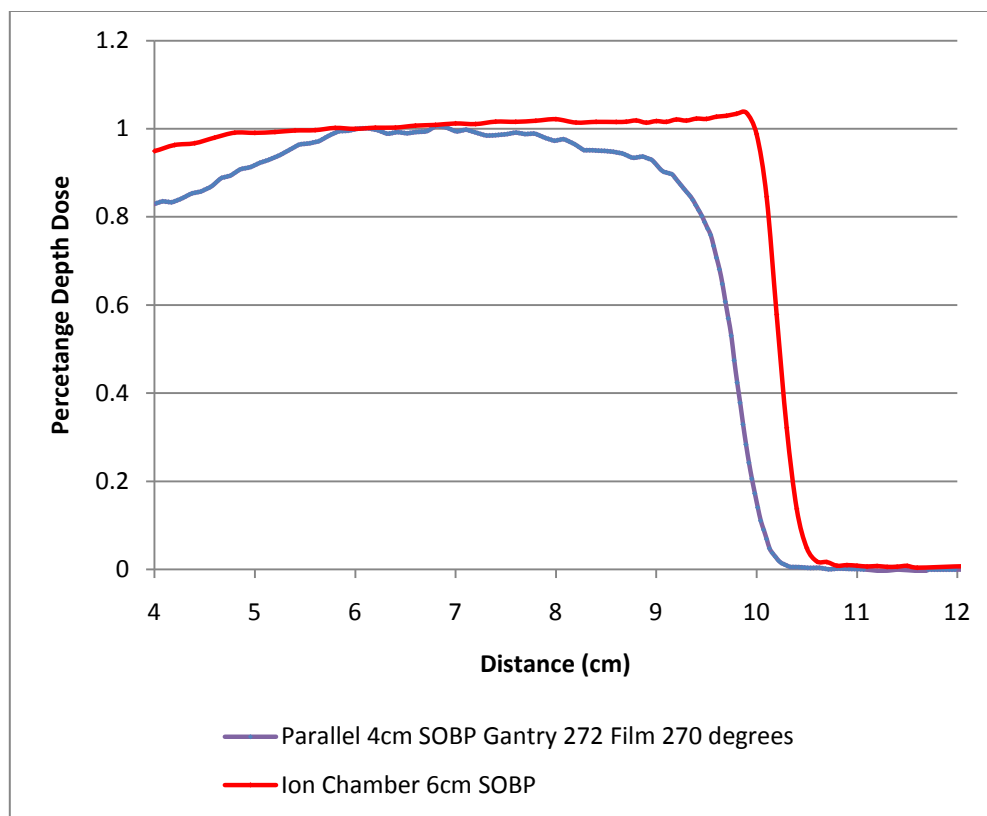


Figure 3.7 Comparison of depth dose curves obtained using parallel GafChromic EBT2 film to depth dose curve obtained with ion chamber from PTC-H at 140 MeV

The result for this scan showed a large disparity between the two sets of data at the distal end of the SOBP. There were many beam tuning issues, and it was decided that a second method should be tried. For this method placing the gantry at 270 degrees and the film bracket at 268 degrees would yield the same angular difference in the orientation of the film and the beam. However the beam selected was set to a 5cm SOBP. This should not affect the distal end of the SOBP as the range was not modified for either trial using a range modifier, and the energy was set to the same value. Both curves were once again normalized at 6cm. The results for this can be seen below in Figure 3-8.

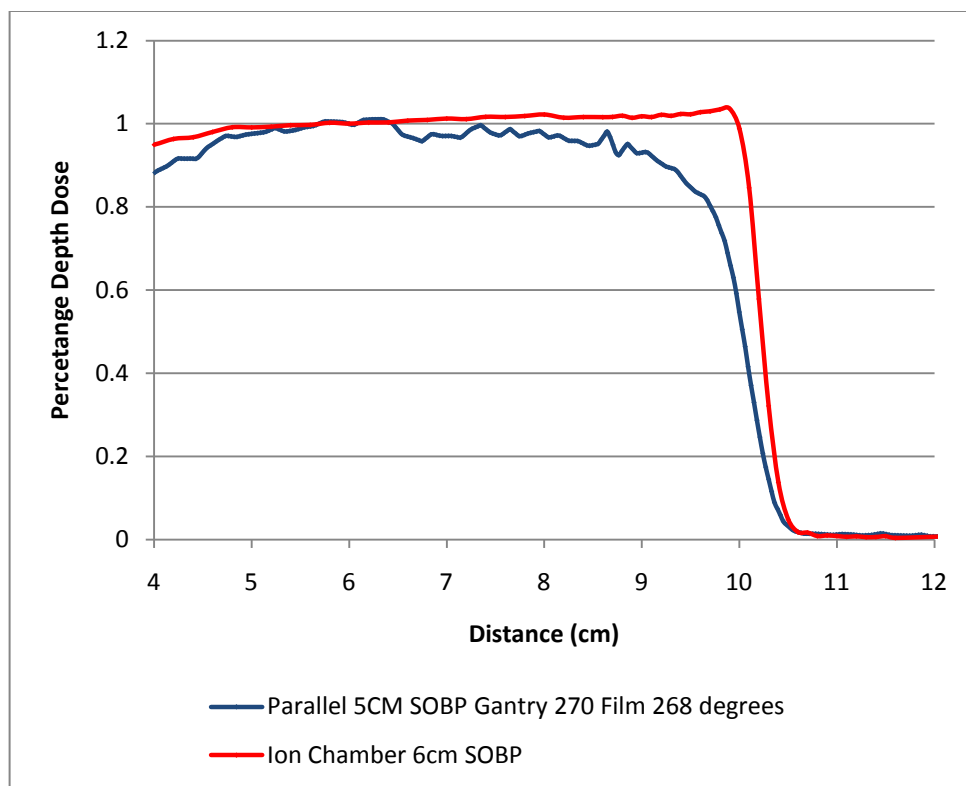


Figure 3.8 Comparison of depth dose curves obtained using alternate method of parallel GafChromic EBT2 film to depth dose curve obtained with ion chamber from PTC-H at 140 MeV

The appearance of this curve more closely resembled that as seen in the literature (Zhao and Das 2010). The percentage difference between the original method and the ion chamber showed an average percentage difference between measured points of 55.4% with a maximum difference of 97.2% at 10.3cm depth. For the alternate method, the average percentage difference of the measured points was 31.0% with a max difference of 54.83% at 10.3cm depth. These results are shown in Table 6.

Depth (cm)	Ion Chamber	Alternate Method		Original Method	
		268 Deg. Film	% Difference	270 Deg. Film	% Difference
5.3	0.995	0.984	1.11%	0.947	4.82%
8.5	1.016	0.948	6.69%	0.949	6.59%
9.6	1.027	0.829	19.28%	0.707	31.16%
9.8	1.034	0.747	27.76%	0.424	58.99%
10.1	0.846	0.393	53.55%	0.059	93.03%
10.2	0.579	0.267	53.89%	0.025	95.68%
10.3	0.321	0.145	54.83%	0.009	97.20%

Table 6 Comparison of Parallel film methods to Ion chamber readings

3.2.2 PERPENDICULAR FILM ORIENTATION

After irradiation in the perpendicular orientation, the film was once again scanned and analyzed. A linear fit was placed between the 5.3 and 8.5cm points to determine a 6.0cm depth value. At this point the film data was then normalized to the ion chamber data. The results are shown in Figure 3-9 . The film values at the distal end once again under performed, with an average percentage difference of 14.7%, with a max percentage difference of 55.1% at 10.3cm, shown in Table 7.

Depth (cm)	Ion Chamber	Perpendicular Film	
		Film	% Difference
5.3	0.995	0.992	0.30%
8.5	1.016	1.027	-1.08%
9.6	1.027	0.999	2.73%
9.8	1.034	0.977	5.51%
10.1	0.846	0.631	25.41%
10.3	0.321	0.144	55.14%

Table 7 Comparison of Perpendicular film method to Ion chamber readings

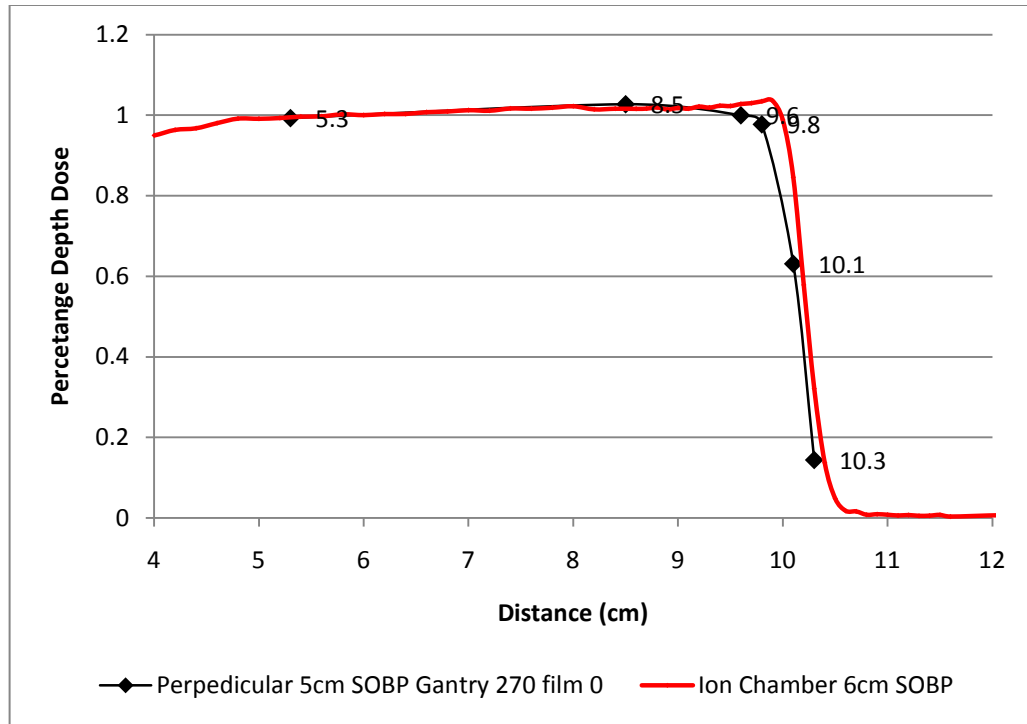


Figure 3.9 Comparison of depth dose curves obtained using ion chamber and perpendicular GAFChromic EBT2 film at 140 MeV

Based on these results, it is to be expected that there will be some type of distal edge LET effect on the film independent of orientation, with more severe effects seen when the film is closer to parallel to the beam path.

3.3 Phantom Irradiation Evaluation

Post irradiation, each of the film sets and TLD sets were then prepared to be analyzed. The TLD was read out by staff at the RPC 30 days post irradiation, and the film was scanned using an in-house scanner to acquire .FIT images for evaluation.

3.3.1 TLD

The TLD utilized for this project is known internally at the RPC as Batch 07, or B07, and had been commissioned by the RPC prior to the start of this project. For this specific batch of TLD, the following constants are utilized in the formulas from section 2.5.1.

X	Days Post Irradiation
N	1.3493
A	1.2815
B	0.00010885
C	0.06781
D	0.071908
Linearity a	2.29840E-08
Linearity b	-2.1190.E-04
Linearity c	1.0615

Table 8 TLD formula constants for B07

3.3.1.1 TLD COMPARISONS

The TLD capsules used contained two loads of TLD-100 powder. Each load is weighed and measured at the RPC, and the two readings for each capsule are averaged together to equal dose at the point of measurement. A comparison of the TLD measurements was made for each trial to the calculated beam data from Eclipse over the contoured volume of each TLD. The TLD data for Plan 1a is shown below in Table 9. The ratios of measured to calculated dose rate indicate that all TLD readings were within 6%, except for trial 3 superior which was under 7%.

	Calculated dose (cGy) Eclipse	Measured dose (cGy) TLD	Measured/ Calculated dose
Plan 1a Trial 1			
PTV Superior TLD	624.4	591.0	0.947
PTV Inferior TLD	617.9	584.1	0.945
Plan 1a Trial 2			
PTV Superior TLD	624.4	590.0	0.945
PTV Inferior TLD	617.9	584.4	0.946
Plan 1a Trial 3			
PTV Superior TLD	624.4	584.6	0.936
PTV Inferior TLD	617.9	590.1	0.955

Table 9 Plan 1a TLD dosimetry data

The ratios of the TLD data for Plan 1b were then calculated. These are shown in Table 10. It should be noted that there was no PTV superior TLD data for trial 1, as there were problems with the readout at the RPC. The ratios of the remaining measured to the calculated doses were all under 6%. For the plan 1b trials, the average ratio of the dose rates is 5.4%.

	Calculated dose (cGy) Eclipse	Measured dose (cGy) TLD	Measured/ Calculated dose
Plan 1b Trial 1			
PTV Superior TLD	624.5	n/a	n/a
PTV Inferior TLD	625.3	591.0	0.945
Plan 1b Trial 2			
PTV Superior TLD	624.5	595.6	0.954
PTV Inferior TLD	625.3	592.6	0.948
Plan 1b Trial 3			
PTV Superior TLD	624.5	587.7	0.941
PTV Inferior TLD	625.3	589.9	0.943

Table 10 Plan 1b TLD dosimetry data

The TLD results for the 3 trials in Plan 1a and Plan 1b were then averaged and the standard deviation of the 3 trials for each plan was also calculated. Utilizing the average and the standard deviation together allows the calculation of the coefficient of variation (CV) between the trials. The CV is unit less, and therefore allows for comparisons between variables. If a variable has a smaller CV then it tends to be less dispersed than a variable with a large CV. (UCLA: Academic Technology Services n.d.) For Plan 1a, the CV is less than 1%, indicating that there is very little spread amongst the values, shown in Table 11. For Plan 1b, even with only two data points for the PTV superior

TLD, the CV is still less than 1%, indicating that there is very little spread amongst the values, shown in Table 12 Plan 1b TLD average, Std. deviation, and CV for 3 trials. This reproducibility of the phantom measurements means that the phantom design can be utilized as an accurate dosimetry device.

Plan 1a	PTV Superior TLD	PTV Inferior TLD
Calculated dose (cGy)	624.4	617.9
Measured dose Average (cGy)	588.5	586.2
Std. Deviation	3.44	3.15
CV	0.58%	0.54%
Measured Avg. dose/ Calculated dose	0.948	0.949

Table 11 Plan 1a TLD average, Std. Deviation and CV for 3 trials

Plan 1b	PTV Superior TLD	PTV Inferior TLD
Calculated dose (cGy)	624.5	625.3
Measured dose Average (cGy)	591.65	586.2
Std. Deviation	5.59	1.4
CV	0.94%	0.24%
Measured Avg. dose/ Calculated dose	0.947	0.937

Table 12 Plan 1b TLD average, Std. deviation, and CV for 3 trials

Applying a one sample t-test data on the TLD data enables us to check for statistical significance of the results. Excluding the Plan 1b Superior TLD (which only had 2 sample points), the values for the two-tailed p-value all were less than 0.05 ($p < 0.05$), and therefore are deemed statistically significant.

3.3.2 CT TO ECLIPSE REGISTRATION

Before any analysis could be performed the computed tomography (CT) image set needed to be registered in CERR to the dose map exported from Eclipse. The image set was registered using 2.5mm CT slices. A series of five landmarks with coordinates shown in Table 13 was utilized to align and register the images, as they are easily visible and results through multiple registrations have proven to be consistent. The first point was selected in the center of the phantom (easily seen by the film cross slot) at the superior edge of the insert wedges. The next three points selected were located at the center of the phantom insert, with two points on the left balsa cylinder wall and top cylinder wall. The center of the film slots was then selected to be the origin (0,0,0) of the entire dose map. The final location selected was the center of the phantom at thin inferior end of the balsa wedges. After selecting these points for registration, the dose map was aligned to the CT images, and the TLD doses were located and compared to the exact doses for the corresponding locations in the eclipse dose plan.

	edge wedge superior	left cylinder wall	center	top cylinder wall	edge wedge inferior
x	0	63	0	0	0
y	0	0	0	63	0
z	-92.4	0	0	0	80.1

Table 13 CT registration landmarks

The five landmarks are then evaluated using the root mean square (RMS) value of the differences between the listed coordinates and the measurements of the pixels on the CT image. This is called the 3D RMS, since all three planes are registered together. For this project a passing value of 3D RMS was to be below 1mm, and all registrations complied. The resulting coordinate system obtained from this registration can then be utilized by RPCFILM to register and analyze the 2D film data.

3.3.3 TLD REGISTRATION

Once the calculated eclipse dose map has been registered to the CT image set, the TLD can then be registered to points on the eclipse dose maps. This is accomplished by selecting the physical location of the TLD as input into RPCFILM by a table in a reference spreadsheet. The values correspond locally to specific dose points on the scanned film images, shown in Table 14, and thereby allow for the calibration of the 2D film dose map to a physical dose that can be directly compared to the Eclipse calculated dose.

	Axial	Coronal		Sagittal	
	inferior TLD	superior TLD	inferior TLD	superior TLD	inferior TLD
X	-4	-4	-4	0	0
Y	4	0	0	4	4
Z	0	5	-5	5	-5

Table 14 Table of TLD physical registration locations for RPCFILM, in mm

3.3.4 FILM SCANNING AND REGISTRATION

Using our in-house film scanner, the separate pieces of film were then aligned based on plane and scanned to .FIT files. For each trial and specific plane, the .FIT images were uploaded into RPCFILM. Each of these “plane” images was then registered to the treatment plan as discussed in section 2.5.4. The coordinates of each of the alignment pricks are shown in Table 15. Any errors in the alignment would be seen as a shift in the DTA profiles, as the eclipse dose and the film dose would not overlay as there would be a misalignment of the physical prick location to the referenced coordinates when the phantom was registered using CERR. An example of each “plane” image with image registration pricks can be seen in Figure 3-10. From this point both gamma analysis and DTA profiles could be acquired by comparing the registered film data to the dose map calculated by Eclipse.

Axial				
	upper right		lower left	
x	29		-12	
y	32		-43	
z	0		0	
Sagittal				
	inferior anterior	inferior posterior	superior anterior	superior posterior
x	0	0	0	0
y	41	-42	42.5	-41.5
z	65	75.5	-75	-70
Coronal				
	inferior right	inferior left	superior right	superior left
x	40	-43	44	-40
y	0	0	0	0
z	75	70	-65	-74.5

Table 15 Film registration prick locations

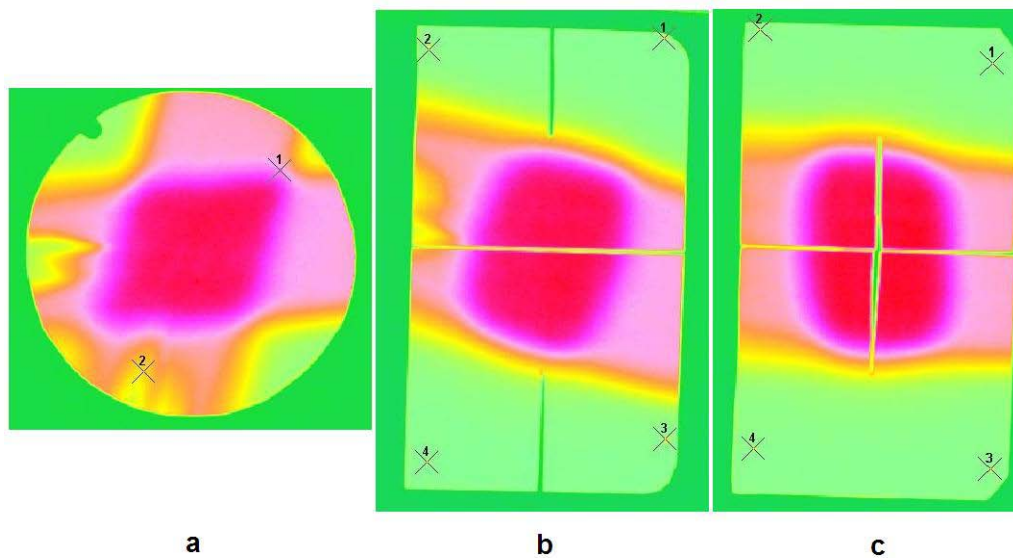


Figure 3.10 Plan 1b trial 2 film prick localizers for three separate .FIT “plane” images: a) axial image, b) coronal image, and c) sagittal image as seen in RPCFILM

3.3.5 GAMMA ANALYSIS

Gamma analysis was performed on the film from each trial to verify that the agreement of the measured and calculated dose. Axial, sagittal, and coronal film sets for each plan and trial set were scanned in and analyzed as discussed in Section 2.6.2. As discussed the software utilized to analyze the images is CERR and RPCFILM. The pass/fail rate for each of the gamma maps is shown in the following sections. These rates are color coded and every point with a gamma greater than 1 will fail the gamma criteria for that test. The percentage passing is listed and shown in a pie chart on the upper right side of the gamma image. The gamma criteria for photon lung phantom treatment for SBRT was agreed upon to be 5%/5mm where each plane must pass with an 80% pass rate, with the average of all 3 planes greater than 85%. The gamma criteria proposed in the hypothesis was set to 5%/3mm, but since no previous data had been recorded, the pass criteria for each film plane and for the total film average was not determined. The films for each trial were analyzed utilizing both criteria sets, and pass rates for 5%/3mm criteria for protons will be determined. The analysis will be shown below for Plan 1a Trial 2 and for Plan 1b Trial 2, with the remaining trials being listed in the appendix.

3.3.5.1 GAMMA ANALYSIS UTILIZING 5%/3MM GAMMA CRITERIA STANDARD PLAN

The gamma analysis for this section is performed utilizing the 5%/3mm criteria on the Std. Plan. The analysis for Plan 1a shows that a large percentage of pixels are failing the gamma criteria, and thus agreement between the measured and calculated dose is very low. Based on the literature, this result is what was expected. The film planes for all 3 planes were directly in line with treatment fields 1 and 2, and although there was no air gap, protons streaming down the film plane were expected to produce errors in the distal end of the SOBP due to the distal edge LET effect discussed in Section 3.2. Another possible explanation could be distal edge degradation due to Multiple Coulomb Scattering (MCS) that occur in the inhomogenities of the phantom materials. (Urie, et al.

1986), (Sawakuchi, et al. 2008) The gamma analysis results for Plan 1b shows an improvement over Plan 1a, with the most significant difference being seen in the axial film plane. These results are shown below in Table 16, and the screen captures of the gamma analysis are shown in Sections 3.3.5.1.1 and 3.3.5.1.2. In looking at the gamma maps, a majority of the pixels that fail are at the far distal end of the SOBP, where the dose has already begun to drop off. It is also worth noting that since the treatment plans were based on clinical patient protocols, as discussed in Section 2.4.1, that a large majority of the failing pixels occur in the region, the so called “dose horns,” caused by the expansion of the aperture and by the smearing of the compensator.

	Plan 1a				Plan 1b			
	Trial 1	Trial 2	Trial 3	Average	Trial 1	Trial 2	Trial 3	Average
Axial	56.13	56.41	53.83	55.46	66.84	74.65	76.15	72.55
Coronal	75.39	69.76	80.98	75.38	82.17	76.18	77.28	78.54
Sagittal	77.82	82.45	76.81	79.03	75.21	81.93	73.86	77.00
3P-Average	69.78	69.54	70.54	69.95	74.74	77.59	75.76	76.03

Table 16 Gamma analysis results for Plans 1a and 1b utilizing a 5%/3mm criteria (displayed in percentage passing)

3.3.5.1.1 Plan 1a

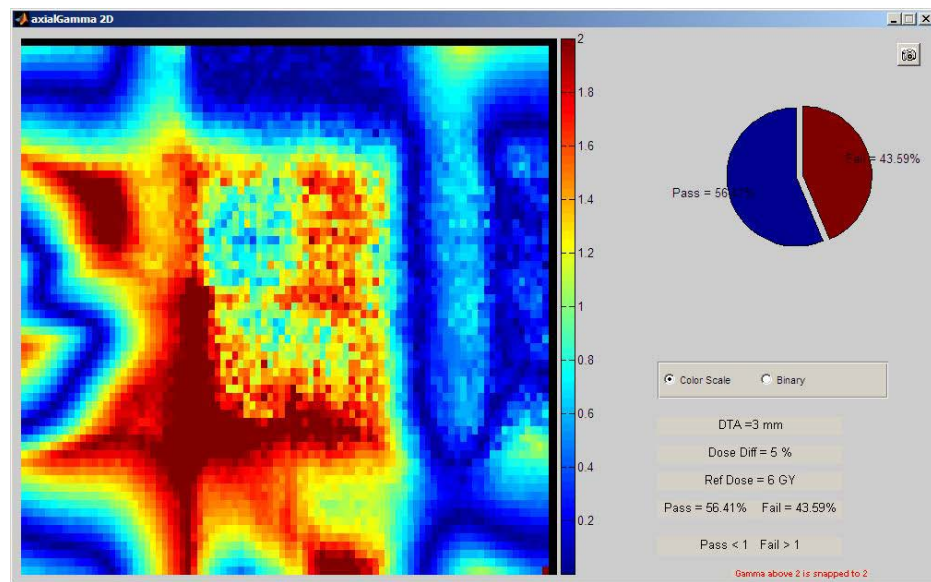


Figure 3.11 Plan 1a Trial 2 Axial Gamma Analysis

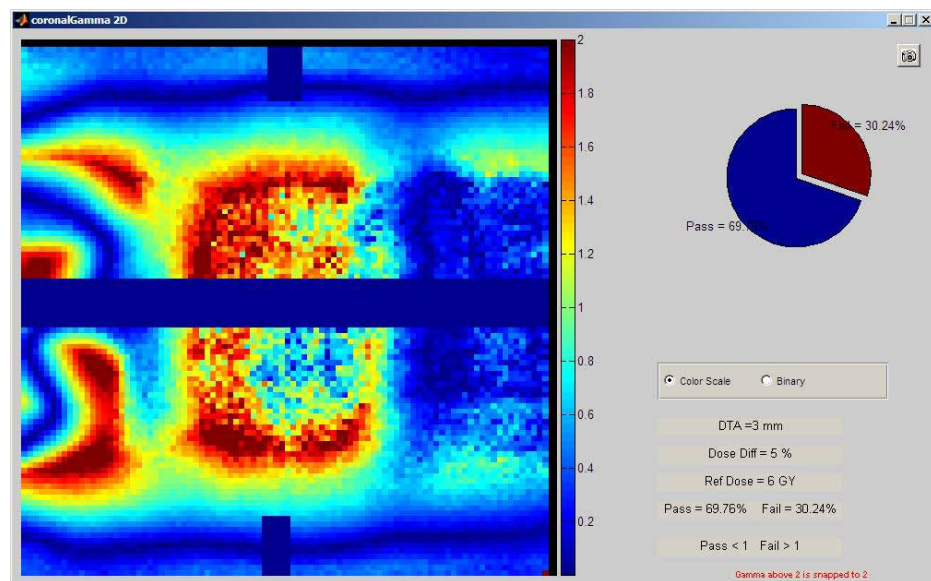


Figure 3.12 Plan 1a Trial 2 Coronal Gamma Analysis

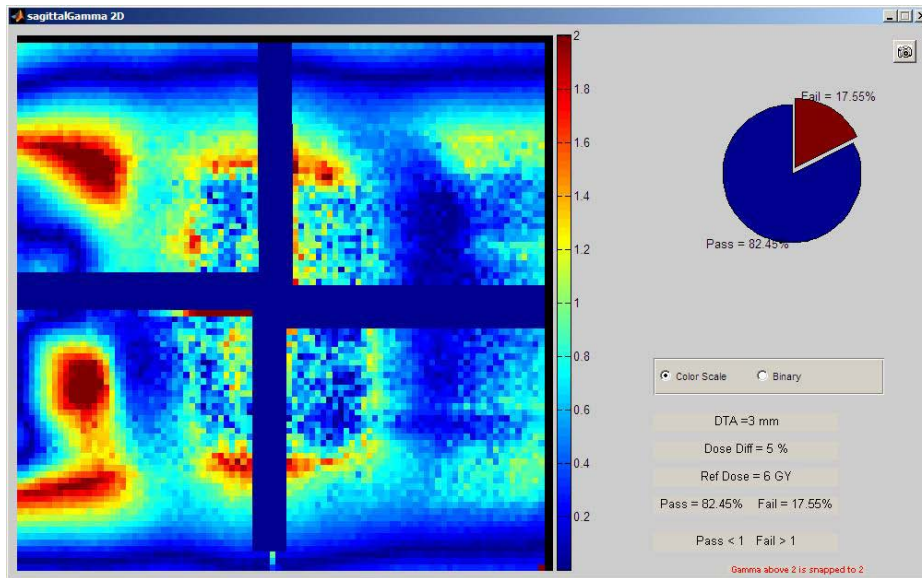


Figure 3.13 Plan 1a Trial 2 Sagittal Gamma Analysis

3.3.5.1.2 Plan 1b

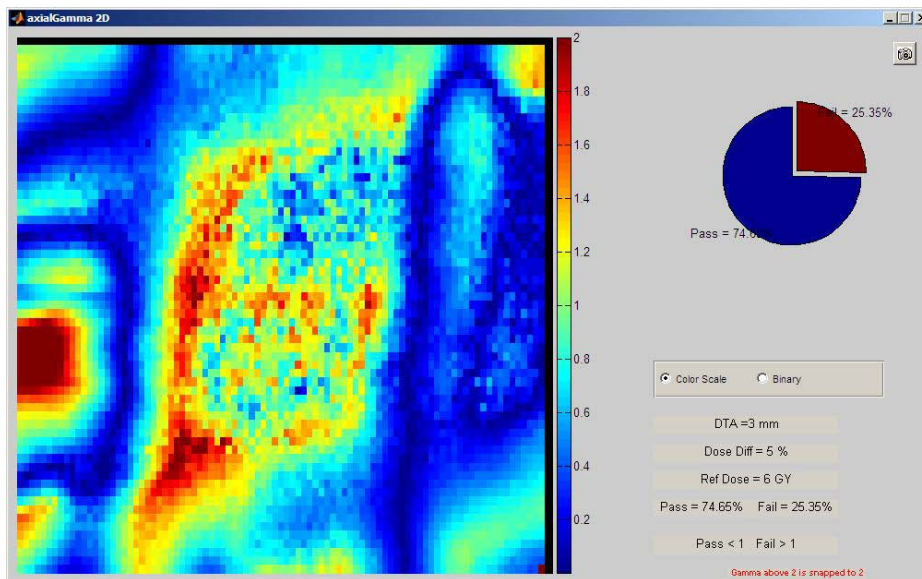


Figure 3.14 Plan 1b Trial 2 Axial Gamma Analysis

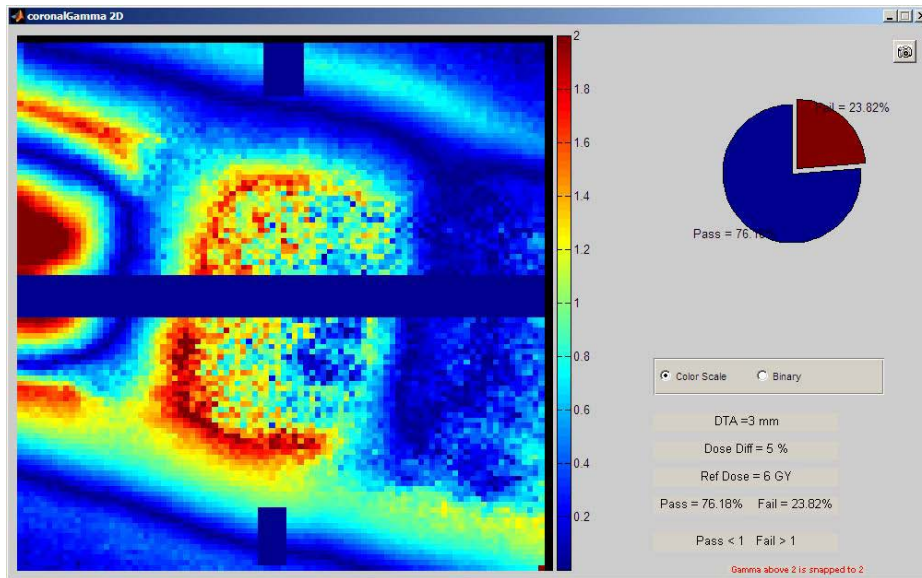


Figure 3.15 Plan 1b Trial 2 Coronal Gamma Analysis

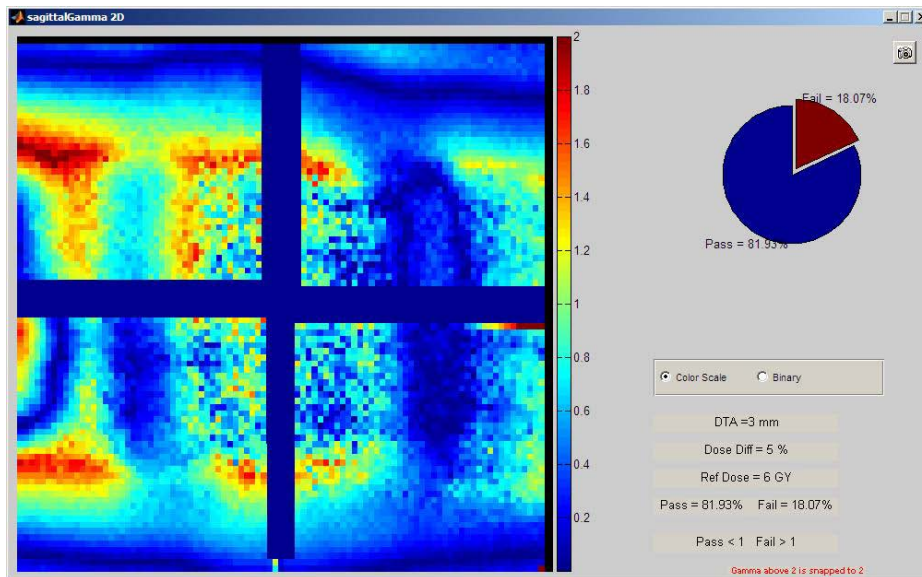


Figure 3.16 Plan 1b Trial 2 Sagittal Gamma Analysis

3.3.5.2 GAMMA ANALYSIS UTILIZING 5%/3MM GAMMA CRITERIA PVC CONTOURED

The gamma analysis for this section is performed utilizing the 5%/3mm criteria on the PVC Contoured Plan. Due to the large shift on the RLSP of the PVC shell as compared to the standard Eclipse curve, gamma analysis was performed to see if any difference would be seen from the Std. plan. The analysis for both Plan 1a and Plan 1b still show that a large percentage of pixels are failing the gamma criteria and no real statistical difference between the contoured and standard plans are visible. This result was surmised in Section 3.1.1, where the comparison of the calculated dose plans yielded very little difference from what was expected. Once again, the gamma analysis results for Plan 1b show an improvement over Plan 1a, with the most significant difference being seen in the axial film plane. These results are shown below in Table 17, and the screen captures of the gamma analysis are shown in Sections 3.3.5.2.1 and 3.3.5.2.2.

	Plan 1a				Plan 1b			
	Trial 1	Trial 2	Trial 3	Average	Trial 1	Trial 2	Trial 3	Average
Axial	55.56	59.72	55.56	56.95	65.59	74.16	75.80	71.85
Coronal	74.41	69.04	80.81	74.75	82.37	75.60	76.46	78.14
Sagittal	78.56	83.89	77.69	80.05	75.52	82.49	73.94	77.32
3P-Average	69.51	70.88	71.35	70.58	74.49	77.42	75.40	75.77

Table 17 Gamma analysis results for Plans 1a and 1b utilizing a 5%/3mm criteria (displayed in percentage passing) and a PVC contoured shell.

3.3.5.2.1 Plan 1a – PVC contoured

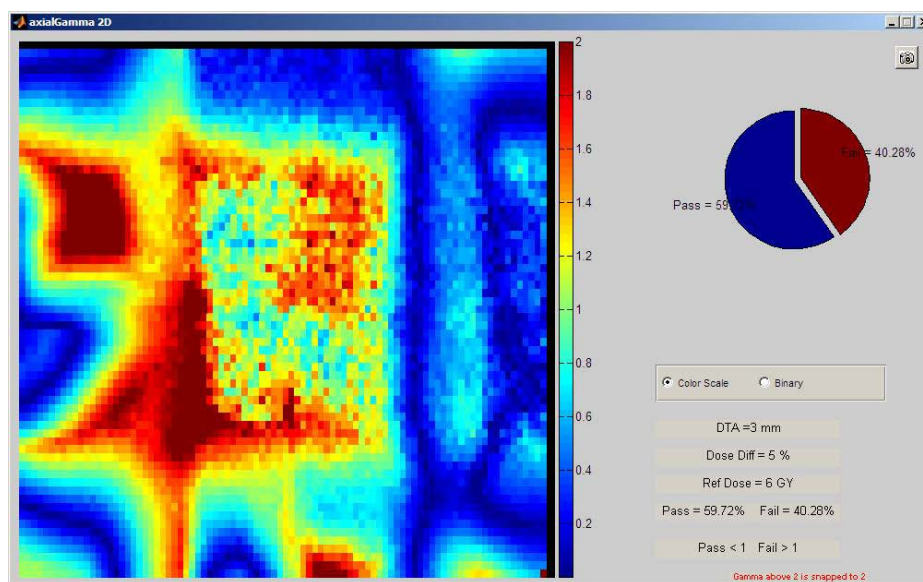


Figure 3.17 Plan 1a Trial 2 Axial Gamma Analysis with PVC Shell contoured and CT Number set to match Eclipse Calibration Curve

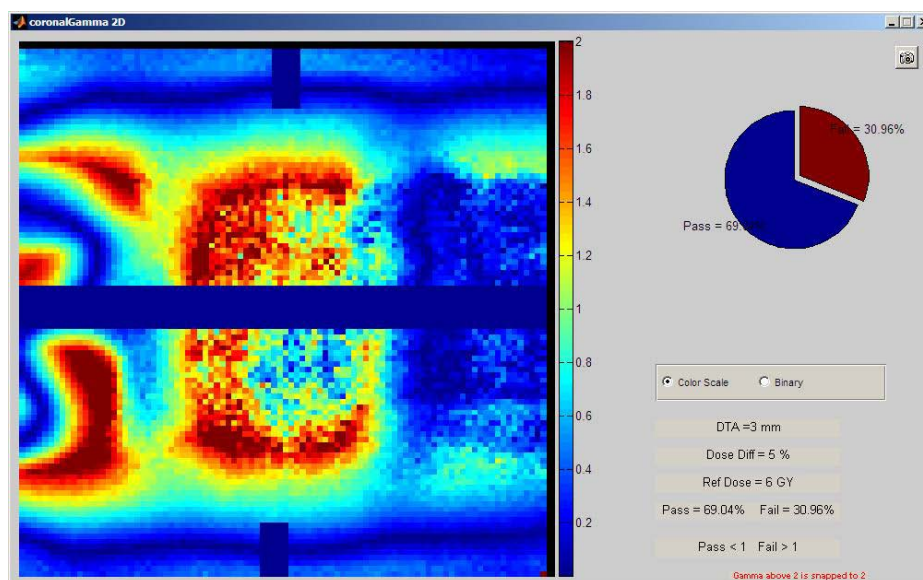


Figure 3.18 Plan 1a Trial 2 Coronal Gamma Analysis with PVC Shell contoured and CT Number set to match Eclipse Calibration Curve

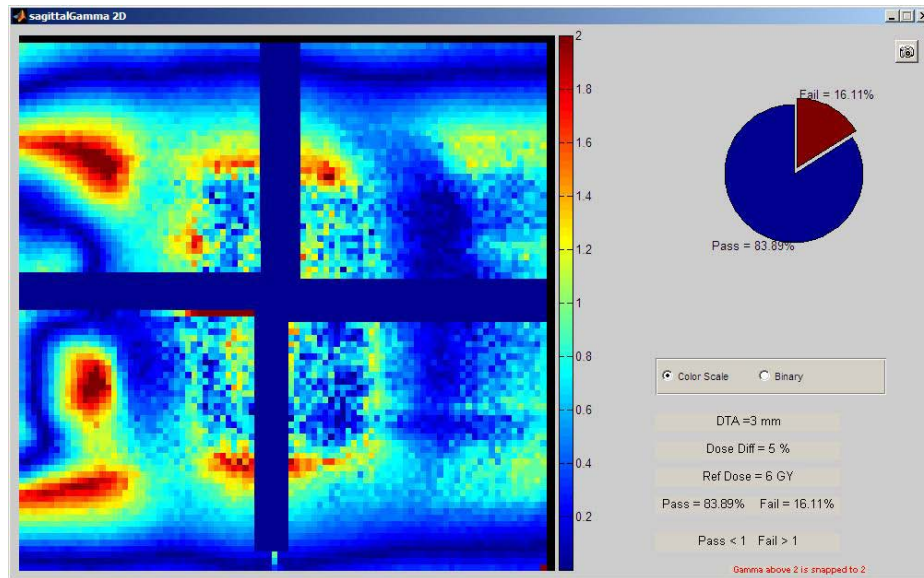


Figure 3.19 Plan 1a Trial 2 Sagittal Gamma Analysis with PVC Shell contoured and CT Number set to match Eclipse Calibration Curve

3.3.5.2.2 Plan 1b- PVC Contoured

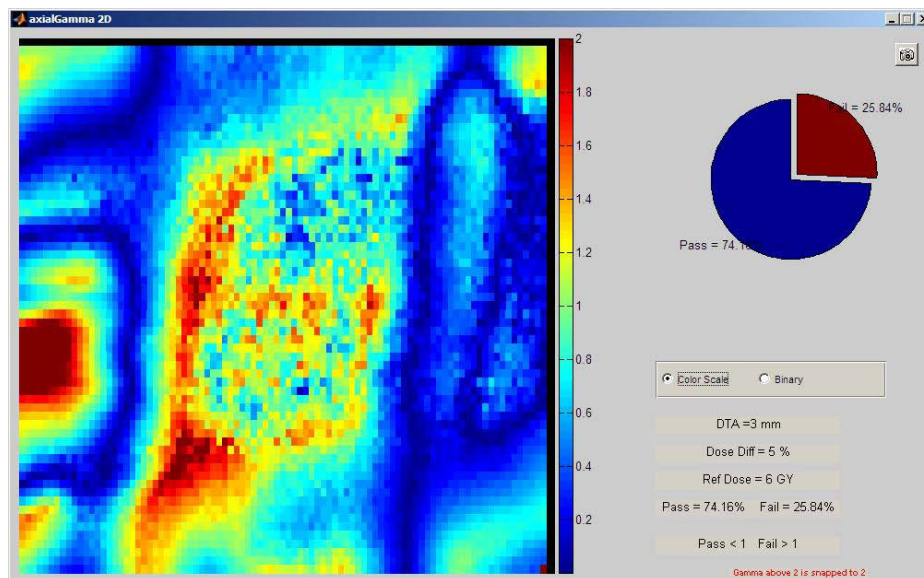


Figure 3.20 Plan 1b Trial 2 Axial Gamma Analysis with PVC Shell contoured and CT Number set to match Eclipse Calibration Curve

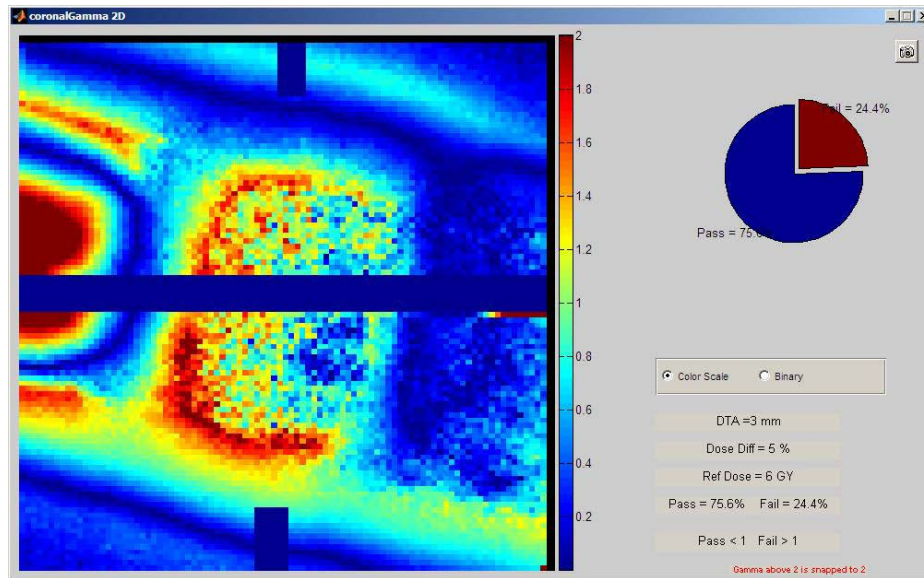


Figure 3.21 Plan 1b Trial 2 Coronal Gamma Analysis with PVC Shell contoured and CT Number set to match Eclipse Calibration Curve

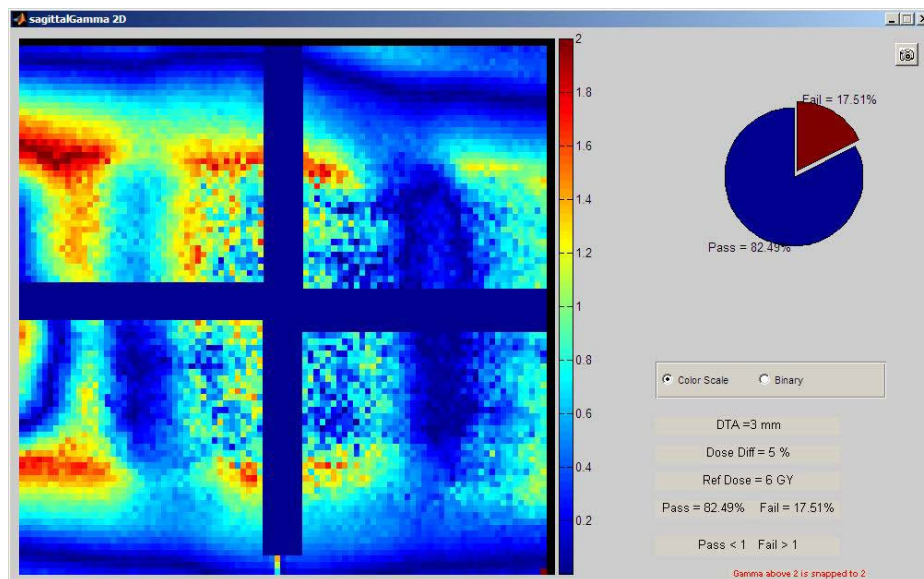


Figure 3.22 Plan 1b Trial 2 Sagittal Gamma Analysis with PVC Shell contoured and CT Number set to match Eclipse Calibration Curve

3.3.5.3 GAMMA ANALYSIS UTILIZING 5%/5MM GAMMA CRITERIA STANDARD PLAN

The gamma analysis for this section is performed utilizing the RPC guidelines of 5%/5mm criteria with 80% individual plane pass criteria, and 85% overall pass criteria, that are based on recommendations of the RTOG. Due to the results from the previous section, only the Std. Plan was analyzed using these criteria, as the contouring of the PVC shell did not introduce any significant improvements to the gamma analysis. The analysis for both Plan 1a and Plan 1b show a much higher percentage of pixels are now passing the gamma criteria, as to be expected with a change of the DTA from 3mm to 5mm. The gamma analysis results for Plan 1b show an improvement over Plan 1a, with the most significant differences being seen in the axial plane with up to a 14.02% improvement. Following the pass criteria set forth by the RPC, all 3 trials for Plan 1b would be classified as passing, by a wide margin. These results are shown below in Table 18, and the screen captures of the gamma analysis are shown in Sections 3.3.5.3.1 and 3.3.5.3.2.

	Plan 1a				Plan 1b			
	Trial 1	Trial 2	Trial 3	Average	Trial 1	Trial 2	Trial 3	Average
Axial	73.56	74.70	72.51	73.59	85.70	87.95	86.53	86.73
Coronal	86.64	84.41	90.45	87.17	92.21	88.68	89.01	89.97
Sagittal	91.03	92.81	88.50	90.78	89.00	93.11	88.26	90.12
3P-Average	83.74	83.97	83.82	83.85	88.97	89.91	87.93	88.94

Table 18 Gamma analysis results for Plans 1a and 1b utilizing a 5%/5mm criteria (displayed in

percentage passing)as established by the RPC based on RTOG recommendations.

3.3.5.3.1 Plan 1a

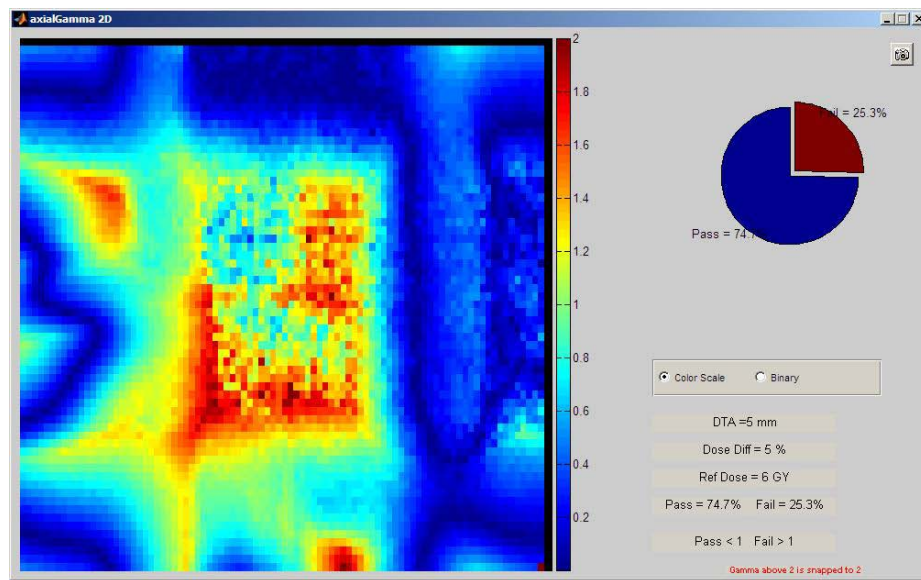


Figure 3.23 Plan 1a Trial 2 Axial Gamma Analysis 5%/5mm

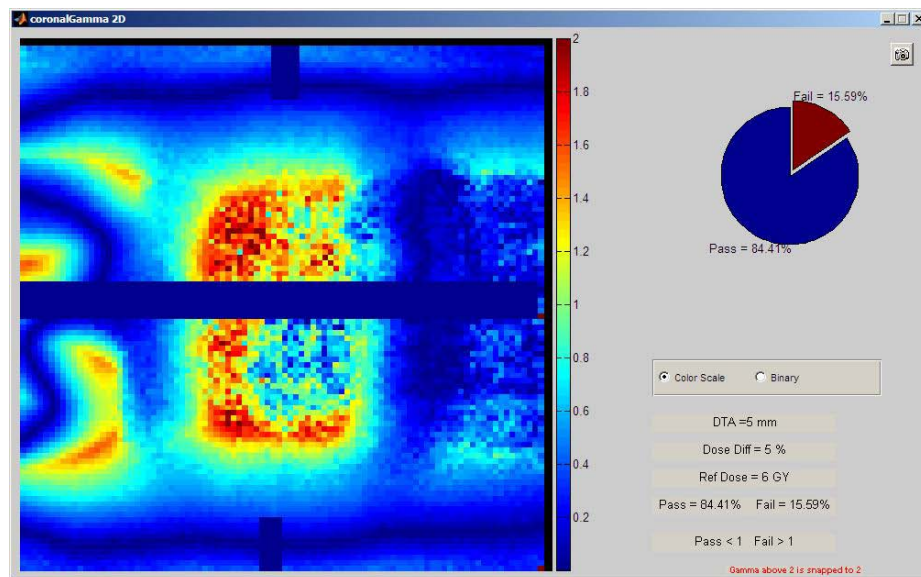


Figure 3.24 Plan 1a Trial 2 Coronal Gamma Analysis 5%/5mm

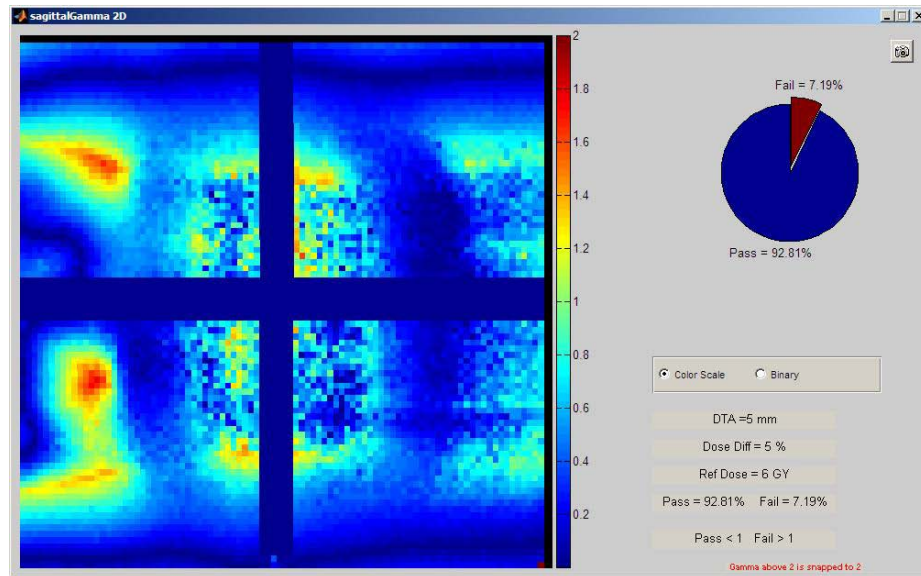


Figure 3.25 Plan 1a Trial 2 Sagittal Gamma Analysis 5%/5mm

3.3.5.3.2 Plan 1b

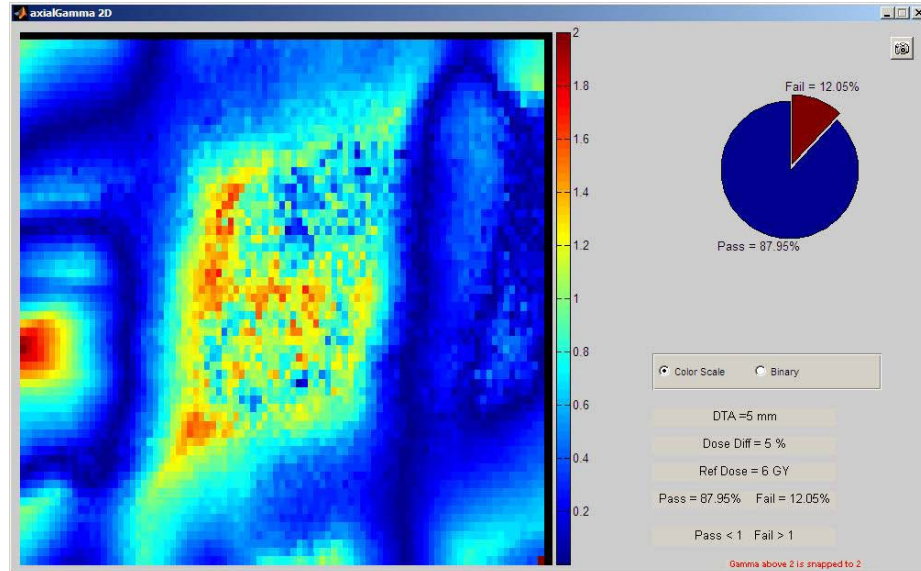


Figure 3.26 Plan 1b Trial 2 Axial Gamma Analysis 5%/5mm

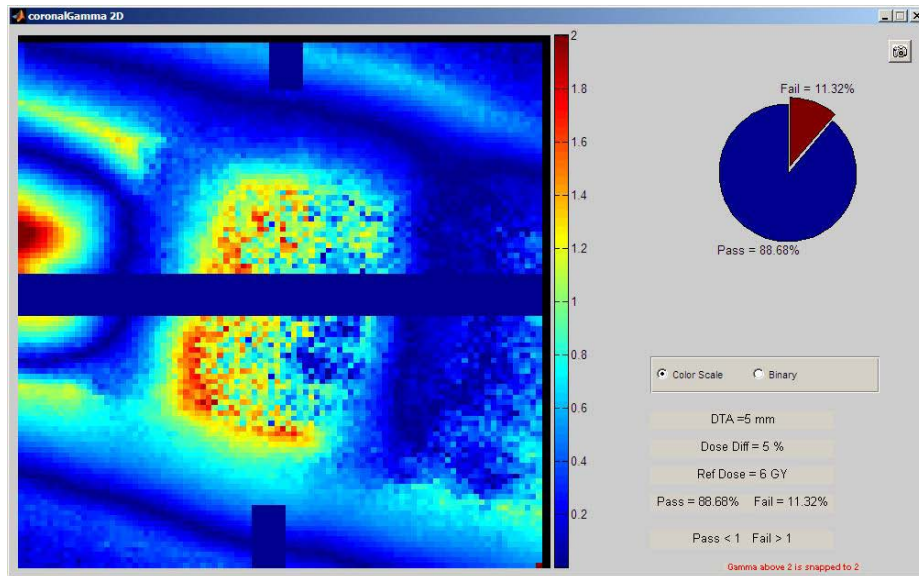


Figure 3.27 Plan 1b Trial 2 Coronal Gamma Analysis 5%/5mm

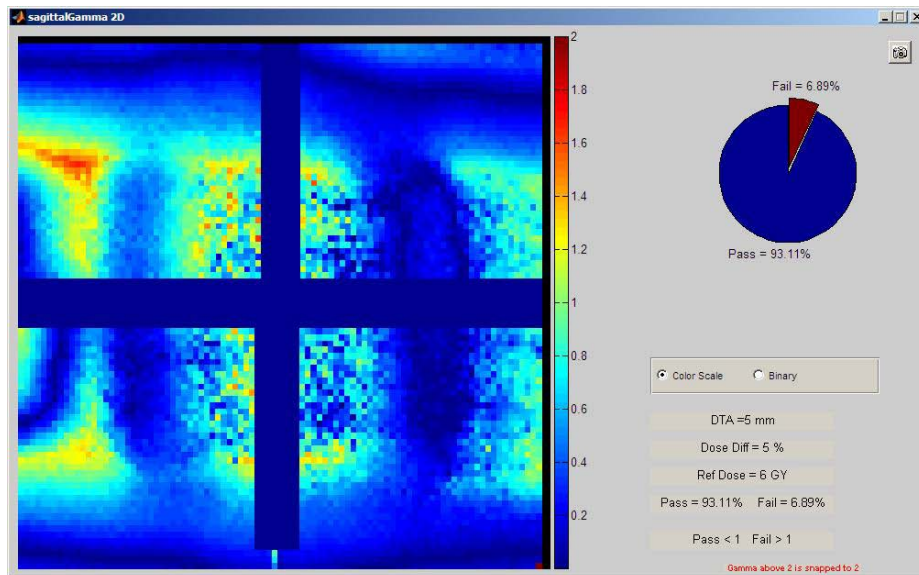


Figure 3.28 Plan 1b Trial 2 Sagittal Gamma Analysis 5%/5mm

3.3.6 DTA PROFILE COMPARISONS

As the gamma analysis takes into account all pixels over the desired area, including the extra dose “horns,” dose profiles were taken through the central region of the tumor target for all plans and then compared to the corresponding TPS data. A linear regression was applied to the sides of

each profile to calculate the distance to agreement of the film to the TPS. Due to the complex nature of the beams the dose levels from which the regression was applied varied both by plan, film plane, and profile direction. These values are shown in Table 19.

		Plan 1a	Plan 1b
Axial	Right Left Profile		
	Patient Right	80%-30%	80%-20%
	Patient Left	80%-60%	80%-60%
	Anterior Posterior Profile		
	Posterior	80%-40%	80%-20%
	Anterior	80%-60%	80%-60%
Coronal	Right Left Profile		
	Patient Right	80%-30%	80%-20%
	Patient Left	80%-60%	
	Superior Inferior Profile		
	Superior	80%-20%	80%-20%
	Inferior		
Sagittal	Anterior Posterior Profile		
	Posterior	80%-40%	80%-20%
	Anterior	80%-50%	80%-50%
	Superior Inferior Profile		
	Superior	80%-20%	80%-20%
	Inferior		

Table 19 Dose levels for linear regressions utilized to calculate DTA

For the following DTA figures, the profile taken from the Eclipse TPS will be shown in blue and designated TPS on the graphs. The Film data will be shown in red and is designated film dose on the graphs. Some of the film curves will show a drop at the origin, which is related to the film slots being cut into the film in the sagittal and coronal films that slows them to interlock, and therefore no dose was recorded in that region.

3.3.6.1 PLAN 1A

Treatment Plan 1a trial 2 had all 3 film planes analyzed for DTA. The first film analyzed is the axial film. Both the Anterior posterior and right left profiles are directly in parallel with the beam

with the entrance of the beam coming from the anterior side and the patient left side. Looking at the Anterior Posterior profile, Figure 3-29, first reveals that there is a 4.9mm average distance over the specified dose levels on the posterior side of the profile, which corresponds to the distal end of the beam. In Figure 3-30, the Right left profile shows an average of 5.8mm difference over the dose levels on the distal end of the treatment beam.

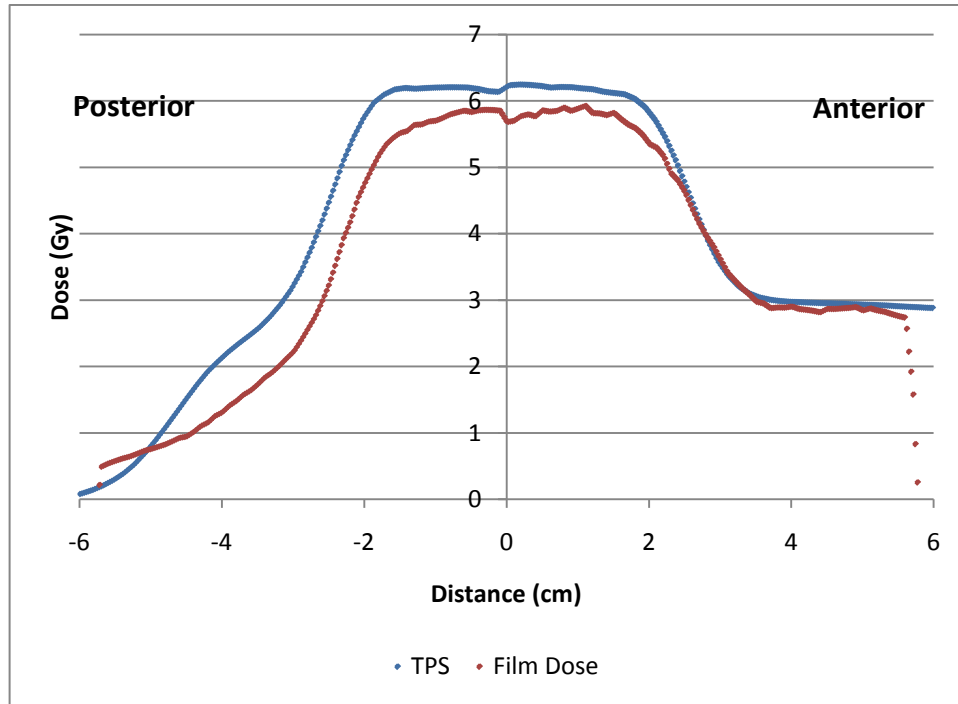


Figure 3.29 Plan 1a Trial 2 Anterior Posterior Profile Axial Plane

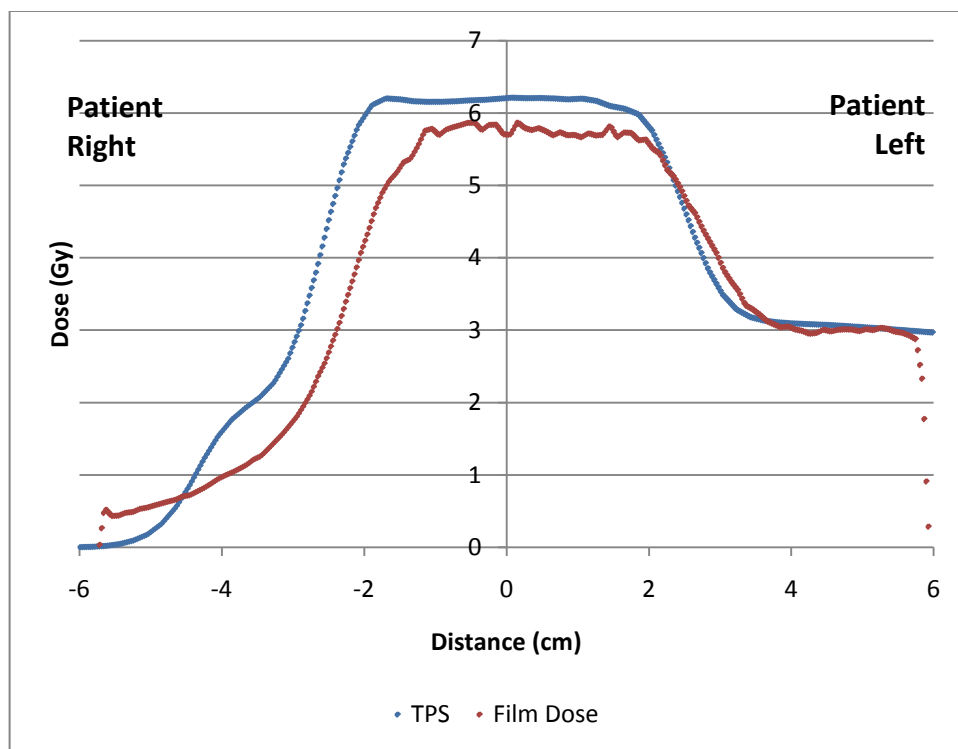


Figure 3.30 Plan 1a Trial 2 Right Left Profile Axial Plane

Depending on the complexity of the interfaces and the position of the detector, the distal edge differences could range from 2mm to 8mm at 80% dose levels (Urie, et al. 1986). Compounding this with the LET effect on the distal edge of the film, and with the protons streaming directly down the film plane, these DTA's were expected to be large.

The profiles drawn across the Coronal planes can be seen in Figure 3-31 and Figure 3-32. for the Coronal plane the superior inferior direction is not directly oriented with the beam path, and therefore no real degradation due to LET or Distal edge degradation should be seen. The DTA for the superior and inferior sides are 1.6 and 1.1mm respectively. The Right left profile, which is in line with one of the treatment fields once again shows a larger DTA with 2.0mm on the patient right side, which corresponds with the distal edge of the beam.

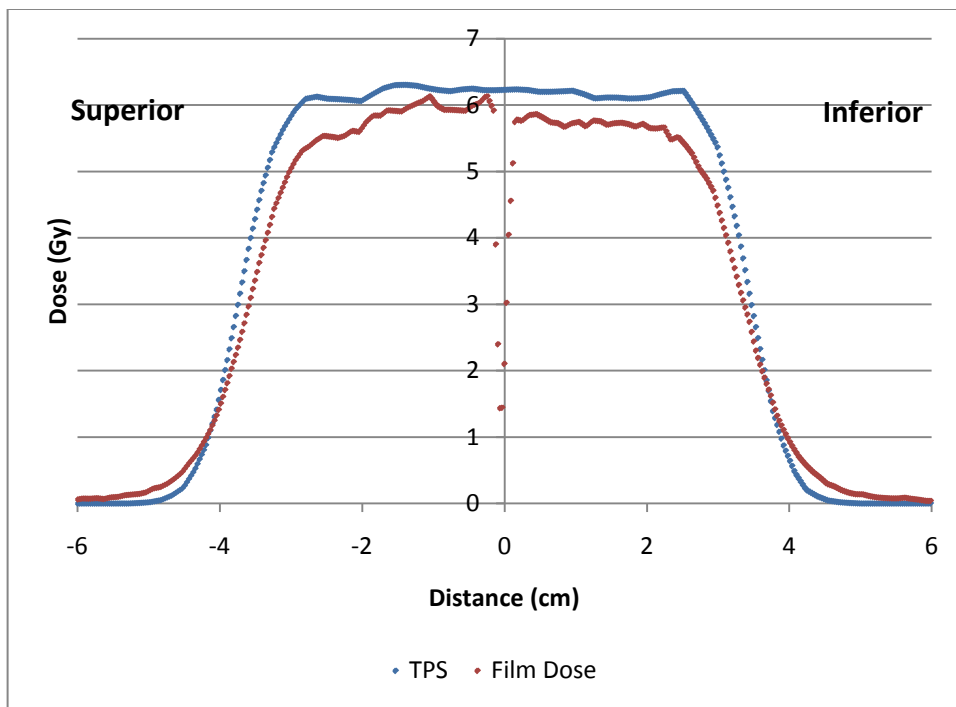


Figure 3.31 Plan 1a Trial 2 Superior Inferior Profile Coronal Plane

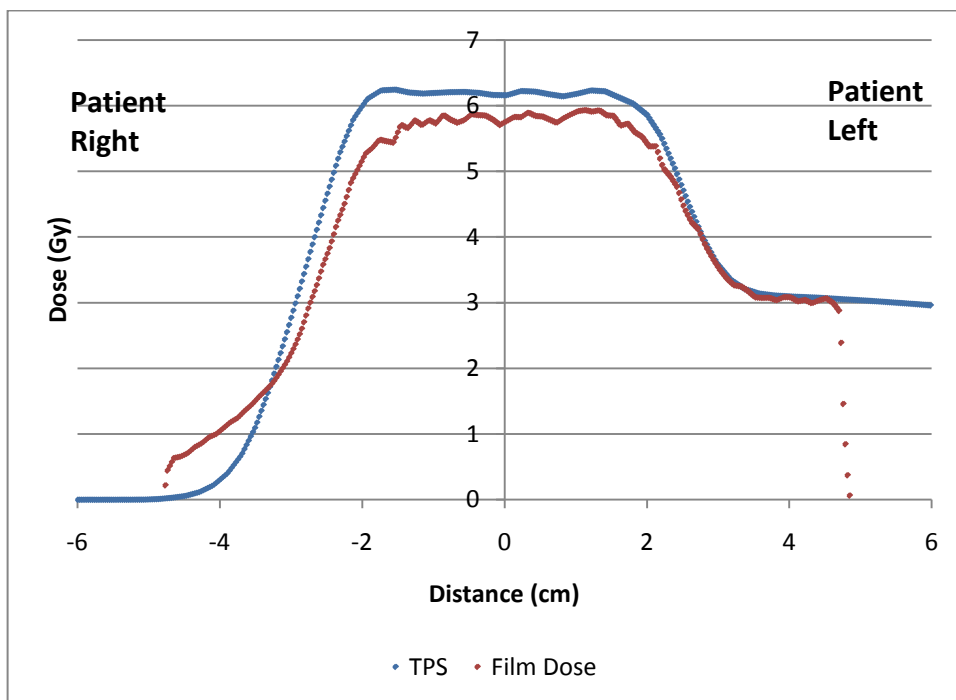


Figure 3.32 Plan 1a Trial 2 Right Left Profile Coronal Plane

The sagittal films are very similar to the coronal films. The anterior posterior profile, Figure 3-33, which is in line with one of the treatment fields, showed a DTA of 2.5mm on the posterior (distal) end of the beam, where the superior and inferior sides of Figure 3-34 are 1.2mm and 1.0mm respectively. The remaining DTA analysis for the other two trials of Plan 1a, as well as a summary of the DTA results, is located in the appendix.

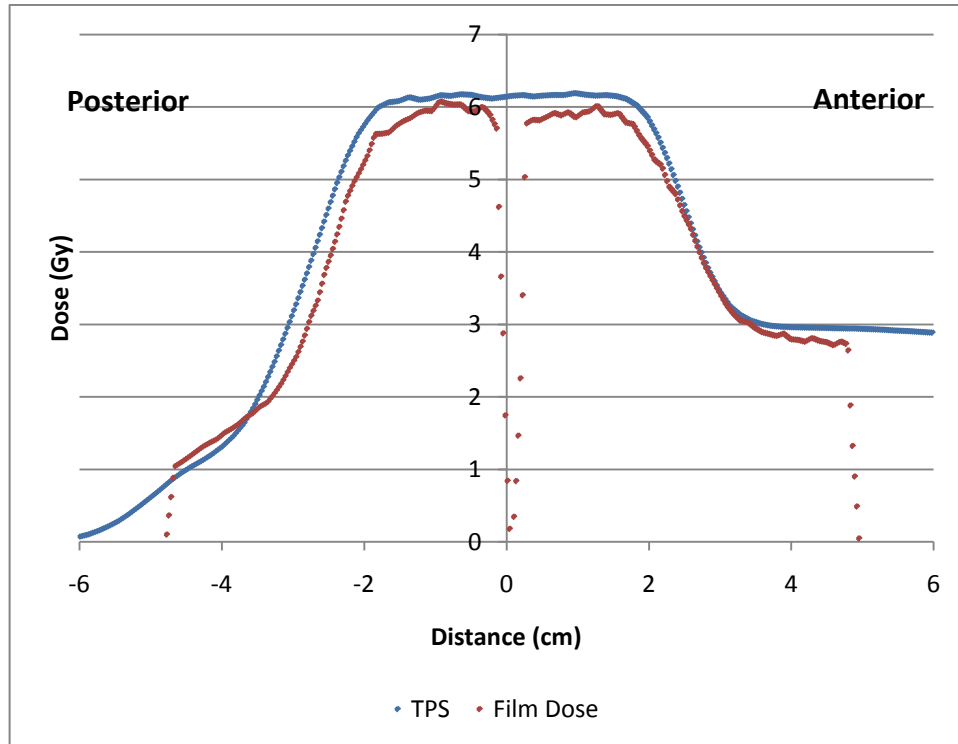


Figure 3.33 Plan 1a Trial 2 Anterior Posterior Profile Sagittal Plane

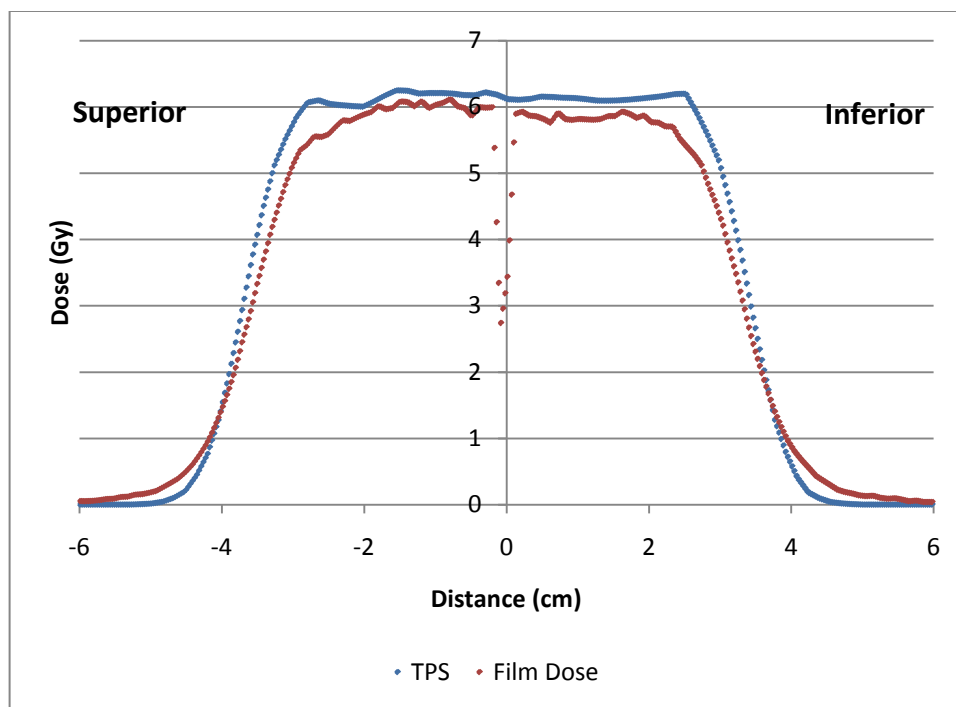


Figure 3.34 Plan 1a Trial 2 Superior Inferior Profile Sagittal Plane

Comparing the averages of the three trials, and utilizing the pass fail criteria of 3mm from the hypothesis, the only failing points come from the distal ends of the axial film profiles, shown below in red in Table 20 Plan 1a DTA data averaged over 3 trials.

Plan 1a DTA Averages				
Axial	Right Left Profile		Anterior Posterior Profile	
	Patient Right	5.3	Posterior	5.6
	Patient Left	1.2	Anterior	0.2
Coronal	Right Left Profile		Superior Inferior Profile	
	Patient Right	1.5	Superior	1.3
	Patient Left	0.6	Inferior	1.1
Sagittal	Anterior Posterior Profile		Superior Inferior Profile	
	Posterior	2.0	Superior	1.0
	Anterior	0.9	Inferior	1.4

Table 20 Plan 1a DTA data averaged over 3 trials

3.3.6.2 PLAN 1B

The same DTA analysis was performed for the films taken from Plan 1b. We would expect to see an improvement in DTA's due to the film channels being offset from the beam paths, and there being a 15 degree couch kick removing the axial film from being directly in line with either field. Analysis of the axial films for Plan 1b trial 2 first reveals that there is a 2.3mm average distance over the specified dose levels on the posterior side of the profile in Figure 3-35, which is drawn through the intersection of the beams, therefore the posterior edge of the profile is composed of regions taken from the lateral sides of the beam from each field, and not entirely from the distal end of the beams. In Figure 3-36, the right left profile shows an average of 1.4mm difference with the largest values coming from around the 80% dose level region. The uptick on the tail of the Patient right side profile is due to the dose overshoot of the dose "horns" and the beam located at 80 degrees.

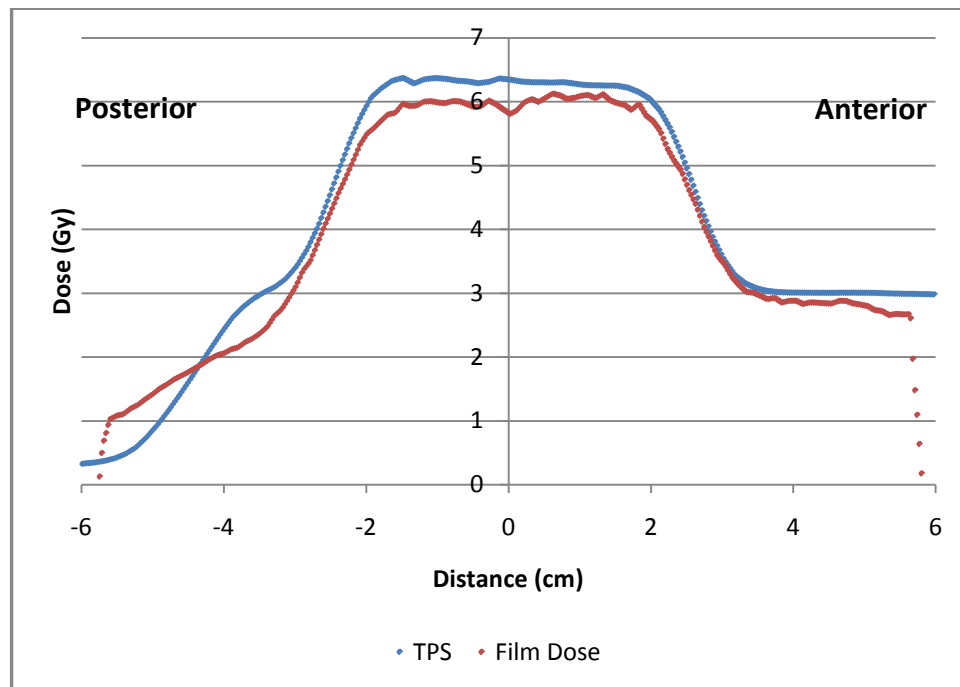


Figure 3.35 Plan 1b Trial 2 Anterior Posterior Profile Axial Plane

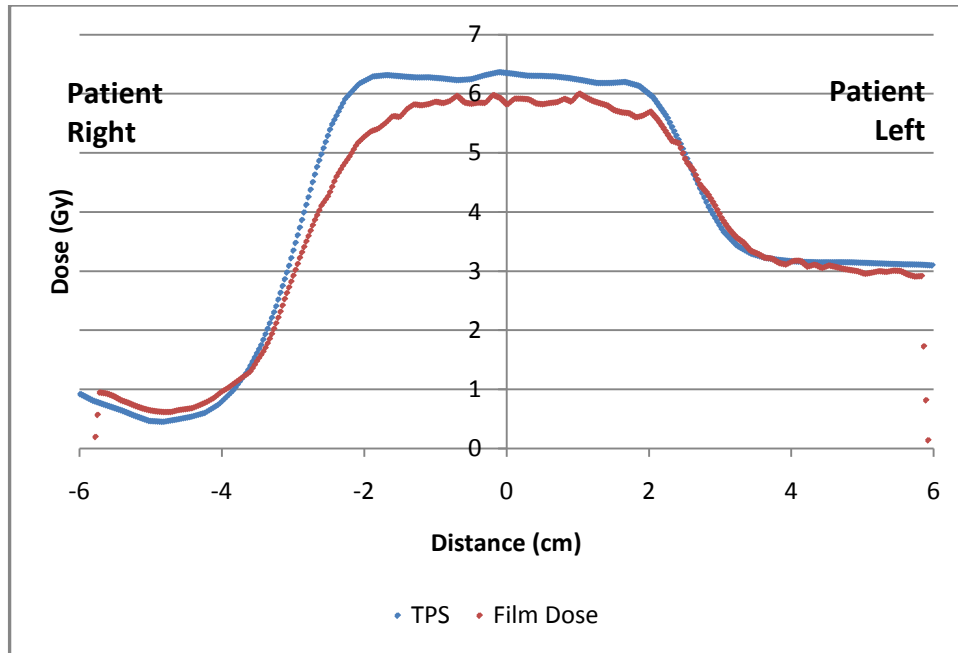


Figure 3.36 Plan 1b Trial 2 Right Left Profile Axial Plane

The film for the coronal plane shows similar results to the one from the orthogonal beam plan, in regards to the superior inferior direction. This was also expected as this plane is not directly oriented with the beam path, and therefore no real degradation due to LET or Distal edge degradation should be seen. The DTA for the superior and inferior sides are 2.3mm and 0.2mm respectively, shown in Figure 3-37. The Right left profile, Figure 3-38, shows an average DTA over the dose region with 0.9mm on the patient right side, exhibiting the same crossover effect seen in the *Urie, 1986* paper. (Urie, et al. 1986)

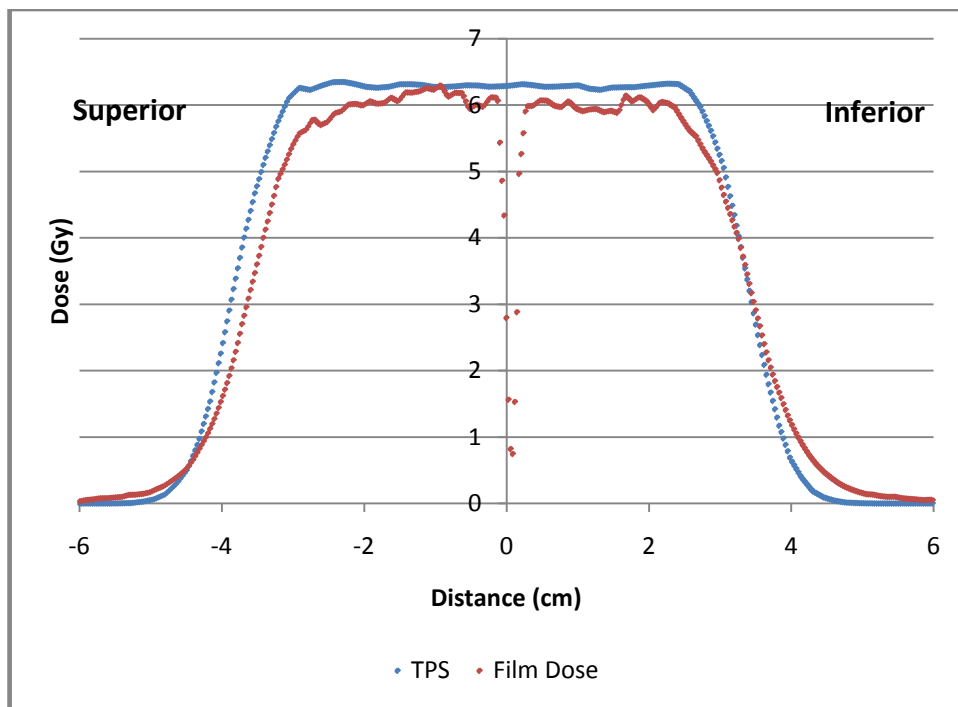


Figure 3.37 Plan 1b Trial 2 Superior Inferior Profile Coronal Plane

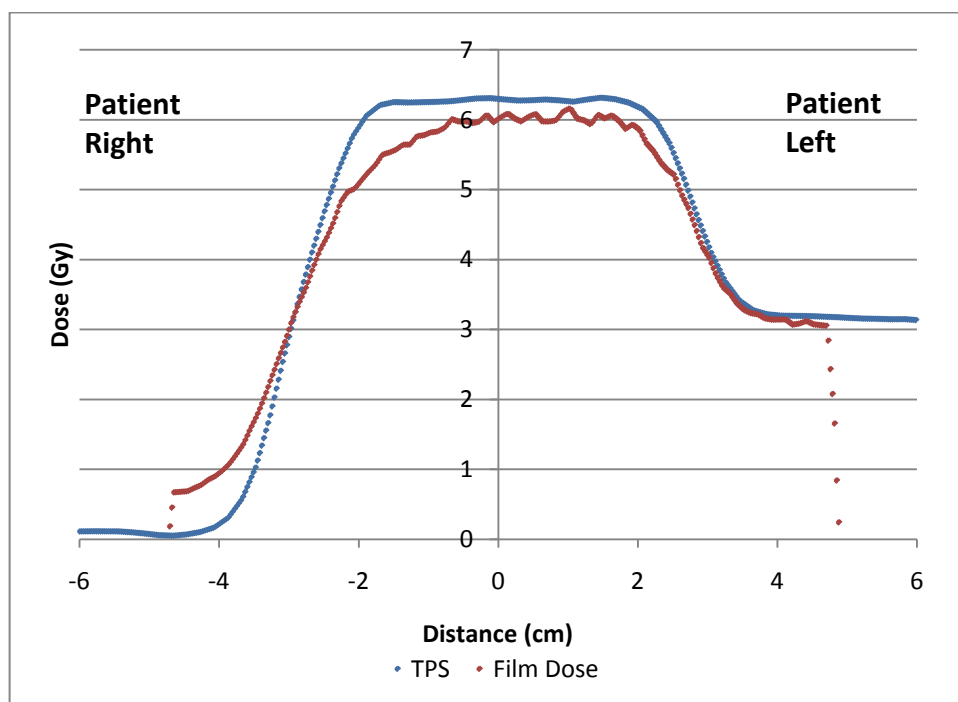


Figure 3.38 Plan 1b Trial 2 Right Left Profile Coronal Plane

The film for the sagittal plane is very similar to the coronal film. The Anterior posterior profile, Figure 3-39, showed a DTA of 2.4mm on the posterior side of the profile, where the superior and inferior sides of Figure 3-40 are 1.1mm and 0.8mm respectively. The remaining DTA analysis for the other two trials of Plan 1b, as well as a summary of the DTA results, is located in the Appendix.

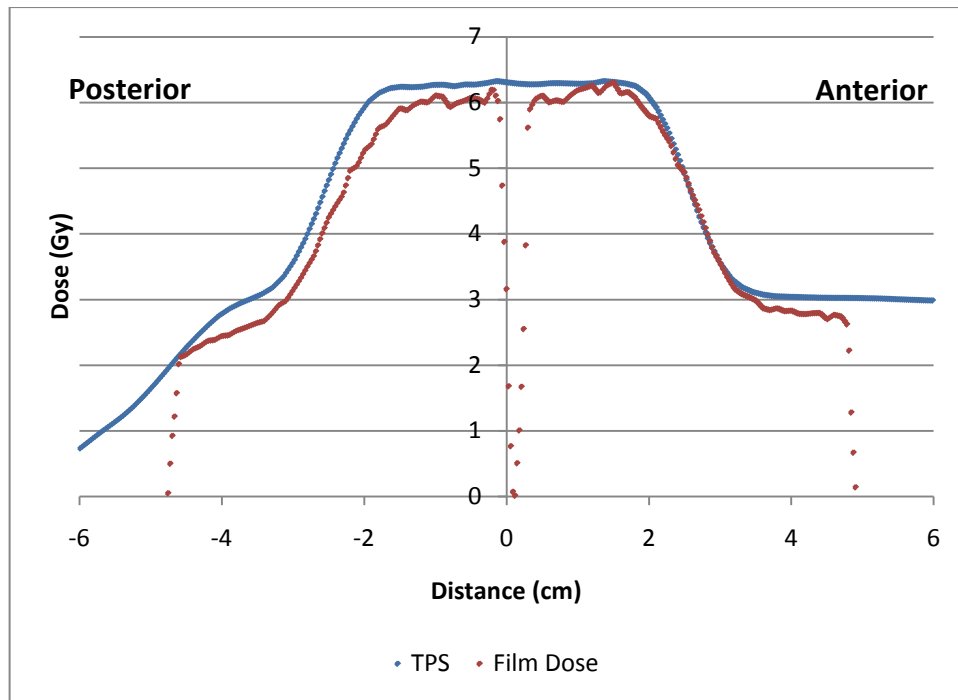


Figure 3.39 Plan 1b Trial 2 Anterior Posterior Profile Sagittal Plane

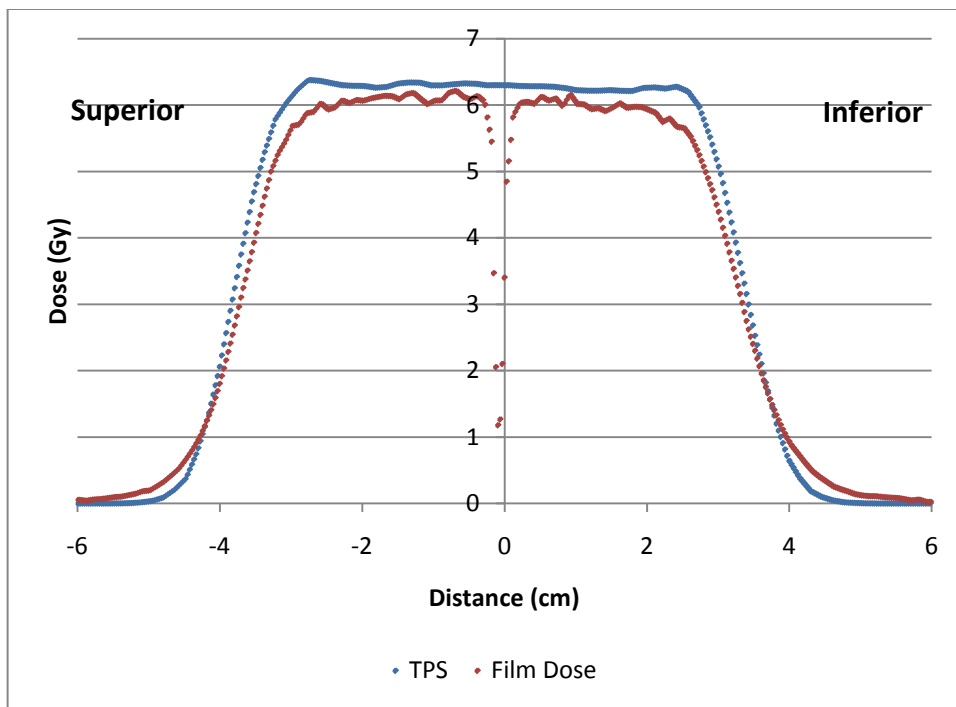


Figure 3.40 Plan 1b Trial 2 Superior Inferior Profile Sagittal Plane

Comparing the averages of the three trials for Plan 1b, and utilizing the pass fail criteria of 3mm from the hypothesis, shown in Table 21, has no failures.

Plan 1b DTA Averages				
Axial	Right Left Profile		Anterior Posterior Profile	
	Patient Right	2.4	Posterior	2.3
	Patient Left	1.7	Anterior	0.9
Coronal	Right Left Profile		Superior Inferior Profile	
	Patient Right	0.4	Superior	1.8
	Patient Left	0.5	Inferior	0.6
Sagittal	Anterior Posterior Profile		Superior Inferior Profile	
	Posterior	1.9	Superior	1.7
	Anterior	0.6	Inferior	1.0

Table 21 Plan 1b DTA averaged over 3 trials

The only individual failure is on the axial film of trial 1, which appears to be misaligned as evident by the right left profile, shown in Figure 3-41. This is entirely possible as the axial film is

pricked by hand and is only aligned by the phantom alignment notch, which might cause the film to rotate when compression is applied. For all 6 trials of the two plans of the phantom, this only occurred this one time Subtracting the offset of 3.5mm from the patient left side from the 4.7mm of the patient right side, would give a passing value of 1.2mm.

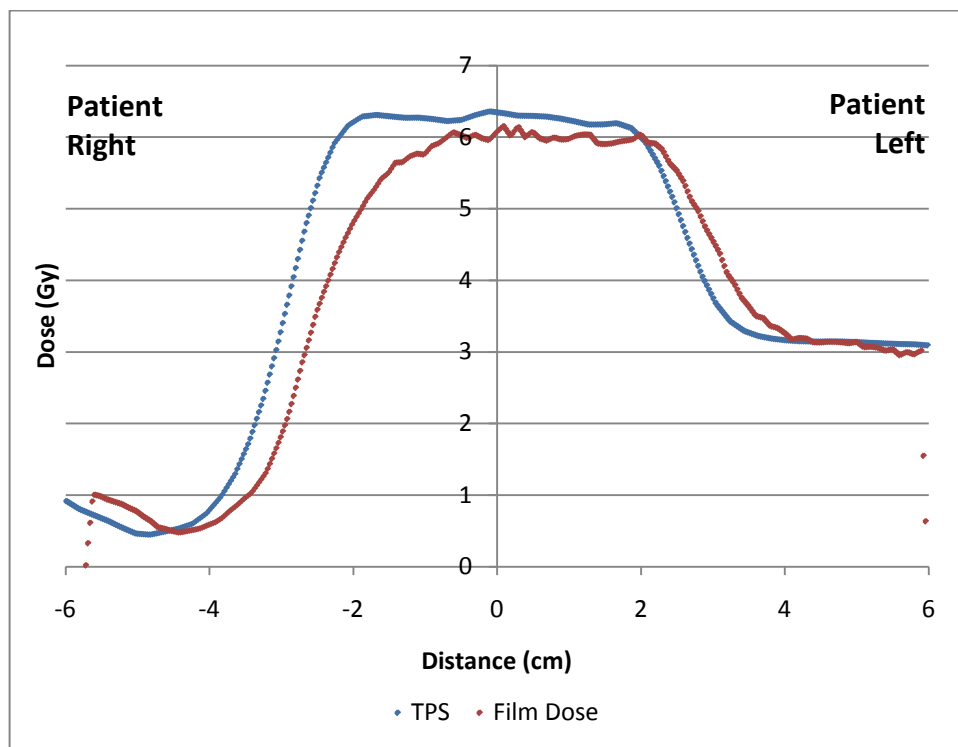


Figure 3.41 Plan 1b Trial 1 Right Left Profile Axial Plane

CHAPTER 4: CONCLUSIONS

4.1 Summary

This project was intended to design and test a proton equivalent lung insert that could be used inside the existing RPC Thorax phantom to allow for auditing of proton lung therapy treatment procedures. The guidelines set forth in the hypothesis for this were to have no more than a 5%/3mm difference between the measured dose and the calculated dose with a reproducibility of 5%.

Selecting a proton equivalent material and designing a new insert was the first part of this project. Relative stopping powers, physical density, and HU's of existing materials were evaluated, and extra heavy balsa wood, a material with comparable density and HU, was selected. The relative stopping power of the balsa was measured to be 0.313 and compared favorably with the calibrated HU-RLSP curve that is used by the Eclipse treatment planning system at the PTC-H. A treatment plan was then developed and the Phantom was treated utilizing two different plans.

The LET of film based on orientation was then tested by submersing film both parallel and perpendicularly in a water phantom. Parallel film irradiation was explored utilizing two different methods of film alignment. A 24.3% difference between the original method and the alternate method was observed and probably was related to beam malfunctioning. When compared to the ion chamber readings, both parallel and perpendicular orientations displayed a quenching effect underperforming the ion chamber, with the alternate parallel orientation showing an average 31.0 % difference and the perpendicular showing an average of 14.7% difference.

The phantom was simulated using a free breathing technique common to all lung patients at M. D. Anderson. The first plan consisted of treatment fields at orthogonal angles, 0 and 90 degrees, with a 0 degree couch kick. This was put in place to verify if there would be noticeable differences due to distal edge degradation with the film channels in the insert parallel to the treatment fields. The second plan consisted of two beams at 10 and 80 degrees, with a couch kick of -15 degrees, thereby

placing all of the film channels at orientations that ensure no parallel artifacts might be present. Both plans were developed to mimic treatment plans on patients, and as such the compensators were smeared by 6mm and the apertures were expanded by 10mm. Both of the plans were then scaled to deliver 200 cGy to the tumor target for 1 fraction. The phantom was then irradiated 3 times for each plan for a total dose to the tumor target of 600 cGy.

A separate plan was then created to see if contouring and setting the PVC shell to a value that corresponds with the HU-RLSP curve from Eclipse would show improvement. Since the shell in that region is only 6.35 mm thick, the HU number was changed and due to the increased treatment area caused by the smearing and expansion of the compensators and apertures, it did not result in any difference when the beam parameters were calculated. A comparison of the two plans showed that no pixels were different with a 5%/3mm gamma criteria. Gamma analysis was then performed utilizing the Contoured PVC dose plan, and no noticeable differences were found.

For both plans the TLD values of the PTV region were within 7% of the dose calculated by Eclipse. The gamma analysis for Plan 1a at the 5%/3mm criteria, revealed individual plane passing percentages much lower than 80%, which was expected due to the alignment of the film and the beams. The average of the three plane averages was 71% for Plan 1a. The gamma analysis for Plan 1b showed better results for each individual plane, even though they also were less than the 80% suggested by the pass criteria. The averages for the individual planes ranged from 72% to 78% with the average of the three plane average having a passing rate of 76%. The plans were then compared utilizing the RPC conventional Lung treatment guidelines set forth by the RTOG, 5%/5mm, with 80% pass rate per plane and an overall pass rate of 85%. Utilizing this criteria Plan 1b was passing for all 3 trials, with an average of the three plane average of 89%. Plan 1a, however, failed the individual plane criteria even at the lower criteria.

Evaluating the DTA using 2D profiles gives a better picture of what is happening in the gamma analysis. Looking at the profiles drawn parallel to the treatment fields shows there is not just a dependence on the LET of the film due to quenching, but also because of distal edge degradation. The overall poor comparison of the film with the plan is primarily caused by the TPS's inability to accurately account for the inhomogeneities of the phantom materials.

4.2 Conclusions

The hypothesis of this project was to modify the existing RPC thorax phantom for usage in proton beams. Based on the design of the new phantom insert and the properties of protons, it is recommended that when the treatment plans are created for evaluation, that the beams need to be placed in orientations that are not parallel to the film channels. This can be accomplished by placing the beams at 10 degrees and 80 degrees, or by placing them at orthogonal angles such as 30 and 120 degrees, being careful not to allow the couch to enter the path of the beam.

The pass criteria set forth in the hypothesis was 5%/3mm with 5% reproducibility, however pass rates were not stipulated. The reproducibility of dose to the tumor site, as displayed by the TLD readings is under 7%. However, when applying the pass rates of an 80% for each single plane, and a 85% overall pass rate to a patient equivalent plan where the smearing and expansion of the compensators and apertures, this pass criteria cannot be met. At this point we do not know if the failure is caused by the inadequacy of the TPS or a failure of the dosimetry system. The failure of the dosimetry system could be due to a combination of the effects of LET on the film, distal edge degradations caused by inhomogeneities of the phantom, and by dose "horns" introduced by the patient equivalent plan, that cause multiple pixel failures downstream of the tumor target. However, when utilizing the existing criteria set forth by the RTOG for photons of 5%/5mm at 80% pass for each single plane, and a 85% overall pass rate is achievable on a patient equivalent plan, as long as the beams are placed correctly..

At this time, when utilizing a patient equivalent plan either the pass rates should be lowered or the phantom should be treated utilizing a tighter PTV that does not allow for smearing and expansion that is traditionally performed on patient exams. Either of these recommendations should allow for the effective evaluation of proton therapy treatment procedures for lung tumors. Further studies could verify that a treatment plan with a tighter PTV can pass at a 5%/3mm with standard pass rates.

4.3 Future Work

The thorax phantom with the modified imaging/dosimetry insert can be an extremely valuable tool for use in evaluating proton therapy procedures. Utilizing a motion sled, existing patient equivalent techniques could be utilized to verify motion gating. Also developing and treating a plan with a tighter PTV to verify passing conditions without the presence of dose overshoot could be evaluated. As for improvements to the insert, applying some type of secondary alignment notch could prevent possible slippage of the axial film, which likely caused the only failure in DTA profiles for Plan 1b.

CHAPTER 5: APPENDIX

5.1 Gamma Analysis – 5%/3mm

5.1.1 PLAN 1A

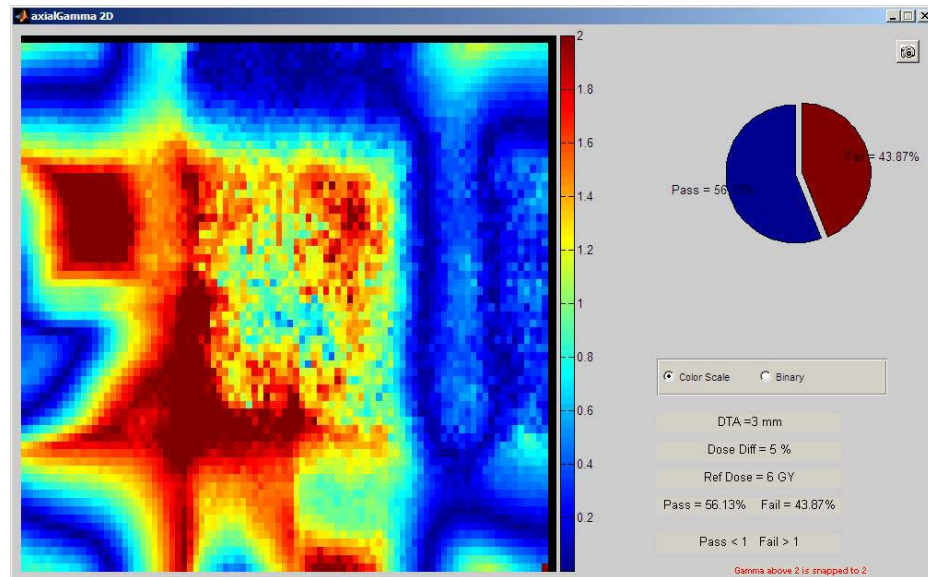


Figure 5.1 Plan 1a Trial 1 Axial Gamma Analysis

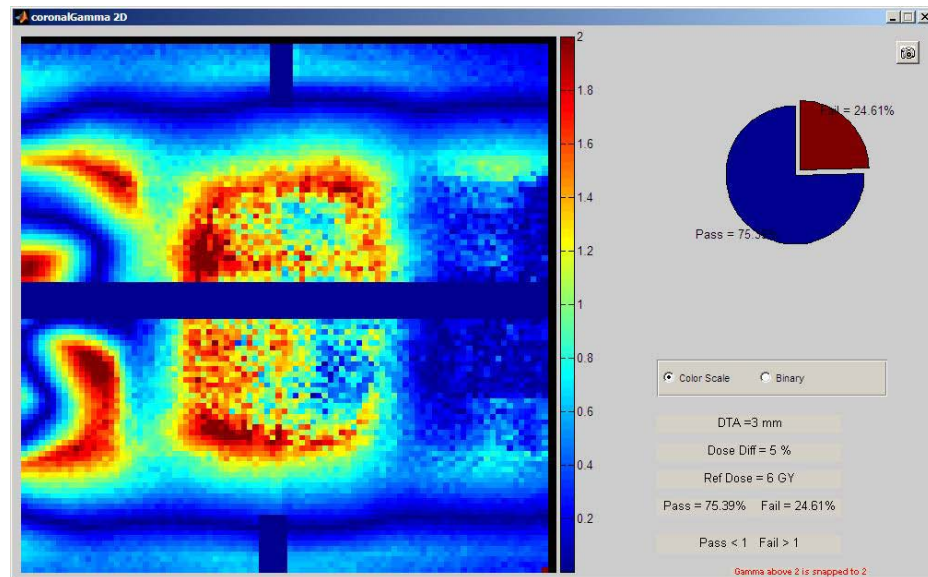


Figure 5.2 Plan 1a Trial 1 Coronal Gamma Analysis

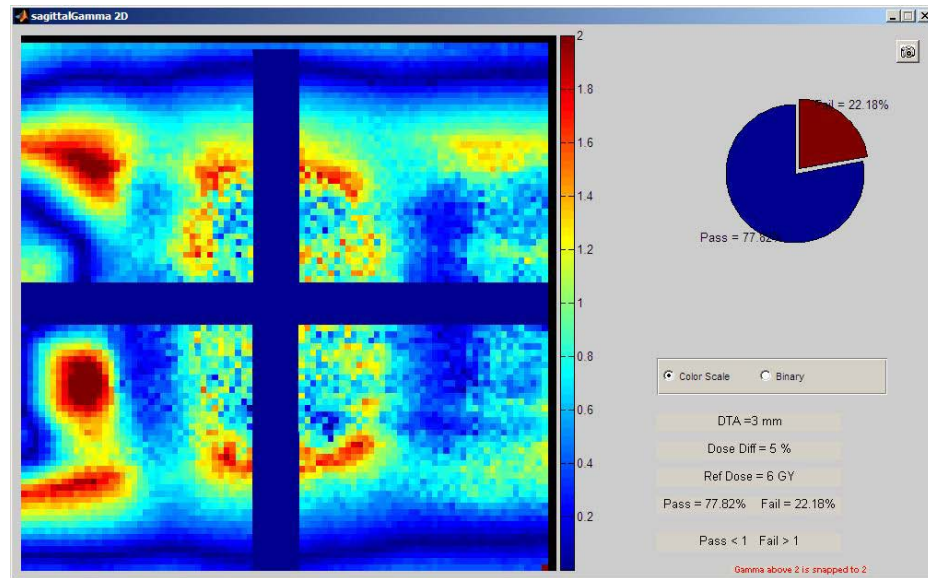


Figure 5.3 Plan 1a Trial 1 Sagittal Gamma Analysis

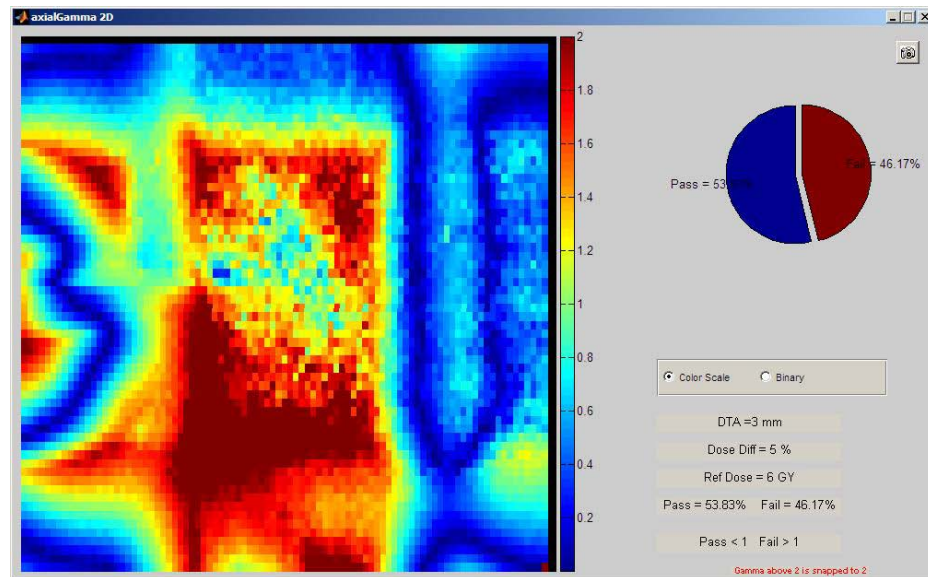


Figure 5.4 Plan 1a Trial 3 Axial Gamma Analysis

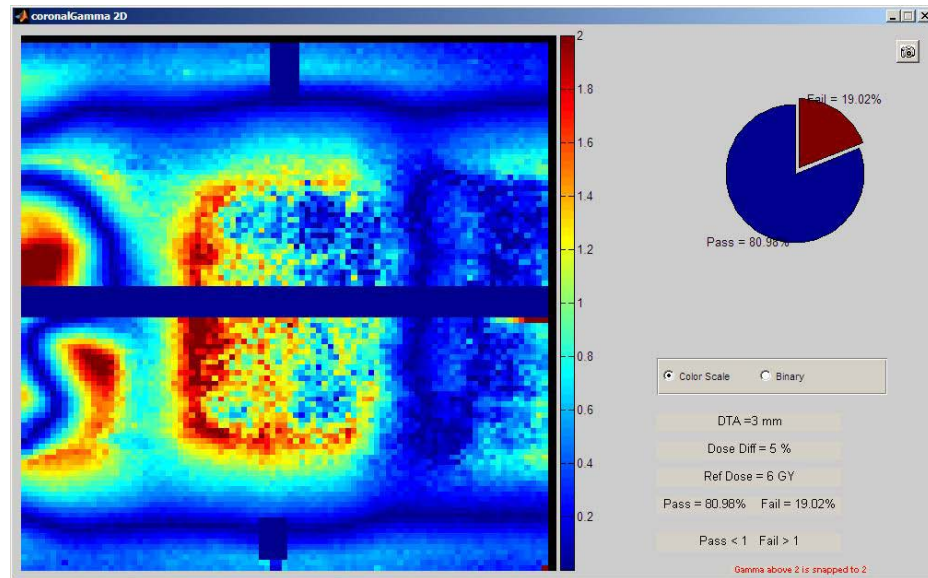


Figure 5.5 Plan 1a Trial 3 Coronal Gamma Analysis

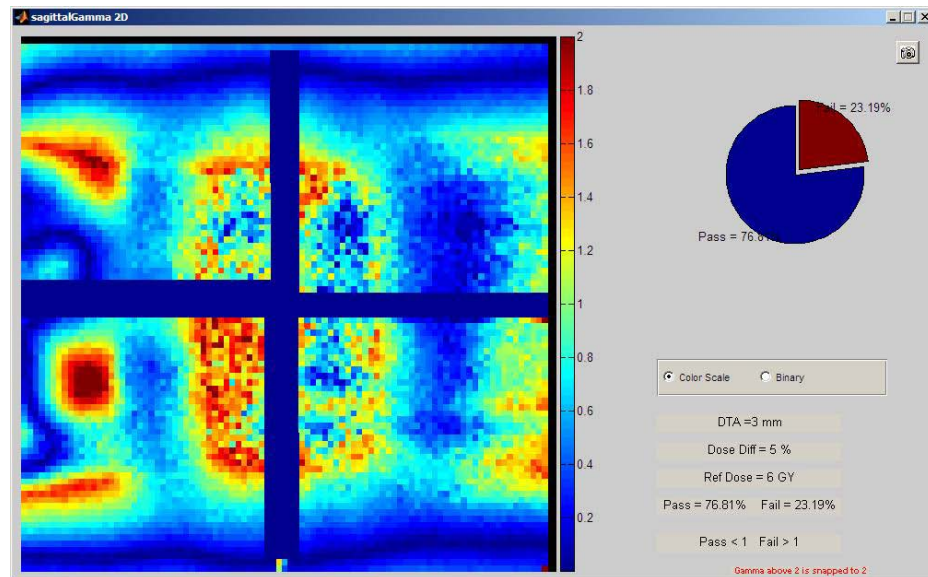


Figure 5.6 Plan 1a Trial 3 Sagittal Gamma Analysis

5.1.2 PLAN 1A – PVC CONTOURED

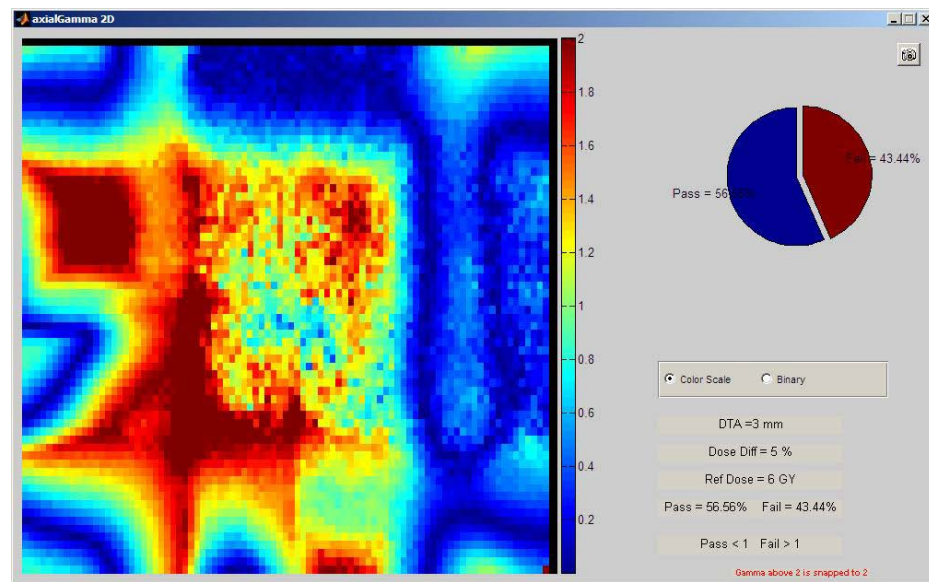


Figure 5.7 Plan 1a Trial 1 Axial Gamma Analysis

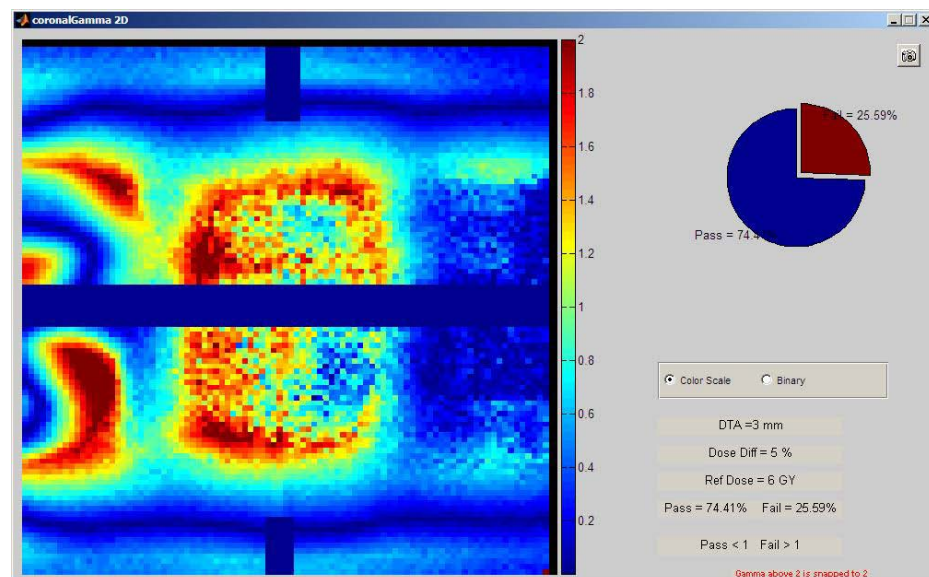


Figure 5.8 Plan 1a Trial 1 Coronal Gamma Analysis

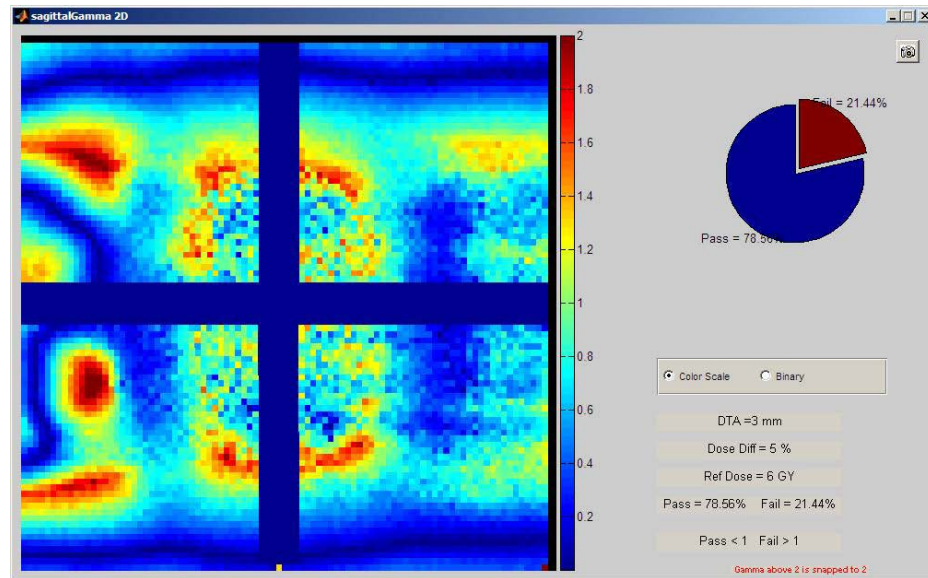


Figure 5.9 Plan 1a Trial 1 Sagittal Gamma Analysis

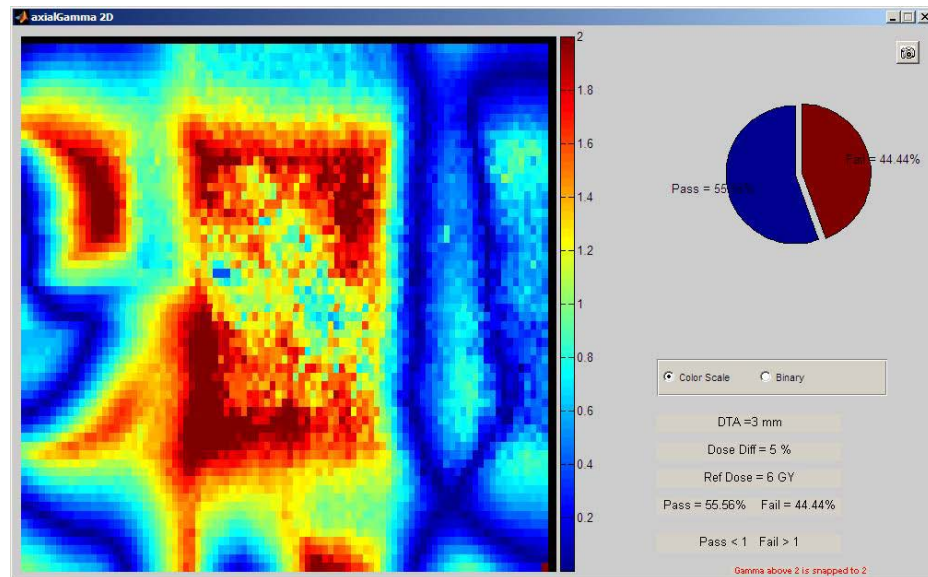


Figure 5.10 Plan 1a Trial 3 Axial Gamma Analysis

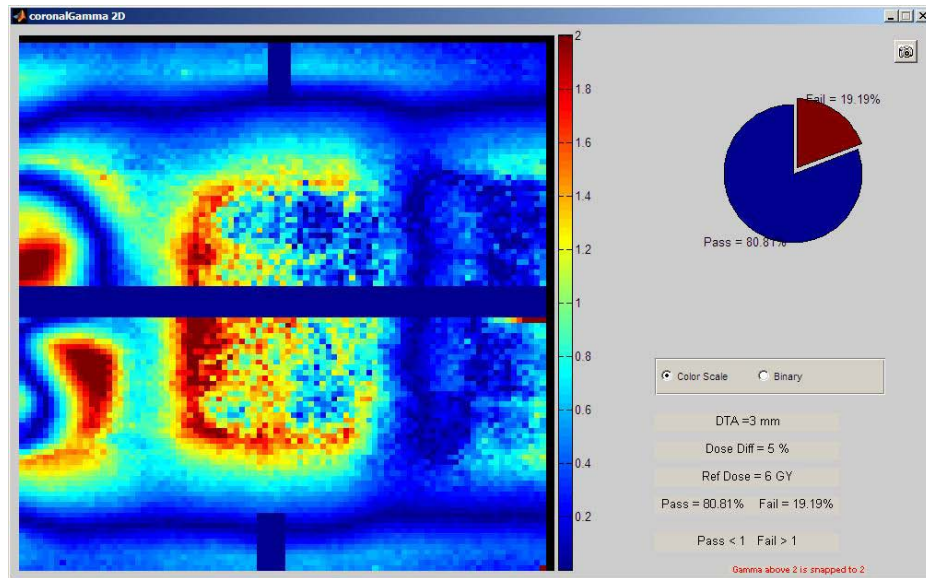


Figure 5.11 Plan 1a Trial 3 Coronal Gamma Analysis

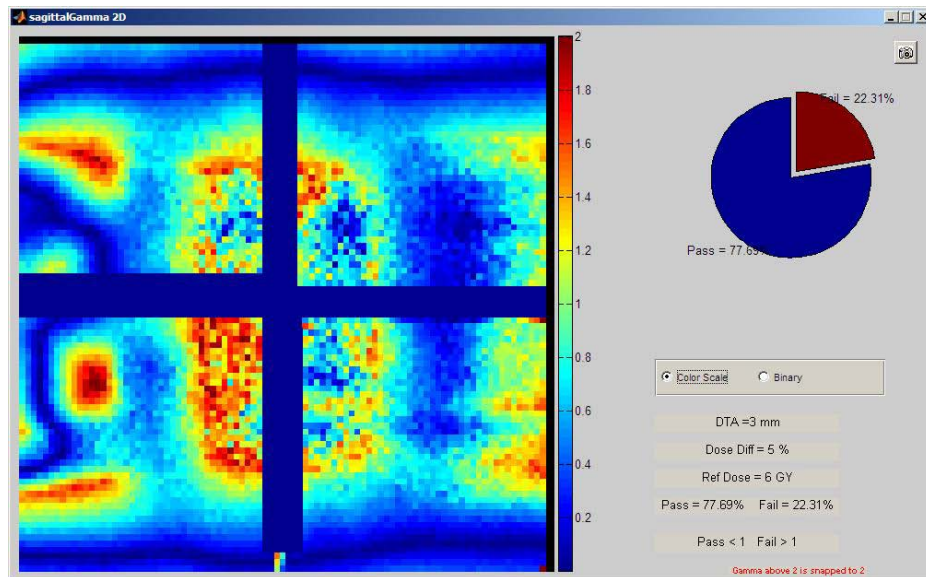


Figure 5.12 Plan 1a Trial 3 Sagittal Gamma Analysis

5.1.3 PLAN 1B

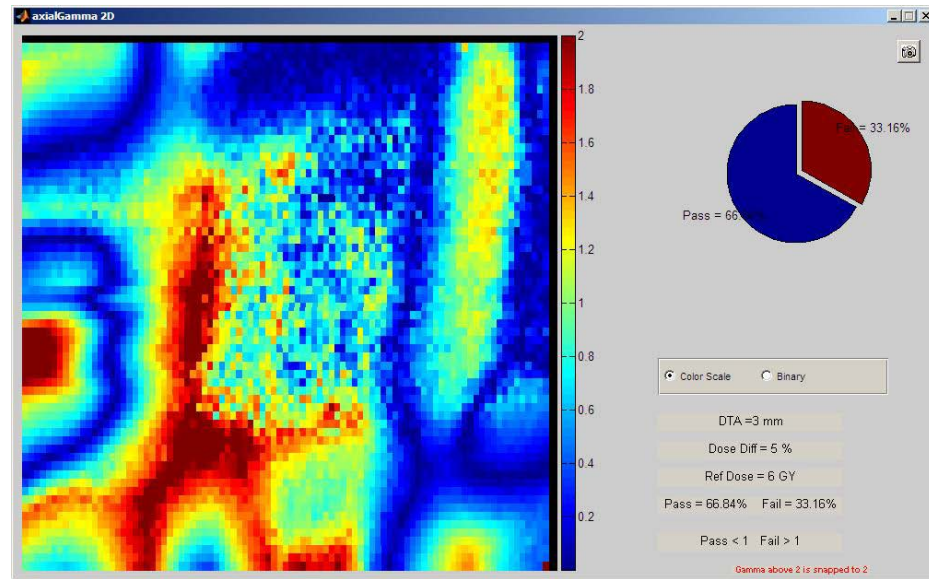


Figure 5.13 Plan 1b Trial 1 Axial Gamma Analysis

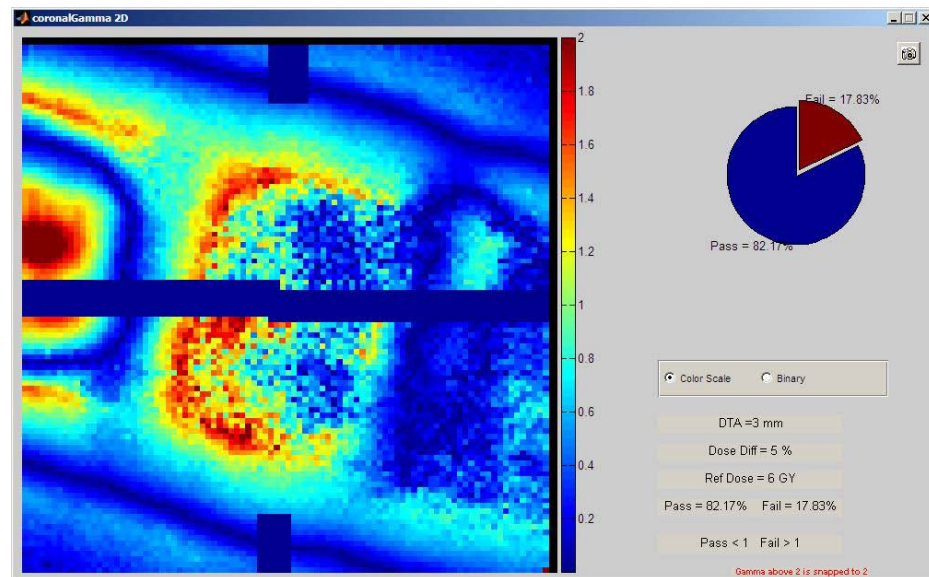


Figure 5.14 Plan 1b Trial 1 Axial Gamma Analysis

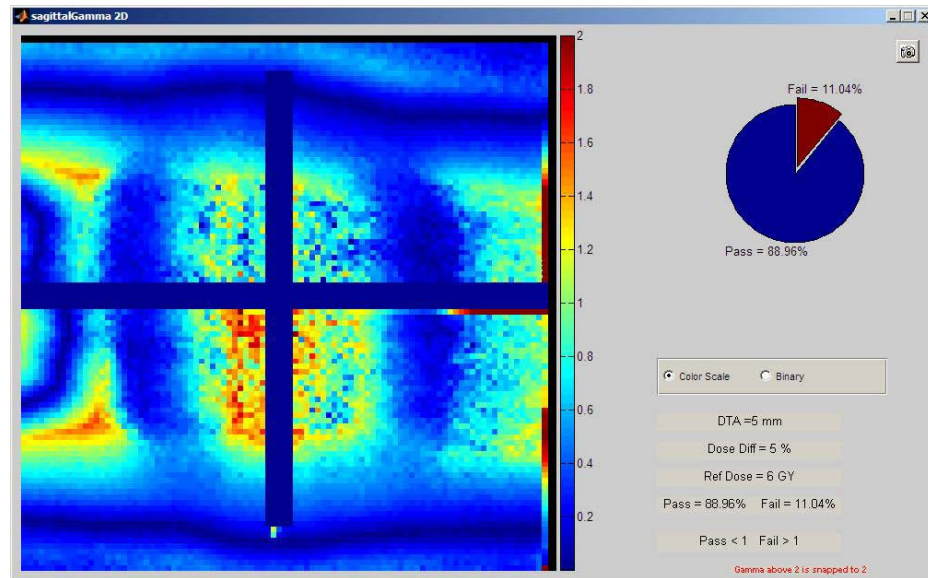


Figure 5.15 Plan 1b Trial 1 Sagittal Gamma Analysis

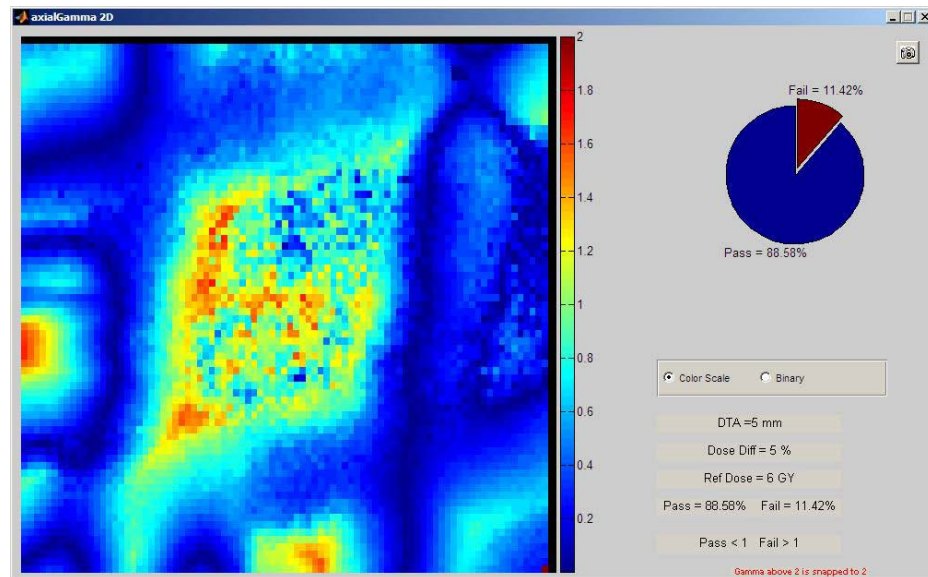


Figure 5.16 Plan 1b Trial 3 Axial Gamma Analysis

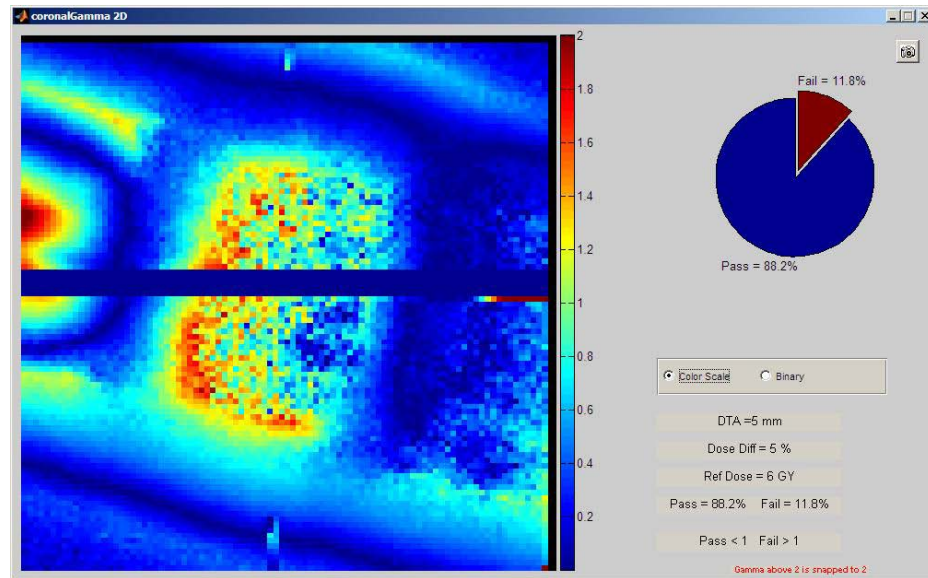


Figure 5.17 Plan 1b Trial 3 Coronal Gamma Analysis

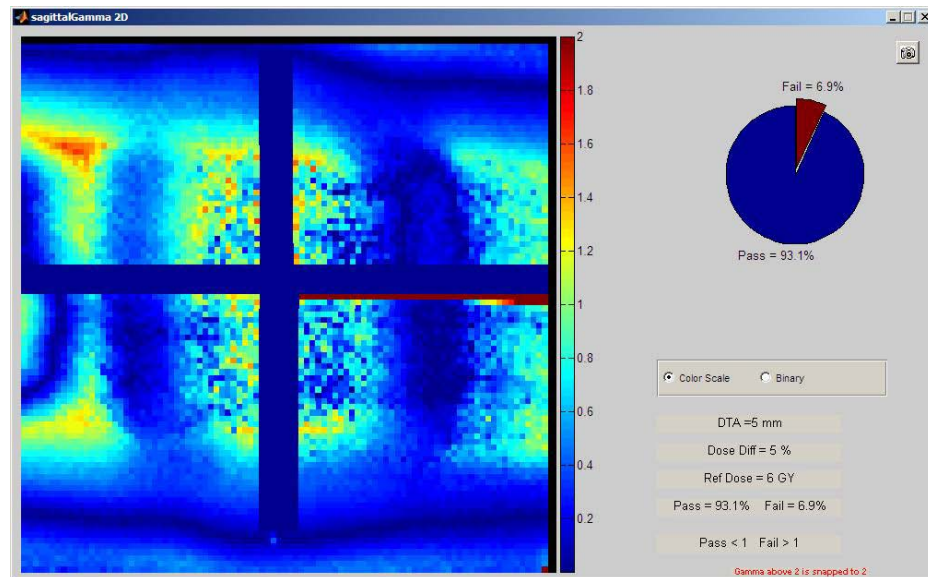


Figure 5.18 Plan 1b Trial 3 Sagittal Gamma Analysis

5.1.4 PLAN 1B- PVC CONTOURED

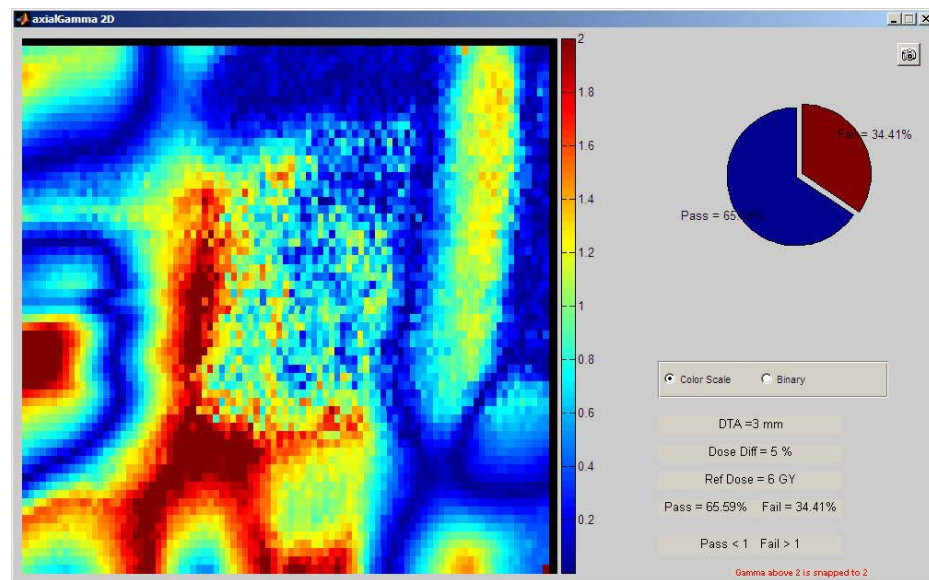


Figure 5.19 Plan 1b Trial 1 Axial Gamma Analysis

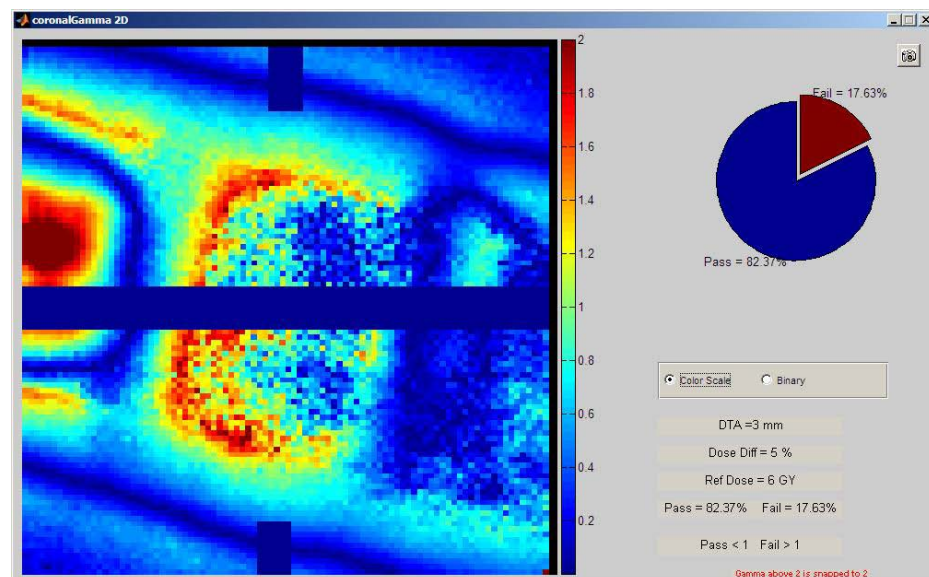


Figure 5.20 Plan 1b Trial 1 Axial Gamma Analysis

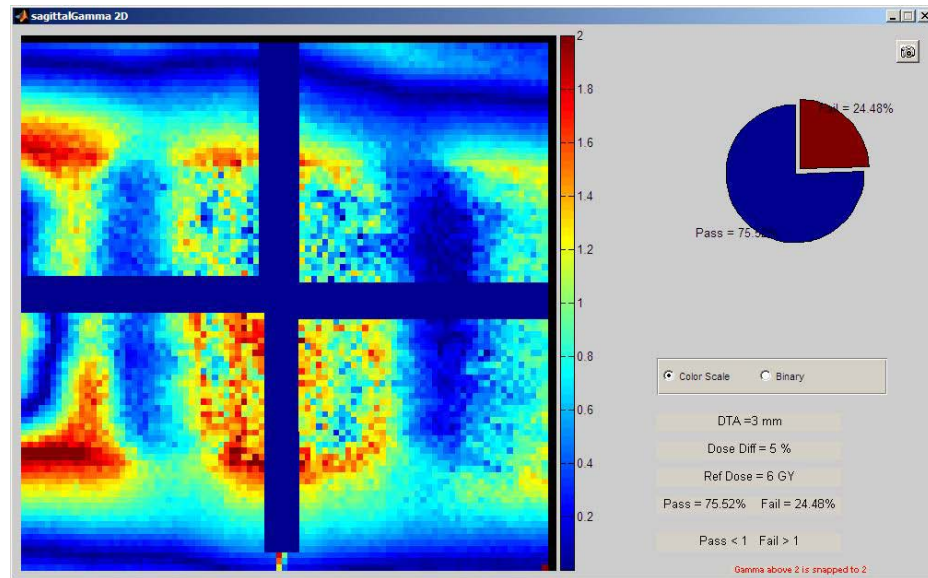


Figure 5.21 Plan 1b Trial 1 Sagittal Gamma Analysis

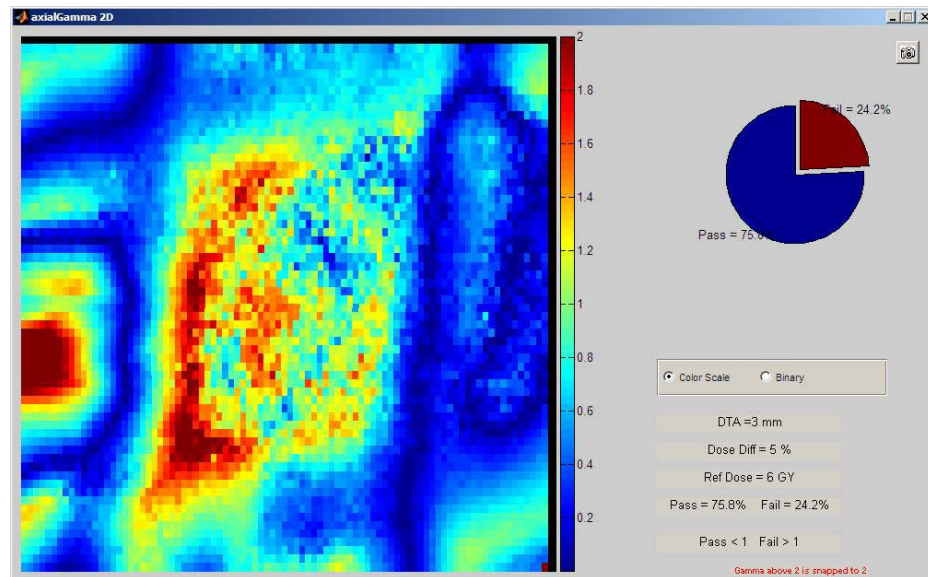


Figure 5.22 Plan 1b Trial 3 Axial Gamma Analysis

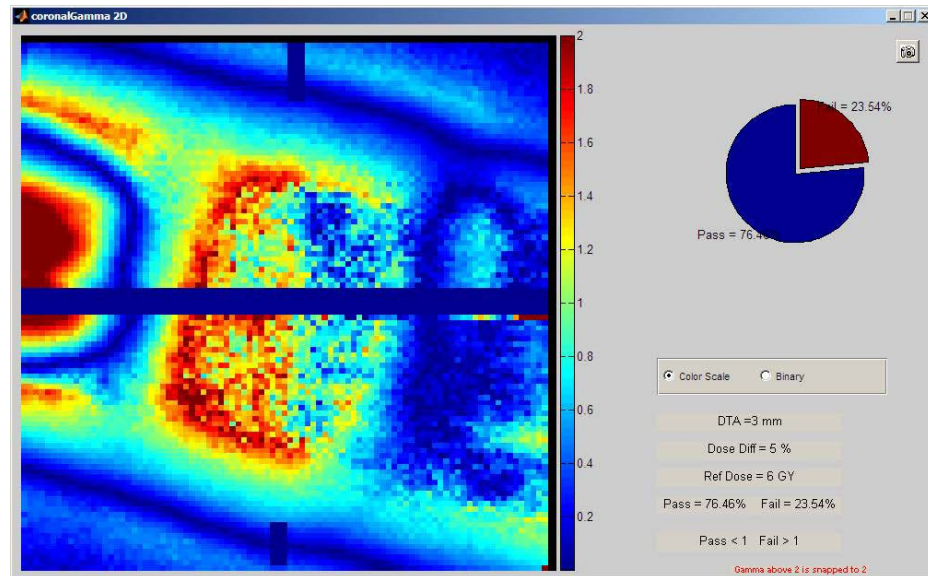


Figure 5.23 Plan 1b Trial 3 Coronal Gamma Analysis

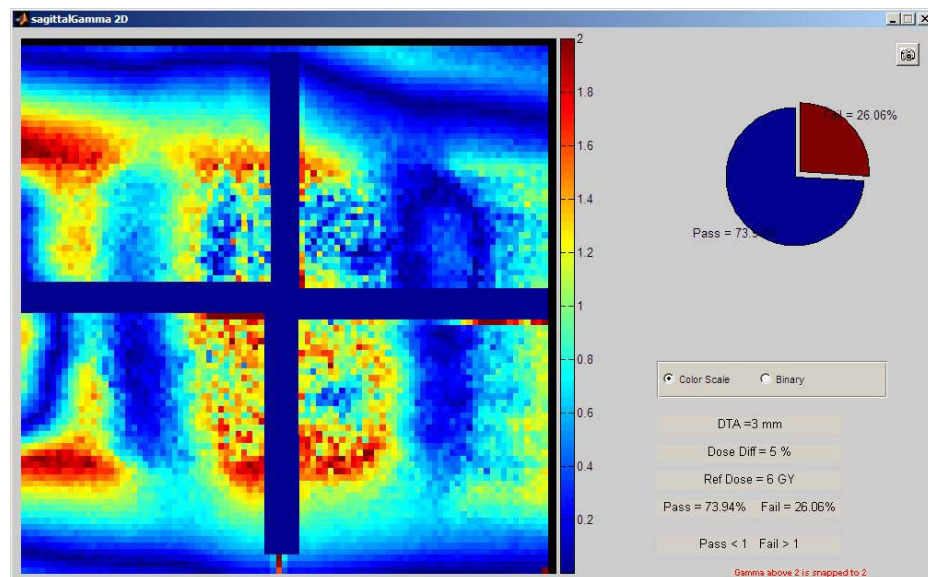


Figure 5.24 Plan 1b Trial 3 Sagittal Gamma Analysis

5.2 DTA Profile Comparisons

5.2.1 PLAN 1A

Trial 1				
Axial	Right Left Profile		Anterior Posterior Profile	
	Patient Right	5.8	Posterior	6.3
	Patient Left	1.2	Anterior	0.2
Coronal	Right Left Profile		Superior Inferior Profile	
	Patient Right	2.2	Superior	1.2
	Patient Left	1.3	Inferior	1.7
Sagittal	Anterior Posterior Profile		Superior Inferior Profile	
	Posterior	1.8	Superior	0.9
	Anterior	1.3	Inferior	1.9
Trial 2				
Axial	Right Left Profile		Anterior Posterior Profile	
	Patient Right	5.8	Posterior	4.9
	Patient Left	1.6	Anterior	0.1
Coronal	Right Left Profile		Superior Inferior Profile	
	Patient Right	2	Superior	1.6
	Patient Left	0.5	Inferior	1.1
Sagittal	Anterior Posterior Profile		Superior Inferior Profile	
	Posterior	2.5	Superior	1.2
	Anterior	0.4	Inferior	1
Trial 3				
Axial	Right Left Profile		Anterior Posterior Profile	
	Patient Right	4.4	Posterior	5.5
	Patient Left	0.8	Anterior	0.4
Coronal	Right Left Profile		Superior Inferior Profile	
	Patient Right	0.4	Superior	1.1
	Patient Left	0.1	Inferior	0.6
Sagittal	Anterior Posterior Profile		Superior Inferior Profile	
	Posterior	1.6	Superior	1
	Anterior	1.1	Inferior	1.3

Table 22 DTA values per film per profiles for Plan 1a, in mm.

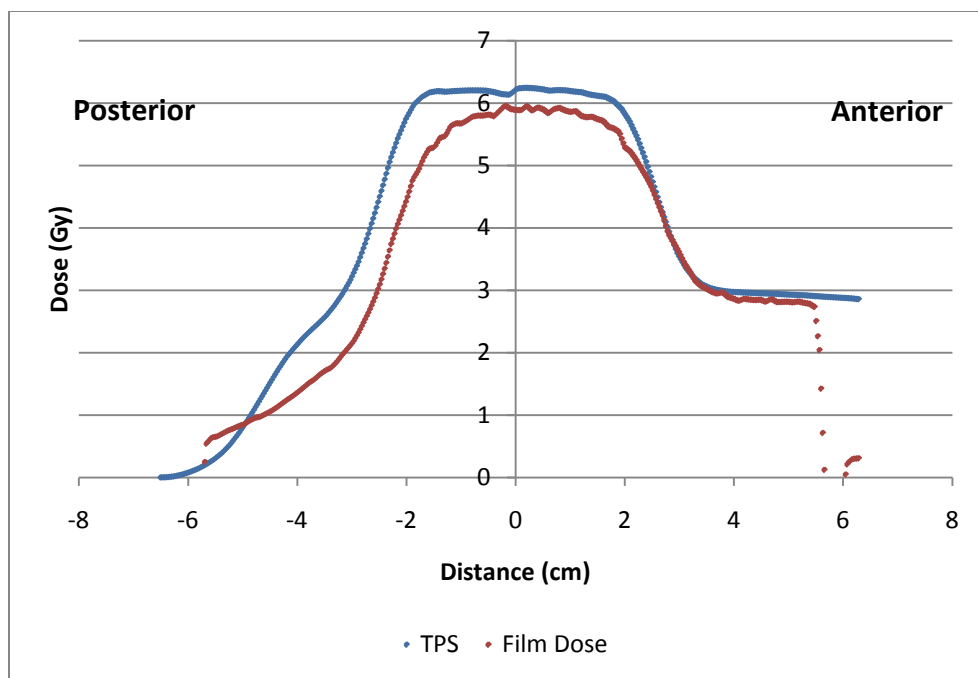


Figure 5.25 Plan 1a Trial 1 Anterior Posterior Profile Axial Plane

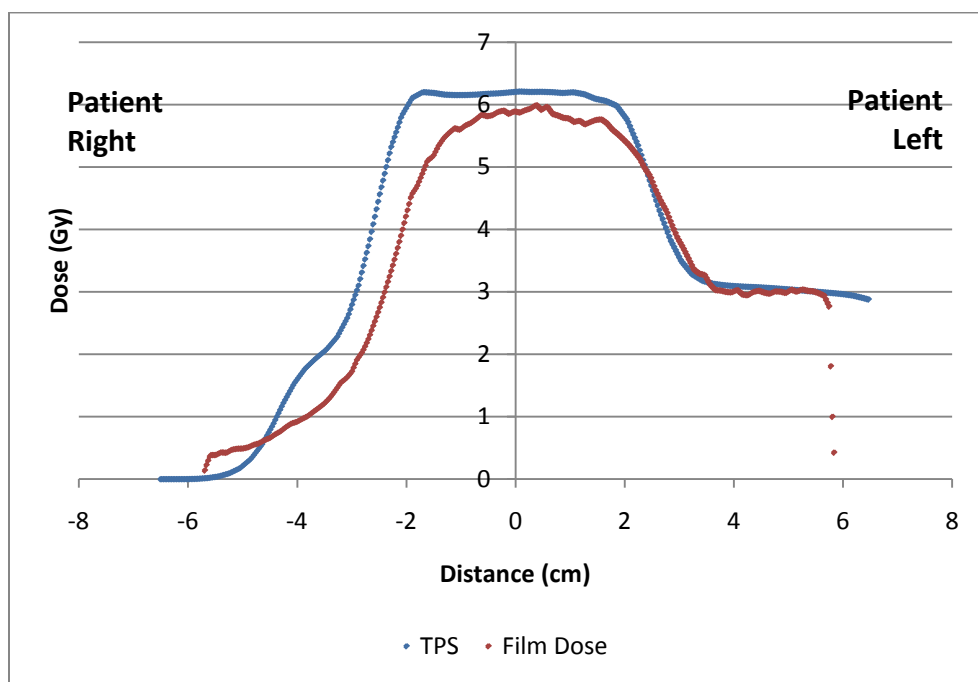


Figure 5.26 Plan 1a Trial 1 Right Left Profile Axial Plane

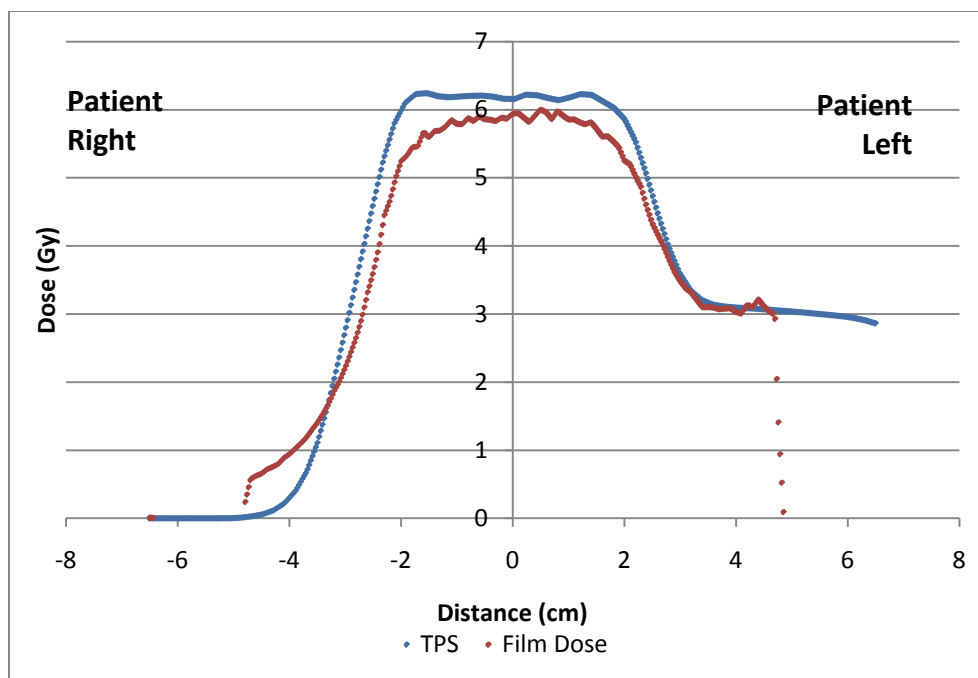


Figure 5.27 Plan 1A Trial 1 Right Left Profile Coronal Plane

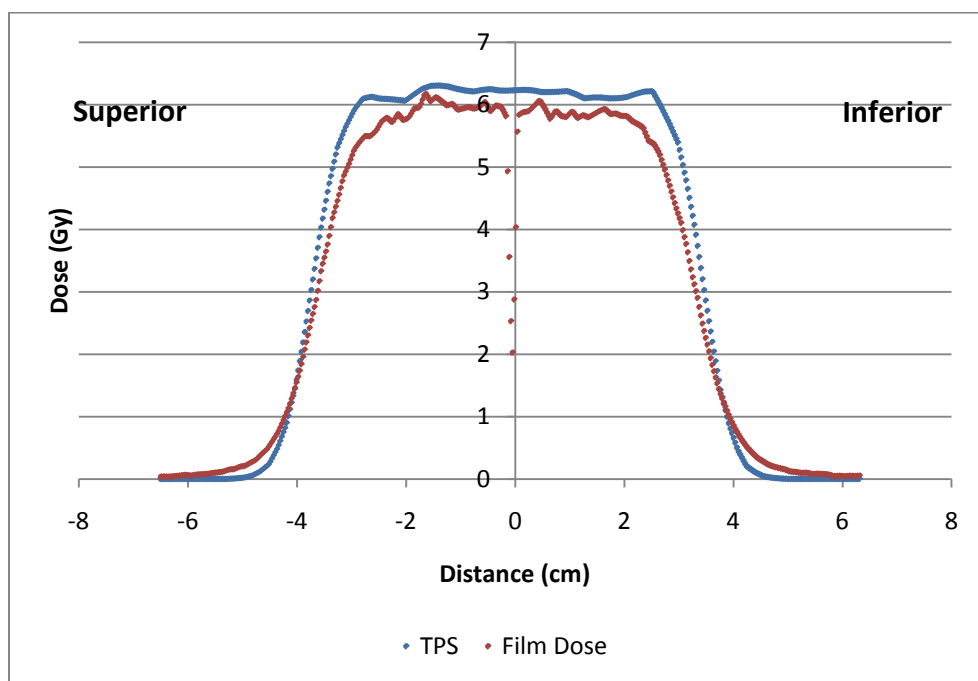


Figure 5.28 Plan 1A Trial 1 Superior Inferior Coronal Plane

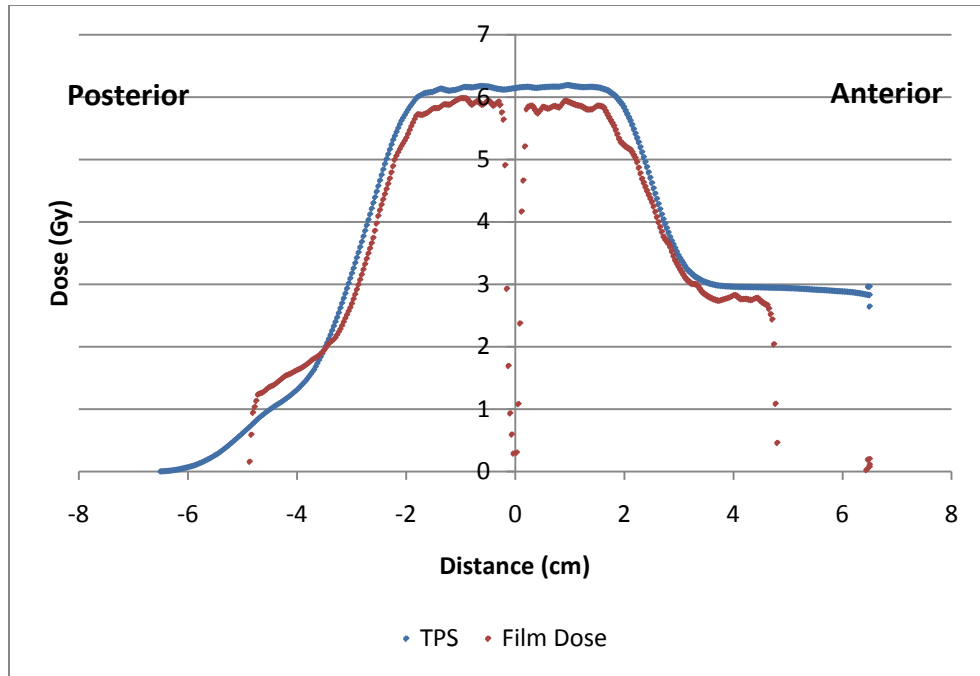


Figure 5.29 Plan 1A Trial 1 Anterior Posterior Sagittal Plane

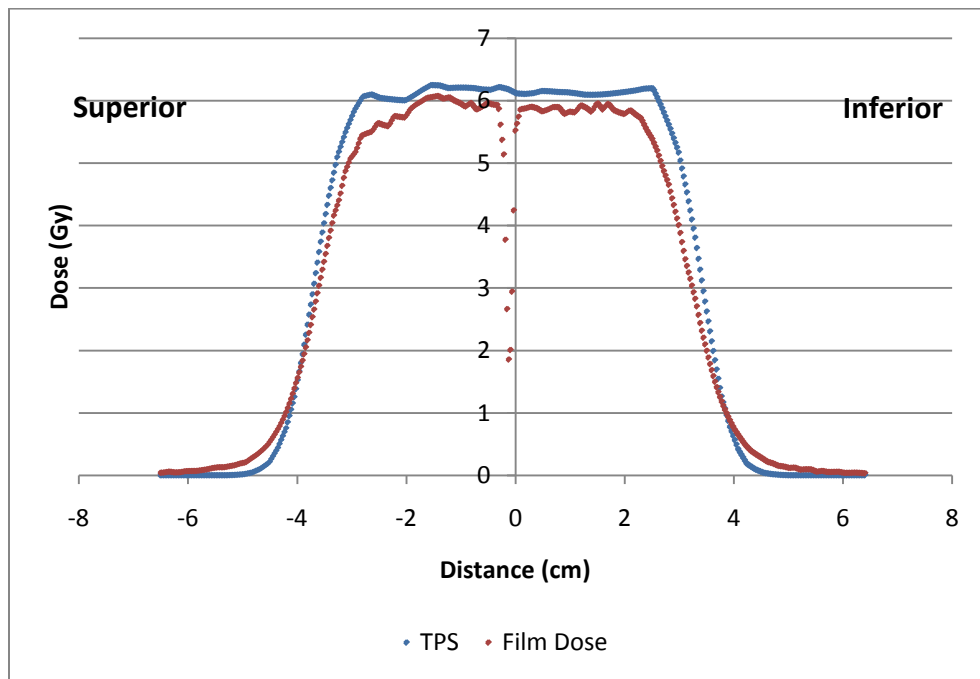


Figure 5.30 Plan 1A Trial 1 Superior Inferior Sagittal Plane

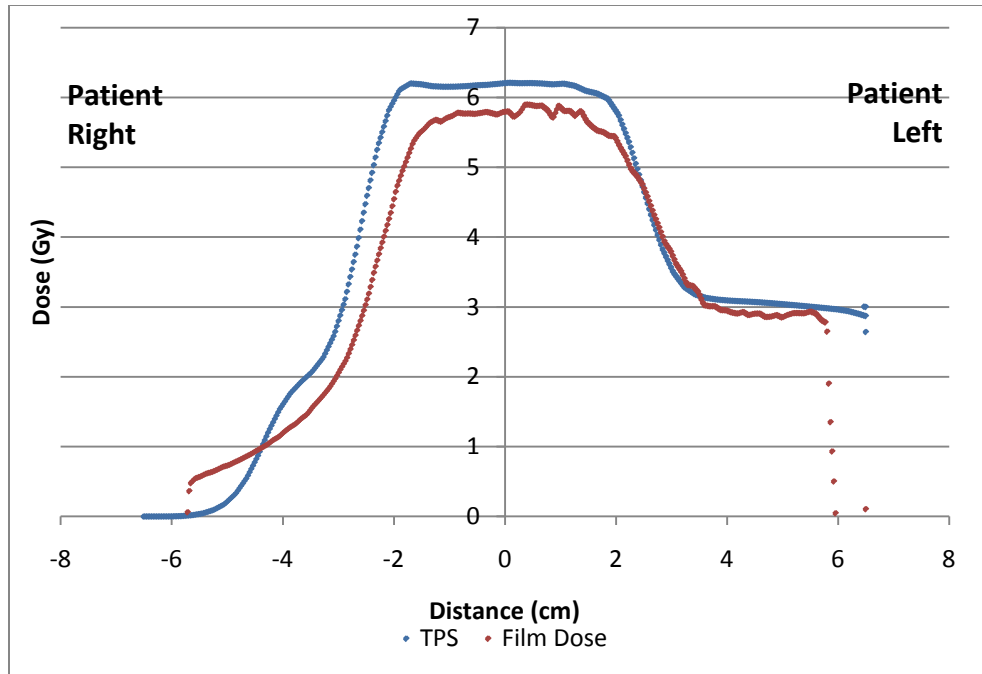


Figure 5.31 Plan 1A Trial 1 Right Left Profile Axial Plane

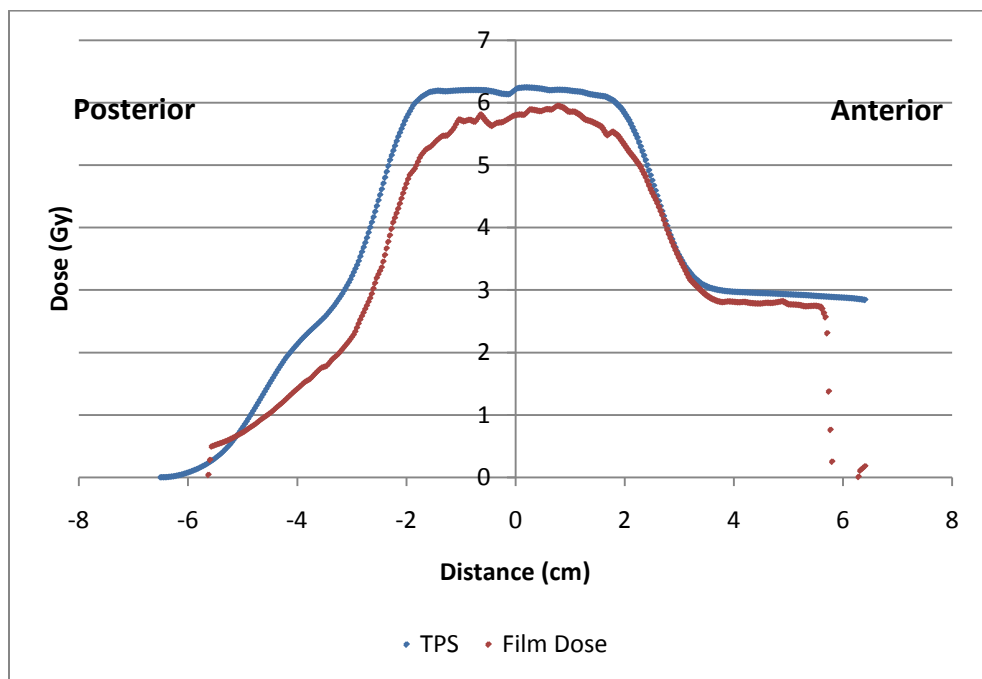


Figure 5.32 Plan 1A Trial 3 Anterior Posterior Axial Plane

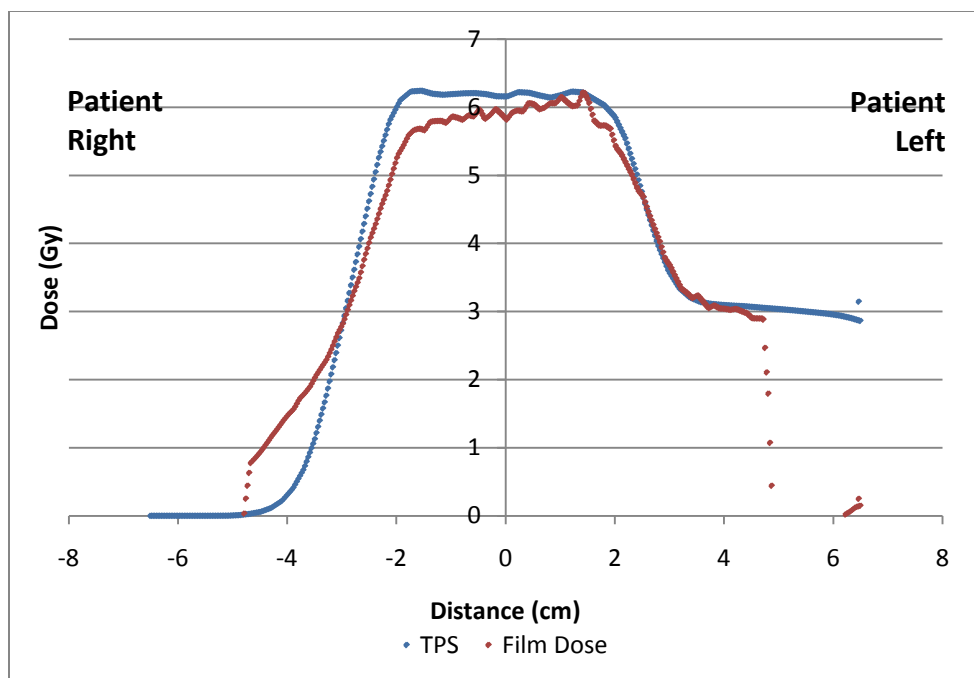


Figure 5.33 Plan 1A Trial 3 Right Left Coronal Plane

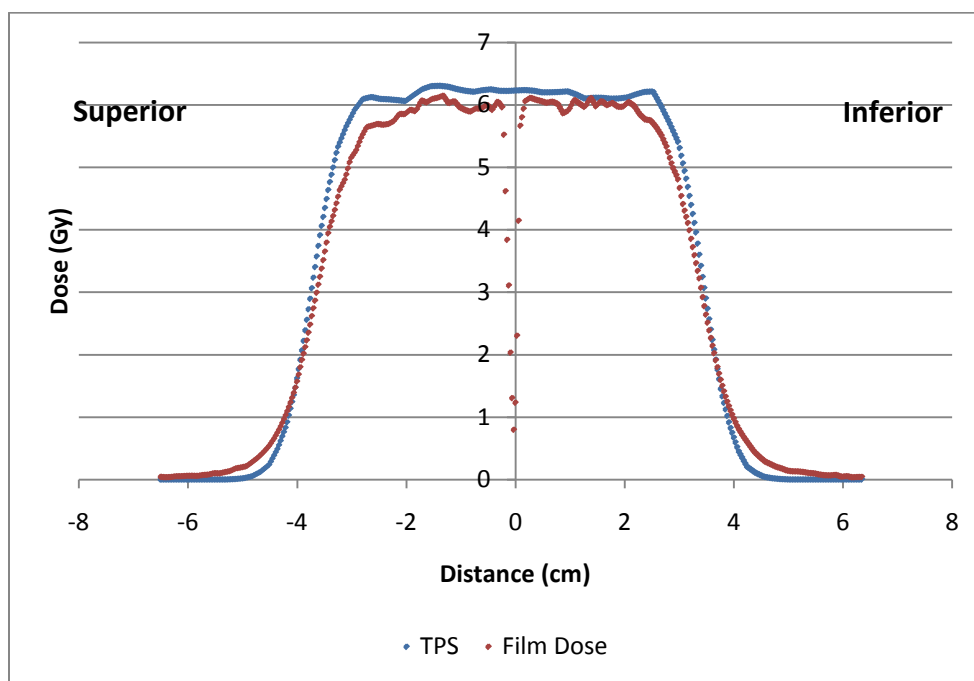


Figure 5.34 Plan 1A Trial 3 Superior Inferior Coronal Plane

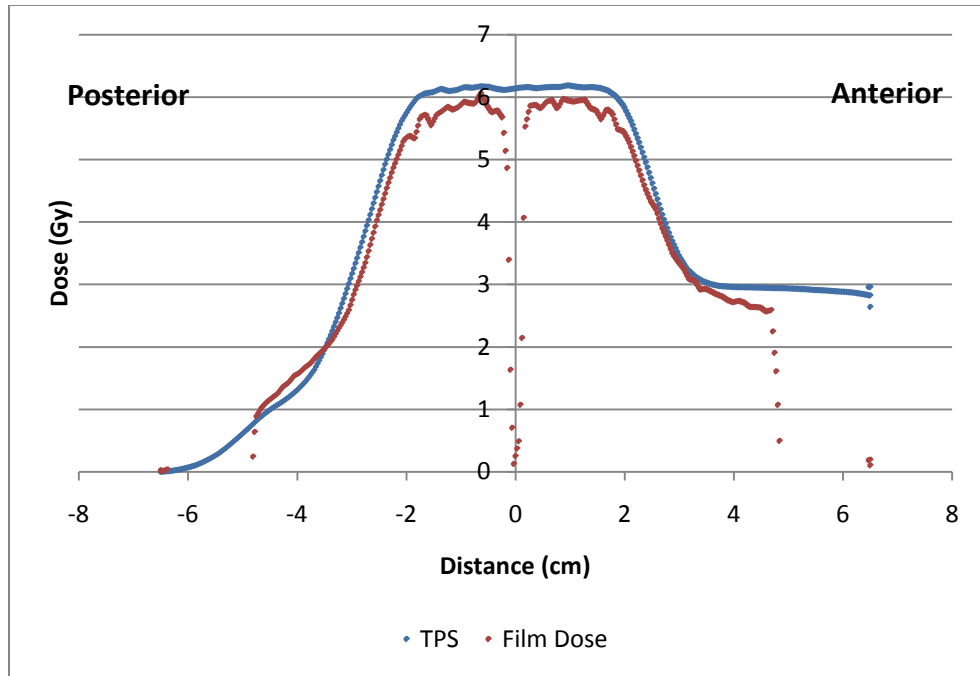


Figure 5.35 Plan 1A Trial 3 Anterior Posterior Sagittal Plane

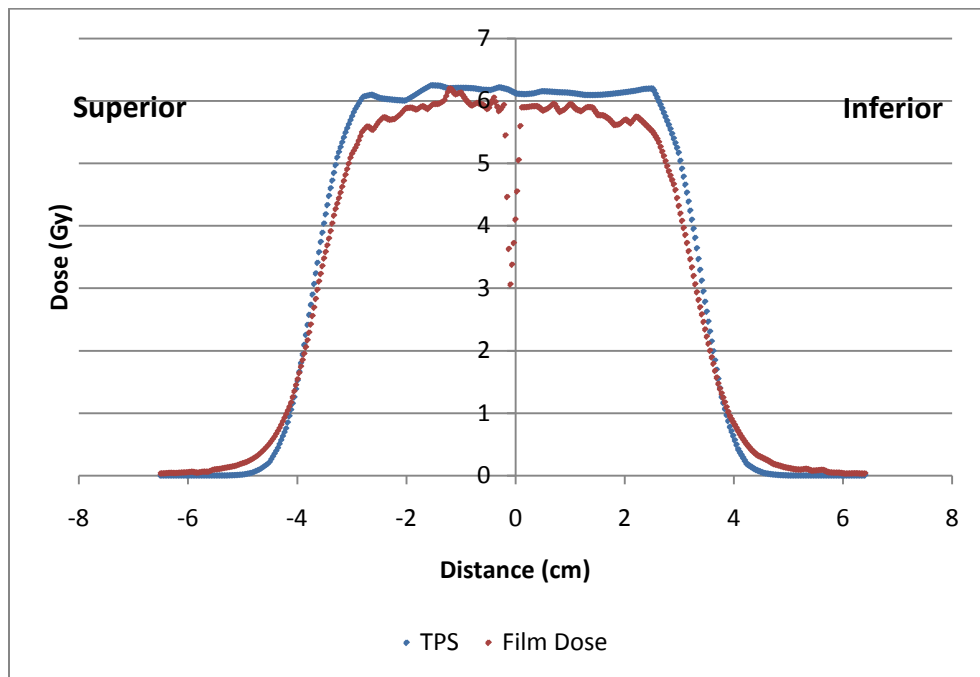


Figure 5.36 Plan 1A Trial 3 Superior Inferior Sagittal Plane

5.2.2 PLAN 1B

Trial 1				
Axial	Right Left Profile		Anterior Profile	Posterior
	Patient Right	4.7	Posterior	2.8
	Patient Left	3.5	Anterior	1.1
Coronal	Right Left Profile		Superior Profile	Inferior
	Patient Right	0.6	Superior	1.3
	Patient Left	0.3	Inferior	0.8
Sagittal	Anterior Posterior Profile		Superior Profile	Inferior
	Posterior	1.2	Superior	2.1
	Anterior	1	Inferior	0.8
Trial 2				
Axial	Right Left Profile		Anterior Profile	Posterior
	Patient Right	1.4	Posterior	2.3
	Patient Left	0.6	Anterior	0.5
Coronal	Right Left Profile		Superior Profile	Inferior
	Patient Right	0.2	Superior	2.3
	Patient Left	0.9	Inferior	0.2
Sagittal	Anterior Posterior Profile		Superior Profile	Inferior
	Posterior	2.4	Superior	1.1
	Anterior	0	Inferior	0.8
Trial 3				
Axial	Right Left Profile		Anterior Profile	Posterior
	Patient Right	1.1	Posterior	1.9
	Patient Left	1.1	Anterior	1
Coronal	Right Left Profile		Superior Profile	Inferior
	Patient Right	0.5	Superior	1.7
	Patient Left	0.2	Inferior	0.7
Sagittal	Anterior Posterior Profile		Superior Profile	Inferior
	Posterior	2	Superior	2
	Anterior	0.7	Inferior	1.5

Table 23 DTA values per film per profiles for Plan 1b, in mm.

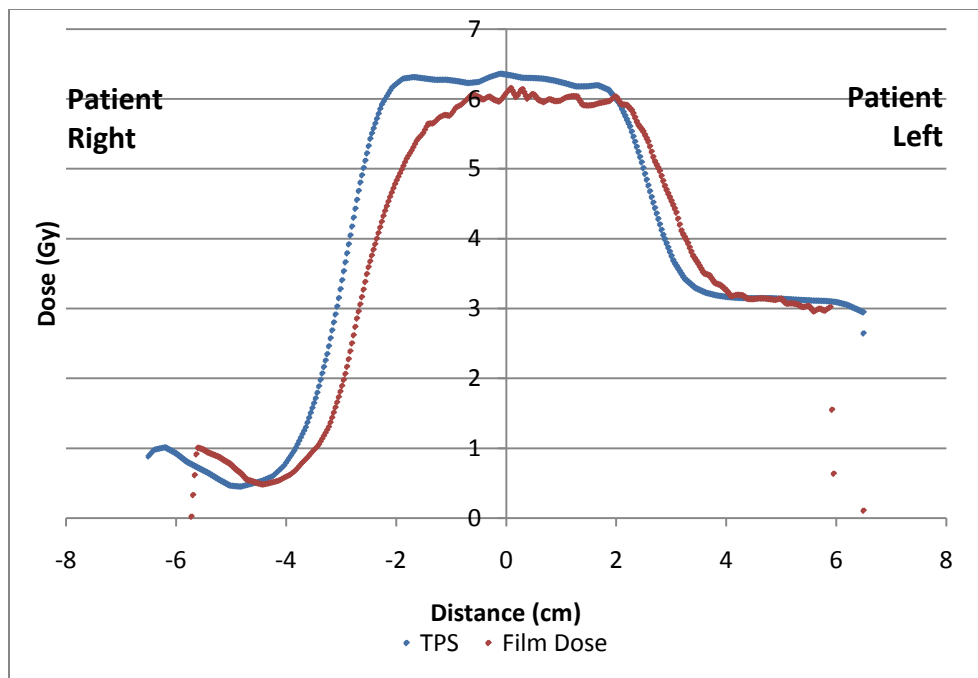


Figure 5.37 Plan 1b Trial 1 Right Left Axial Plane

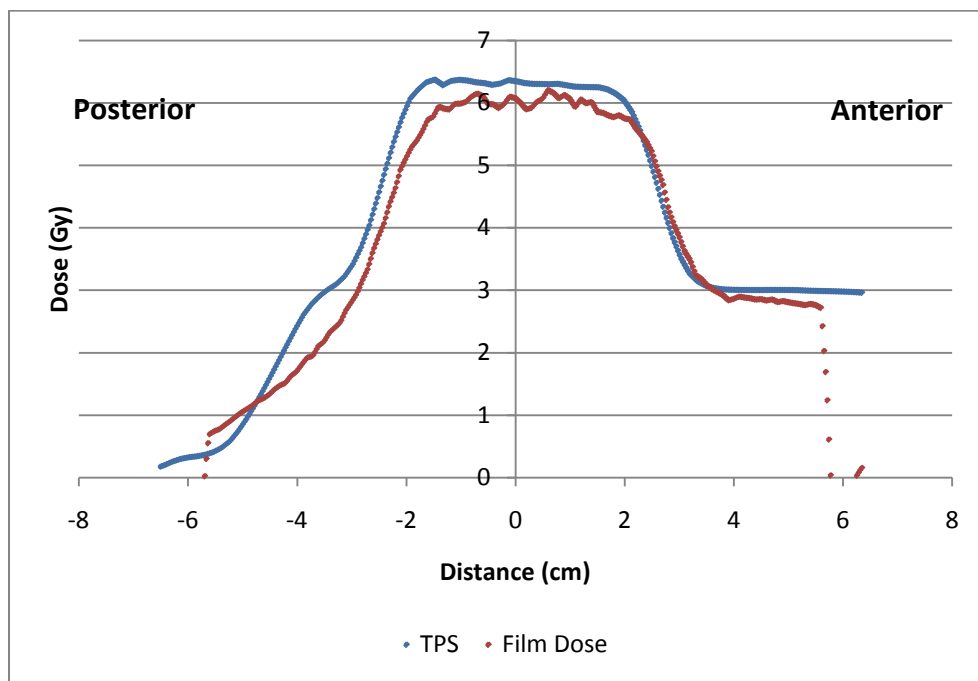


Figure 5.38 Plan 1b Trial 1 Anterior Posterior Axial Plane

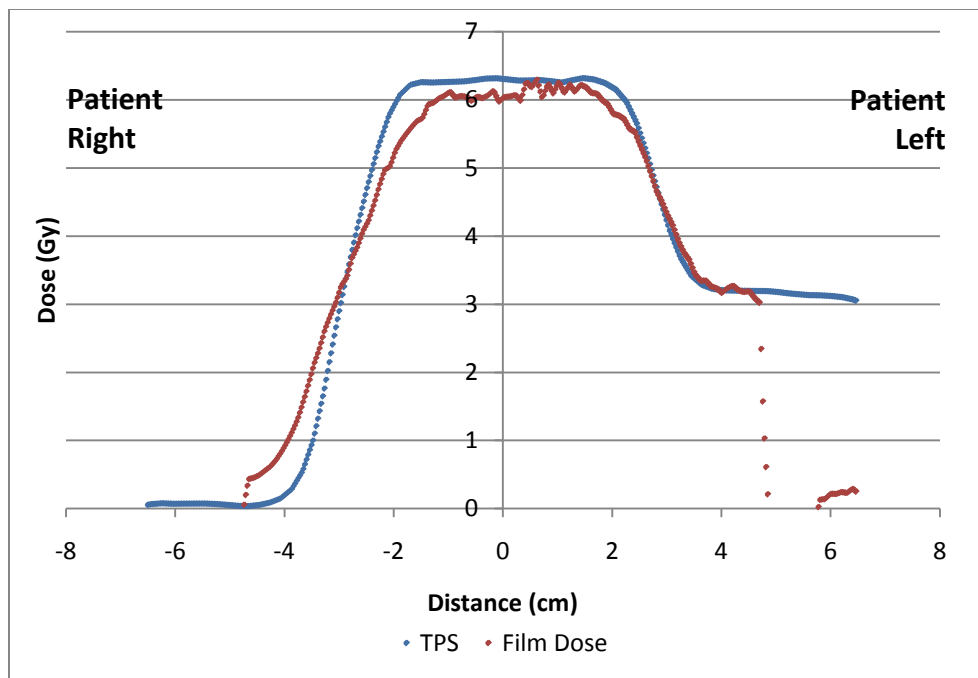


Figure 5.39 Plan 1b Trial 1 Right Left Coronal Plane

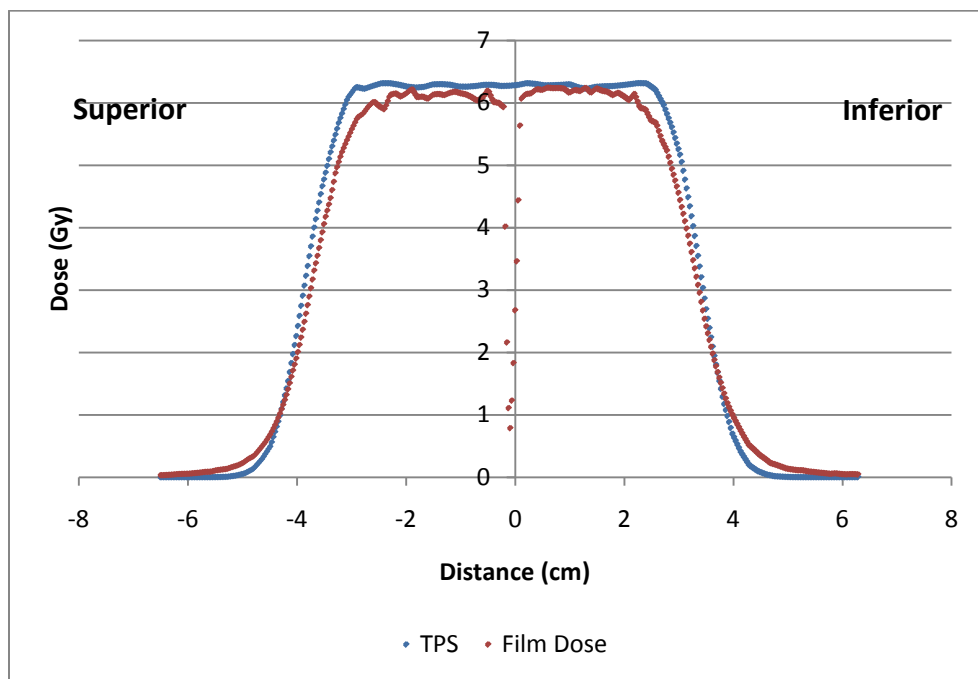


Figure 5.40 Plan 1b Trial 1 Superior Inferior Coronal Plane

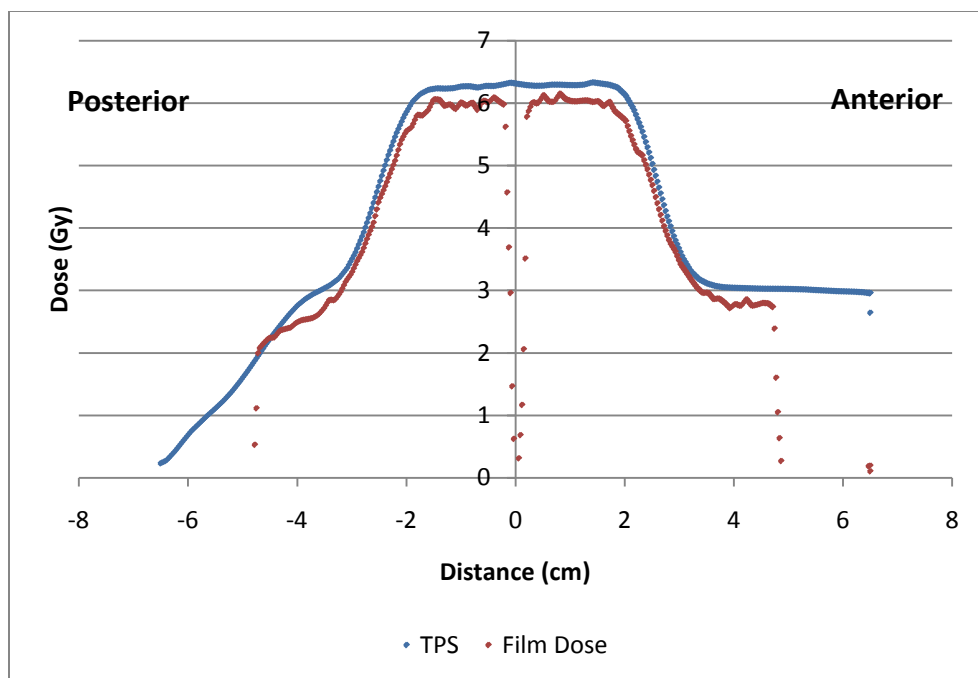


Figure 5.41 Plan 1b Anterior Posterior Sagittal Plane

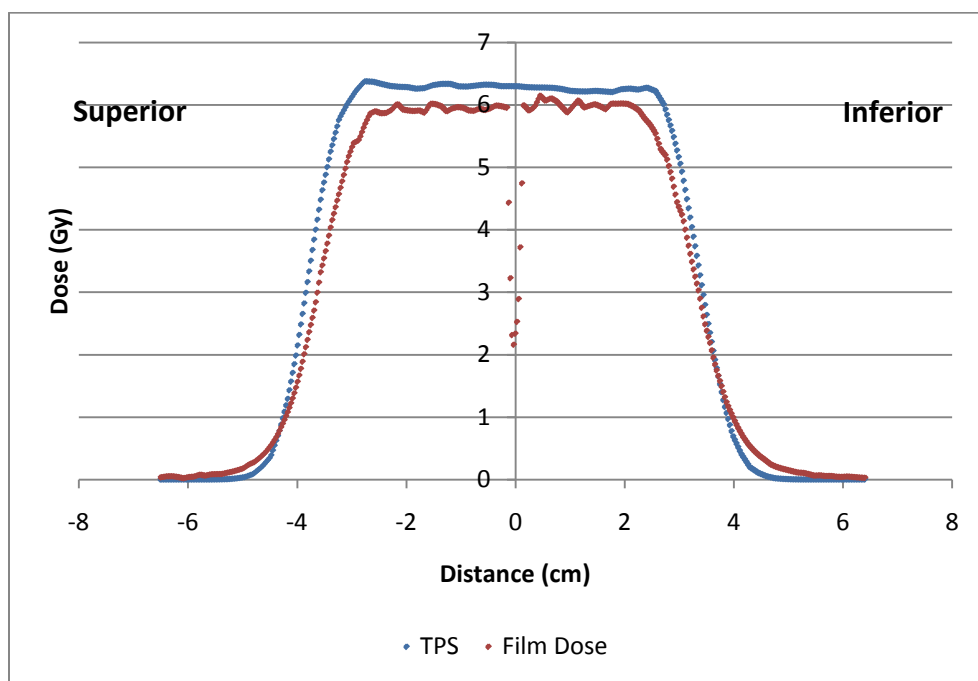


Figure 5.42 Plan 1b Trial 1 Superior Inferior Sagittal Plane

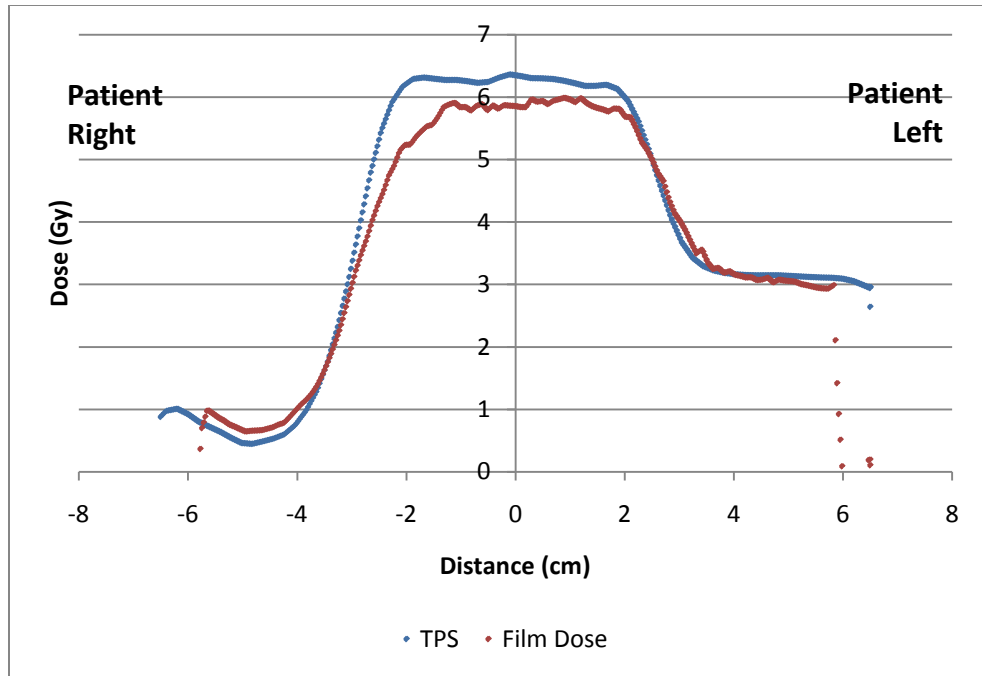


Figure 5.43 Plan 1b Trial 3 Right Left Axial Plane

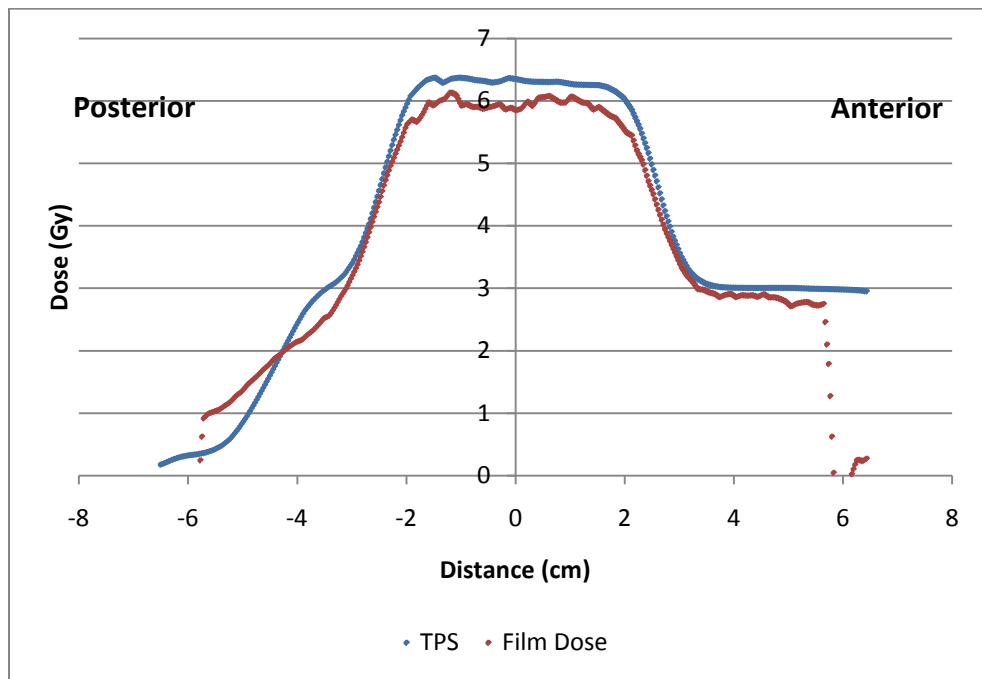


Figure 5.44 Plan 1b Trial 3 Anterior Posterior Axial Plane

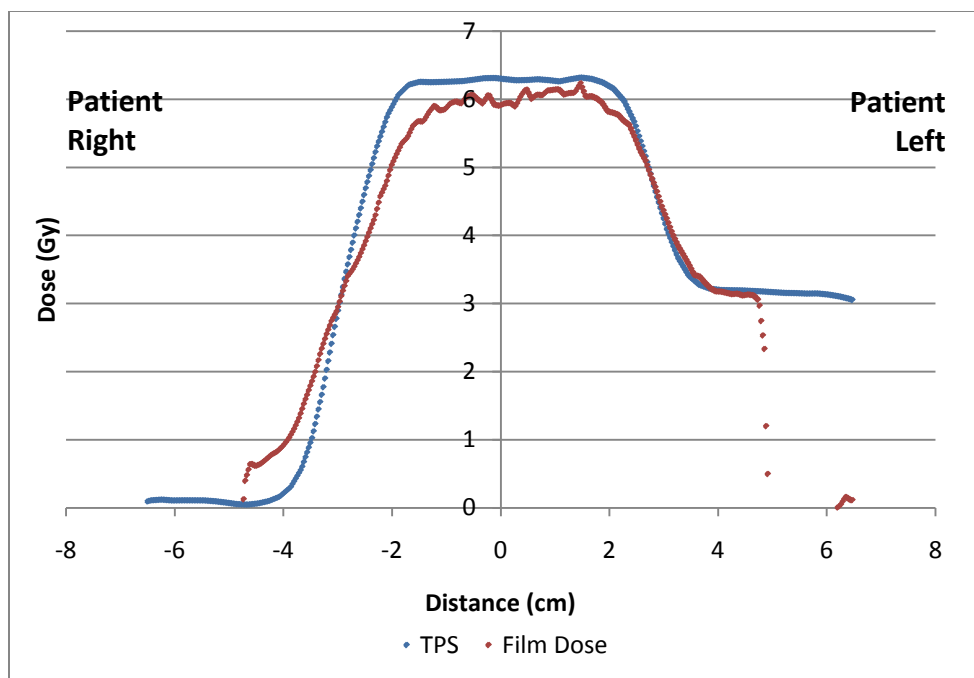


Figure 5.45 Plan 1b Trial 3 Right Left Coronal Plane

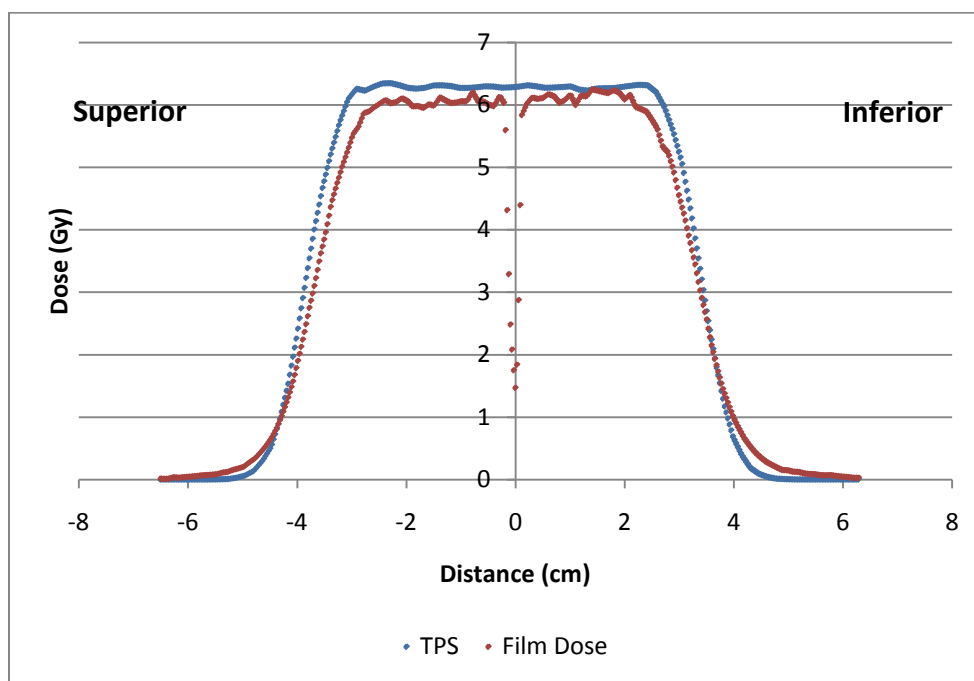


Figure 5.46 Plan 1b Trial 3 Superior Inferior Coronal Plane

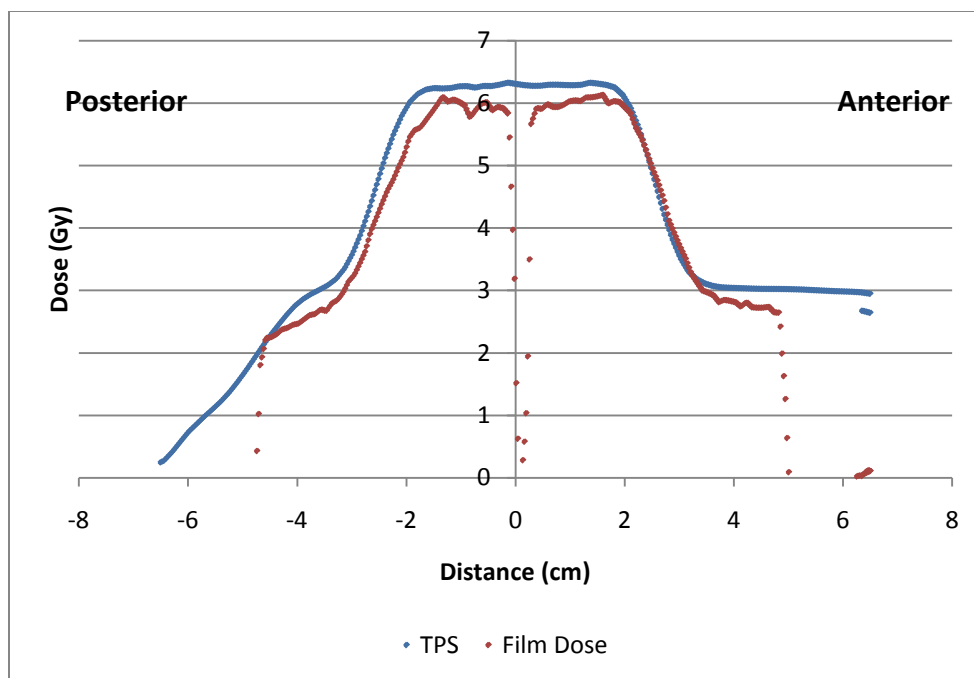


Figure 5.47 Plan 1b Trial 3 Anterior Posterior Sagittal Plane

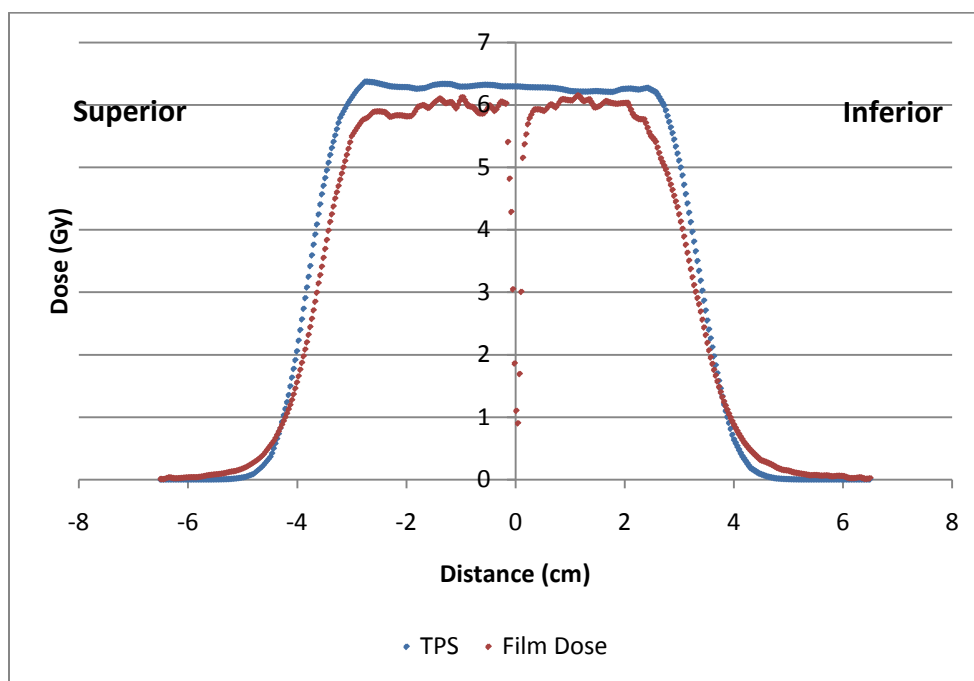


Figure 5.48 Plan 1b Trial 3 Superior Inferior Sagittal Plane



Monitor Unit Calculation

Proton Therapy Center, Houston

Date: **August 16, 2010**

Patient Name **ZZLUNG NO FID, Phantom** MR # **ZZ082410**

Prescription	Dose (CcGyE)	Fractions	Isodose	Dose / fx. (CcGyE)	Dose / fx. To IDL (CcGyE)
	400	1	100.0%	400	400.0

Plan	Plan1a	Plan1a	Plan3	Plan3
Plan ID	ALL1A	BAP1A	CLA1A	DLA1A
Field ID	ALL1A	BAP1A	CLA1A	DLA1A
Field Name	ALL1A	BAP1A	CLA1A	DLA1A
Energy (MeV)	140/85	160/84	140/85	160/84
Gantry/Couch positions (deg)	90/0	0/0	80/345	10/345
Snout Position (cm)	30	30	30	30
Range (cm)	8.1	11.9	8.1	11
SOBP Width (cm)	5	5	5	5
SOBP Center (cm)	5.6	9.4	5.6	8.5
Dose reference point (DRP)	ALL1A	BAP1A	CLA1A	DLA1A
Depth in Water Phantom (cm)	5.6	9.4	5.6	8.5
SSD (cm) (DRP)	264.4	260.6	264.4	261.5
DRP Dose (VP_NC)(CcGyE)	103.1	101.6	105.9	101.4
DRP Dose(VP_NC) (cGy)	103.1	101.6	105.9	101.4

Calculated MU	ALL1A	BAP1A	CLA1A	DLA1A
Patient Specific Parameters				
Field	ALL1A	BAP1A	CLA1A	DLA1A
Location	ALL1A	BAP1A	CLA1A	DLA1A
Range Shift (cm)	2.1	1.5	2.1	2.4
Relative OF	0.927	0.865	0.927	0.865
Range Shifter Fctr.	0.947	0.973	0.947	0.958
SOBP Factor	1.073	1.295	1.073	1.295
SOBP Off-Center Factor (OCF)	1.000	1.000	1.000	1.000
Other	1.000	1.000	1.000	1.000
MU Required	109.5	93.2	112.4	94.5

MU=PointDose (cGy)/(Relative OF*Range Shifter Fctr*SOBP factor*other)

NOTE : Factors not considered in measurement and calculation

1. The end effect in dose measurement is not used. It was estimated to be in the range of 0.2 to 0.3 MU, which is less than 0.5% of the MU used for treatment.
2. Temperature factor, which is expected to be very small, is not considered in the calculated MU, but is included in the determination of measurement of required MU.

_____**Jin Lii**_____**ID #: 123548**_____**Certification MP0121**_____**Date 08/16/2010**

Calculated by:

_____**Narayan Sahoo**_____**ID #: 148706**_____**Certification Ph.D.**_____**Date 08/18/2010**

Reviewing Physicist

5.49 Monitor Unit Calculation Sheet

REFERENCES

- American Cancer Society (Accessed July 28, 2010) What are the key statistics about lung cancer?
Available at: "<http://www.cancer.org/Cancer/Lung Cancer-Non-Small Cell/ Detailed Guide/ non-small-cell-lung-cancer-key-statistics>"
- Childress, NL., Bloch, C., White, RA., Salehpour, M., Rosen, I. (2005) Detection of IMRT delivery errors using a quantitative 2D dosimetric verification system. *Medical Physics* **32(1)**, 153-162.
- Deasy, JO., Blanco, AI., Clark, VH. (2003) CERR: A computational environment for radiotherapy research. *Medical Physics* **30(5)**, 979-985.
- DeLaney, TF., Kooy, HM. (2008) *Proton and Charged Particle Radiotherapy*. Lippincott Williams & Wilkins, Philadelphia, PA.
- Followill, D. S., Evans, D. R., Cherry, C., Moileu, A., Fisher, G., Hanson, W. F., Ibbott, G. S. (June 2007) Design, development, and implementation of the Radiological Physics Center's pelvis and thorax anthropomorphic quality assurance phantoms. *Medical Physics* **34(6)**, 2070-2076.
- Followill, D.S. (Accessed January 20, 2010) Radiological Physics Center - RPC Website. Available at: "<http://rpc.mdanderson.org/rpc/>"
- Grant, R. (May 2010) *Implementation of an Anthropomorphic Pelvis Phantom for the Evaluation of Proton Therapy Treatment Procedures*. Graduate School of Biomedical Sciences.
- ICRU (1993) *Stopping Power and Ranges for Protons and Alpha Particles*. ICRU Report 49, Bethesda, MD.

- International Specialty Products (February 2009) *GAFCHROMIC EBT2 self-developing film for radiotherapy dosimetry.*, 2009.
- Johns, H. E., Cunningham, J. R. (1983) *The Physics of Radiology*. Thomas, Springfield, Ill..
- Khan, F. M. (2010) *The Physics of Radiation Therapy* 4th edn. Lippincott Williams & Wilkins.
- Kirby, D., Green, S., Palmans, H., Hugtenburg, R., Wojnecki, C., Parker, D. (2010) LET dependence of GafChromic films and an ion chamber in low-energy proton dosimetry. *Physics in Medicine and Biology* **55**, 417-433.
- Kirby, TH., Hanson, WF., Johnston, DA. (1992) Uncertainty analysis of absorbed dose calculations from thermoluminescence dosimeters. *Medical Physics* **19(6)**, 1427-1433.
- Knoll, G. F. (2000) *Radiation detection and measurement*. John Wiley & Sons., New York.
- Low, DA., Harms, WB., Mutic, S., Purdy, JA. (1998) A technique for the quantitative evaluation of dose distributions. *Medical Physics* **25(5)**, 656-661.
- Moyers, M. F., Sardesai, M., Sun, S., Miller, D. W. (2010) Ion Stopping Powers and CT Numbers. *Medical Dosimetry* **35(3)**, 179-194.
- Nerbun, C. (2005) *Analysis of MD-55-2 Gafchromic Film as a Dosimetry Ausit System for Proton Therapy*. Graduate School of Biomedical Sciences.
- Paganetti, H., Niemerko, A., Ancukiewicz, M., Gerweck, L. G., Goitein, M., Loeffler, J. S., Suit, H. D. (2002) Relative Biological Effectiveness (RBE) Values for Proton Beam Therapy. *Int. J Radiation Oncology Biol. Phys.* **53(2)**, 407-421.

- Sahoo, N., Zhu, R. X., Arjomandy, B., Ciangaru, G., Lii, M., Amos, R., Wu, R., Gillin, M. T. (2008) A procedure for calculation of monitor units for passively scattered proton radiotherapy beams. *Medical Physics* **35**(11), 5088-5097.
- Sawakuchi, G. O., Titt, U., Mirkovic, D., Mohan, R. (2008) Density heterogeneities and the influence of multiple Coulomb and nuclear scatterings on the Bragg peak distal edge of proton therapy beams. *Physics in Medicine and Biology* **53**, 4605-4619.
- Slater, J. M., Archambeau, J. O., Miller, D. W., Notarus, M. I., Preston, W., Slater, J. D. (1992) The proton treatment center at Loma Linda University Medical Center: Rationale for and description of its development. *International Journal of Radiation Oncology Biology Physics* **22**(2), 383-389.
- Smith, A. R. (2006) Proton Therapy. *Phys Med Biol* **51**(13), 491-504.
- Smith, A., Newhauser, W., Latinkic, M., Hay, A., McMaken, B., Styles, J., Cox, J. (2003) The University of Texas M.D. Anderson Cancer Center Proton Therapy Facility. In : *AIP Conference Proceedings*, vol. **680**, 1073-1076.
- Sundaresan, MK. (2001) Handbook of Particle Physics. CRC Press LLC, Boca Raton, FL 6.
- UCLA: Academic Technology Services FAQ: What is the coefficient of variation? Available at: http://www.ats.ucla.edu/stat/mult_pkg/faq/general/coefficient_of_variation.htm
- Urie, M., Goitein, M., Holley, WR., Chen, T.Y., G. (1986) Degradation of the Bragg Peak due to inhomogeneities. *Physics in Medicine and Biology* **31**(1), 1-15.

- Van Dyk, J., Keane, TJ., Rider, WD. (1982) Lung density as measured by computerized tomography: implications for radiotherapy. *International Journal of Radiation Oncology Biology Physics* **8**, 1363-1372.
- Vatnitsky, S. M., Schulte, R. WM., Galindo, R., Meinass, H. J., Miller, D. W. (1997) Radiochromic film dosimetry for verification of dose distributions delivered with proton-beam radiosurgery. *Physics in Medicine and Biology* **42**, 1887-1898.
- Wilson, RR. (November 1946) Radiological use of fast protons. *Radiology* **47(11)**, 487-491.
- Zhao, L., Das, I. J. (April 2010) Gafchromic EBT film dosimetry in proton beams. *Physics in Medicine and Biology* **55**, N291-301.

VITA

Anthony Blatnica, who goes by Tony, was born in Syracuse, New York on March 30, 1975 to Joe and Geri Blatnica. He is married to Becky Blatnica and has a 6 year old son, Jake. He graduated from Texas State University, back when it was known as Southwest Texas State University, in December 2002. He first worked as an Associate Engineer at Advanced Micro Devices, and later Spansion, LLC. in Austin, TX before moving to Houston, TX in 2004. Upon arrival in Houston, he began work for The University of Texas at M. D. Anderson Cancer center as a Physics Technologist in Imaging Physics. He remained working part time at this position upon entering the University of Texas Health Science Center at Houston Graduate school of Biomedical Sciences. He enjoys reading, science fiction, and playing with his family.

Permanent address:

12502 Antean Way Court

Houston, TX 77065